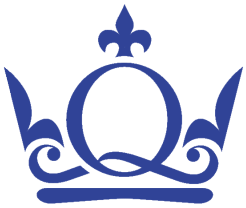

Queen Mary
University of London

DNA Nanotechnology and Nanopatterning:

Biochips for Single-Molecule Investigations

Da Huang

Supervised by Dr. Matteo Palma

School of Biological and Chemical Sciences

Queen Mary University of London

Thesis submitted for the degree of Doctor of Philosophy

2017

Statement of Originality for Inclusion in Research Degree Thesis

I, Da Huang, confirm that the research included within this thesis is my own work or that where it has been carried out in collaboration with, or supported by others, that this is duly acknowledged below and my contribution indicated. Previously published material is also acknowledged below.

I attest that I have exercised reasonable care to ensure that the work is original, and does not to the best of my knowledge break any UK law, infringe any third party's copyright or other Intellectual Property Right, or contain any confidential material.

I accept that the College has the right to use plagiarism detection software to check the electronic version of the thesis.

I confirm that this thesis has not been previously submitted for the award of a degree by this or any other university.

Signature: 

Date: 05th December, 2017

Details of Collaboration and Publications:

1. Huang, D., Freeley, M. & Palma, M. “DNA-Mediated Patterning of Single Quantum Dot Nanoarrays: A Reusable Platform for Single-Molecule Control,” *Sci. Rep.* **7,** 45591 (2017).

2. Huang, D., Freeley, M. & Palma, M. “Single-Molecule Patterning via DNA Nanostructure Assembly: A Reusable Platform” Methods in Molecular Biology (2017), *in press*.

3. Keseroglu, K., Huang, D., Palma, M. & Sapelkin, A. “Super-Resolution Imaging via Spectral Separation of Quantum Dots” (2017), *submitted*.

4. Huang, D., Patel K., Perez-Garrido, S., Marshall, J. & Palma, M. “Patterned DNA Origami for Cancer Cell Adhesion: Multi-valent Investigations with Single-Molecule Control”, *in preparation.*

Acknowledgements

Firstly, I would like to thank my supervisor Dr. Matteo Palma for offering me the chance to work in his group and for his many suggestions, advices, encouragement and patience throughout the years. I benefited a lot from his interest in nanotechnology and expertise in nanofabrication techniques. Without his support in my research and studies, this project would have not been possible.

Many thanks to all the members in Palma Group for an active and harmonious atmosphere. I would like to thank Mark Freeley for the work on surface modifications in my paper and this thesis. Thanks Sandra Perez for the help in cell culturing and the peptide characterisations. I am also grateful to Jingyuan Zhu, Joseph McMorrow, Antonio Attanzio and our postdoctor Dr. Pierrick Clement for all the advices and support you gave me.

I am very grateful to Dr. Russell Bailey and Dr. Nadja Tarakina for the training and support of Focused Ion Beam and Scanning Electron Microscopy. Many thanks to Michaela Egertova for the training and support of Confocal and Differential Interference Contrast Microscopy. I would also like to thank Geoff Gannaway, George Nevill and Dr. Ken Scott for the support in the clean room and the evaporation lab. Thanks also to Samantha Court, Dr Lingzhi Gong, Dr Ruth Rose, Yumiko Tashiro, Agha Shah and Jay Paul for all the helps and technical support in the lab.

I would also like to thank all my collaborators without whom essential experiments in this thesis would not have been possible. Thanks Dr. Andrei Sapelkin and Kemal Keseroglu in School of Physics and Astronomy for the super-resolution imaging of quantum dots. I also would like to express my gratitude to Professor John

Marshal in Barts Cancer Research Institute for his patience, advices and support in cell adhesion studies. Thanks to Ketan Patel in Barts Cancer Research Institute for helping in some cell experiments and his kindly advices.

Lastly, I would like to thank my family for their love. Thanks to my parents and my parents-in-law, you always encourage and believe in me wherever you are. Thank you Dexu, my dear wife, for everything you shared with me and your giving to this family. You inspired and help me a lot in both of my research and life. Thanks Cooper for choosing to live with me and making this family full with happiness.

Abstract

The controlled organization of individual molecules and nanostructures with nanoscale accuracy is of great importance in the investigation of single-molecule events in biological and chemical assays, as well as for the fabrication of the next generation optoelectronic devices. In this regard, the precise patterning of individual molecules into hierarchical structures has attracted substantial research interest in recent years. DNA has been shown to be an ideal structural material for this purpose, due to the specificity of its programmability and outstanding chemical flexibility. DNA origami can display a high degree of positional and precise binding sites, allowing for complex arrangements and the assembly of different nanoscale architectures.

In this project, we present a novel platform based on the use of DNA scaffolds for the organization of individual nanomoieties (with nanoscale spatial control), and their selective immobilisation on surfaces for single-molecule investigations. In particular, semiconductor quantum dots (QDs), fluorescence molecules, linear small peptides, and structural proteins were tethered with single-molecule accuracy on DNA origami; their subsequent organization in array configuration on nanopatterned surfaces allowed us to fabricate and test different platforms for single-molecule studies.

In particular, we developed a Focused Ion Beam (FIB) nanofabrication strategy and demonstrated its general applicability for the assembly of functionalised DNA nanostructures in highly uniform nanoarrays, with single-molecule control. In addition, we further explored this nanofabricated platform for biological investigations at the single-molecule level, from protein-DNA interactions to cancer cell adhesion studies with single-molecule control. Investigations have been carried out via fluorescence

microscopy, scanning electron microscopy (SEM), Focused Ion Beam (FIB) and atomic force microscopy (AFM).

By and large, combining the programming ability of DNA as a scaffolding material with a one-step lithographic process, we have developed a platform of general applicability for the fabrication of nanoscale chips that can be employed in a variety of single-molecule investigations.

Keywords: DNA Nanotechnology, DNA origami, Nanofabrication, Single-molecule, AFM, FIB

Table of Contents

List of Figures

Abbreviations

AFM	Atomic Force Microscopy
BSA	Bovine Serum Albumin
CAD	Computer-aided Design
CLSM	Confocal Laser Scanning Microscopy
CNT	Carbon Nanotube
DI Water	Deionized Water
DIC	Differential Interference Contrast
DMEM	Dulbecco´s Modified Eagle Medium
DNA	Deoxyribonucleic Acid
DPBS	Dulbecco's Phosphate-buffered Saline
dsDNA	Double Stranded Deoxyribonucleic Acid
ECM	Extracellular Matrix
EDC	1-Ethyl-3-(3-dimethylaminopropyl)carbodiimide
EDTA	Ethylenediaminetetraacetic Acid
EGF	Epidermal Growth Factor
FA	Focal Adhesion

FBS	Foetal Bovine Serum
FIB	Focused Ion Beam
FOV	Field of View
GDSC-SMLM	Genome Damage and Stability Centre Single Molecule Light Microscopy
GFP	Green Fluorescent Protein
HMDS	Hexamethyldisilazane
HPLC	High-performance Liquid Chromatography
LMIS	Liquid-metal Ion Source
MCP	Multichannel Plate
MOPS	3-Morpholinopropane-1-sulfonic acid
MWCO	Molecular Weight Cut-off
NMP	N-Methyl-2-pyrrolidone
OD	Optical Density
PAGE	Polyacrylamide Gel Electrophoresis
PBS	Phosphate-buffered Saline
PCR	Polymerase Chain Reaction
PEG	Polyethylene Glycol
PMMA	Poly(methyl methacrylate)
QD	Quantum Dot

QDOSS	Quantum Dot-based Optical Spectral Separation
RGD	Arginyl-Glycyl-Aspartic Acid
RPM	Revolutions Per Minute
RT	Room Temperature
RTFI	Room-temperature Formamide Incubation
SEM	Scanning Electron Microscopy
SR	Super Resolution
ssDNA	Single Stranded Deoxyribonucleic Acid
STM	Scanning Tunnelling Microscope
Sulfo-NHS	N-Hydroxysulfosuccinimide
SWCNT	Single Wall Carbon Nanotube
TAE	Tris-acetate-EDTA
TIRF	Total Internal Reflection Fluorescence
UV	Ultraviolet
2D	Two-dimension
3D	Three-dimension

The 20 Natural Amino Acids and Their Abbreviations

A	Alanine	Ala
C	Cysteine	Cys
D	Aspartic Acid	Asp
E	Glutamic Acid	Glu
F	Phenylalanine	Phe
G	Glycine	Gly
H	Histidine	His
I	Isoleucine	Ile
K	Lysine	Lys
L	Leucine	Leu
M	Methionine	Met
N	Asparagine	Asn
P	Proline	Pro
Q	Glutamine	Gln
R	Arginine	Arg
S	Serine	Ser
T	Threonine	Thr
V	Valine	Val
W	Tryptophan	Trp
Y	Tyrosine	Tyr

Chapter 1

Background

In recent years, there has been a growing interest in controlling matter at smaller and smaller scale. This has not only been driven by the semiconductor industry to fabricate devices at the nanoscale, but it is also a highly-motivated research field in investigating life science at the molecular level. Most biochemical and biophysical processes occur at the nanoscale, so it is important to study nature at the scale at which it occurs. Moreover, the study at the nanoscale encourages the strategy of designing and fabricating functional materials based on the understanding the molecular basis of nature.

In this context, self-assembly is an important supramolecular strategy seen in nature, and represents the perfect bridge between life sciences and materials science: self-assembly processes provide routes to the formation of a range of materials with regular structures, and offer one of the most general strategies now available for generating new architectures at the nanoscale. In return, these artificial structures and the tools developed based on the inspiration from nature, can be employed back to understand the basic science of Life.

In nanotechnology and nano-biotechnology, methods of detecting samples with small scale play an important role. Probing dynamics and monitoring interactions at the single-molecule level is essential for investigating many fundamental processes and issues in living systems. Biomolecular folding and assembly, function of proteins and other cellular machines need to be performed and imaged using newly developed technologies. As a result, low-cost platforms to study biological interactions separately at the nanoscale and with single-molecule resolution are highly demanded.

In this regard, the controlled organization of individual molecules and nanostructures with nanoscale accuracy is of great importance in the investigation of single-molecule events in biological and chemical assays, as well as for the fabrication of the next generation optoelectronic devices. A key requirement for such applications is the controlled organisation of single molecules and nanomoieties from solution to surfaces. For these reasons, the precise patterning of individual molecules into hierarchical structures has attracted substantial research interest in recent years.

While various approaches have been applied for the controlled assembly of single-molecules and individual nanostructures, DNA has been shown to be an ideal structural material for this purpose. DNA origami, in which single- or double- stranded DNA are folded or synthesized into various nano-structures using ‘staple strands’, can display a high degree of positional and precise binding sites, allowing for complex arrangements and the assembly of different nanoscale architectures [1]. In particular, this can be used to pattern bioactive structures precisely at the scale of individual molecules.

In this thesis, we present a novel platform based on the use of DNA scaffolds for the organization of individual nanomoieties (with nanoscale spatial control), and their selective immobilisation on surfaces, in nanoarrays, for single-molecule

investigations. We initially demonstrated the use of this platform for the organization of single quantum dots (QDs) at predefined locations on silicon and transparent glass surfaces. We have then employed this platform and strategy for dynamic enzymatic investigations and in cell adhesion studies. In this regard, patterned peptide modified DNA origami nanoarrays were employed to mimic the extracellular matrix and investigate integrin binding behaviour for specific cancer cells.

The strategies developed make use of molecular nano-fabrication techniques, surface biochemical functionalization strategies, Focused Ion Beam (FIB) patterning and other nanotechnology tools. Investigations have been carried out via fluorescence microscopy, Scanning Electron Microscopy (SEM), and Atomic Force Microscopy (AFM).

In this chapter, the importance of single-molecule investigations, the background of DNA nanotechnology and surface fabrication technologies will be presented. Moreover, surface pattering and nanofabrication will be briefly discussed, Finally, the goals of the thesis will be outlined in section 1.4.

1.1 Single-molecule Investigations

In recent years, the rapid development of single-molecule investigation techniques has opened up a new era in scientific research. The main reasons for developing single-molecule investigations lie in the prospect of understanding matter and its transformations at the most fundamental level and the potential of constructing novel devices and materials.

There are several purposes of studying under single molecule level. Since the atoms and molecules are basic building blocks of matter, their properties represent the origin of the phenomenon at large scale. These intrinsic properties of molecules cannot be simply investigated in a group of molecules where average properties are measured. However, individual molecular effects and their environment can be detected via several strategies such as local potentials or energetic inhomogeneity. As a result, the capability to investigate single molecules makes it possible to manipulate and control nature process at the spatial limit. The properties of individual molecules are hidden in larger systems. The study of single atoms and molecules provides novel insights into quantum mechanics [2]. The nature of chemical bonding or biological reaction can be reveal in a new way and studied to reach the critical bases.

Many chemical and biological processes are complex and cannot be study using ensemble techniques. In the conventional strategies, group of molecules from one or various species are investigated at the same time. In such a bulk approach, the properties of each molecule in the reaction are summarised to yield a measurable signal. In contrast, the single-molecule studies obtain data from individual molecule instead of obtaining from the ensemble-averaged measurements [2]. The conventional measurement cannot observe and manipulate the dynamic behaviour using the statistic results. These reactions of bulk molecules cannot be synchronised even if they are initiated at the same time [3]. As a result, it is important to explore new techniques to study dynamic and mechanistic properties of molecule, which is single-molecule investigation technology. The differences of bulk and single-molecule investigation are distinct in biological processes. Biomolecules are evolved in a complicated heterogeneous system. Biochemical reactions are linked together to formed a large

dynamic network with different types of molecules. Utilising ensemble-averaged measurements in quantitatively detecting dynamic behaviour in a such complicated system becomes difficult. Single-molecule investigation allows revealing the dynamic connection of molecules directly even in real time [4]. The difficulties in bulk investigations can be overcome using single-molecule approaches by simplified the network into individual detections. Via investigating the single molecular signal, the researchers can even reveal the dynamic of bioreaction and draw the detail images of the molecular behaviour.

Single-molecule techniques can also utilise the study of individual behaviours of biomolecules to assemble molecular devices. Revealing the sophisticated signal pathways and the mechanism of specific cell signalling molecules allow researchers to use nano particles or nano materials to mimic the biological reactions with single-molecule resolution. Artificial nanostructures can be synthesised to apply on biotechnology and medical engineering [5].

Recently, DNA based nanotechnology is developed quickly for single-molecule analytical techniques. Single-molecular sensor or detecting device for low-cost, high-throughput analysis is the important application of studying individual molecule properties. Building biochips based on single DNA nanostructures were rapid progressed and draw great attention of researchers. DNA was used in the preparation of increasingly complex shapes and lattices to achieve more and more functions. Since its inception, the single-molecular techniques have gained much attention in the field of structural DNA nanotechnology. The DNA nanostructures can be easily constructed with defined size and shape and detected under individual level. Moreover, specific enzymatic DNA provides powerful material to apply in the individual investigation of

biochemical reaction mechanism. The nature of complementary base pairing of DNA allows self-assembly of various nanostructures for large range of research [6]. As a result, DNA becomes an important substrate in applying single-molecule studies. In the following section, the DNA nanotechnology and functional DNA nanostructures will be discussed.

1.2 DNA Nanotechnology and DNA Origami

Deoxyribonucleic Acid, or DNA is the genetic material in most of living organisms. The genetic information is coded and stored based on the specific structure of DNA.

DNA is a polymer having a backbone containing sugar and phosphate with four different bases attached to the side (nucleoside) [7]. Nucleotides are the simpler monomer units to form the polymer. Each nucleotide contains a five-carbon sugar group (deoxyribose), a phosphate group and a nitrogenous base. There are four different types of nitrogenous bases including Adenine (A), Thymine (T), Cytosine (C), and Guanine (G). With different combinations of nucleotides, DNA polymer is formed to code the genetic information. The alternating sugar and phosphate group backbone structure defines the direction of DNA strands. The phosphate group terminal is defined as 5' end and 3' end is on the sugar hydroxyl group. Hydrogen bond bounds two single stranded DNA (ssDNA) together to form double stranded DNA (dsDNA) (Figure 1.1) [8]. Different nucleotides exhibit specific hydrogen binding according to so called base paring rules: between A and T, there are two hydrogen bonds, meanwhile, three hydrogen bonds bind C to G (Figure 1.2). A double helix structure is formed based on

two antiparallel complementary ssDNA, making 5' end and 3' end of two single strand DNA align to each other.

The double helix structure of dsDNA is a cylinder shape and has a diameter of approximately 2 nanometres (nm). The two strands loop around single axis, and have a repeat pitch of 3.4 nm (10 base pairs per turn). Based on the interaction between the DNA molecule and the environment, researchers also revealed a diameter of 2.2 nm to 2.6 nm for the double helix structure when detected in liquid solution [9].

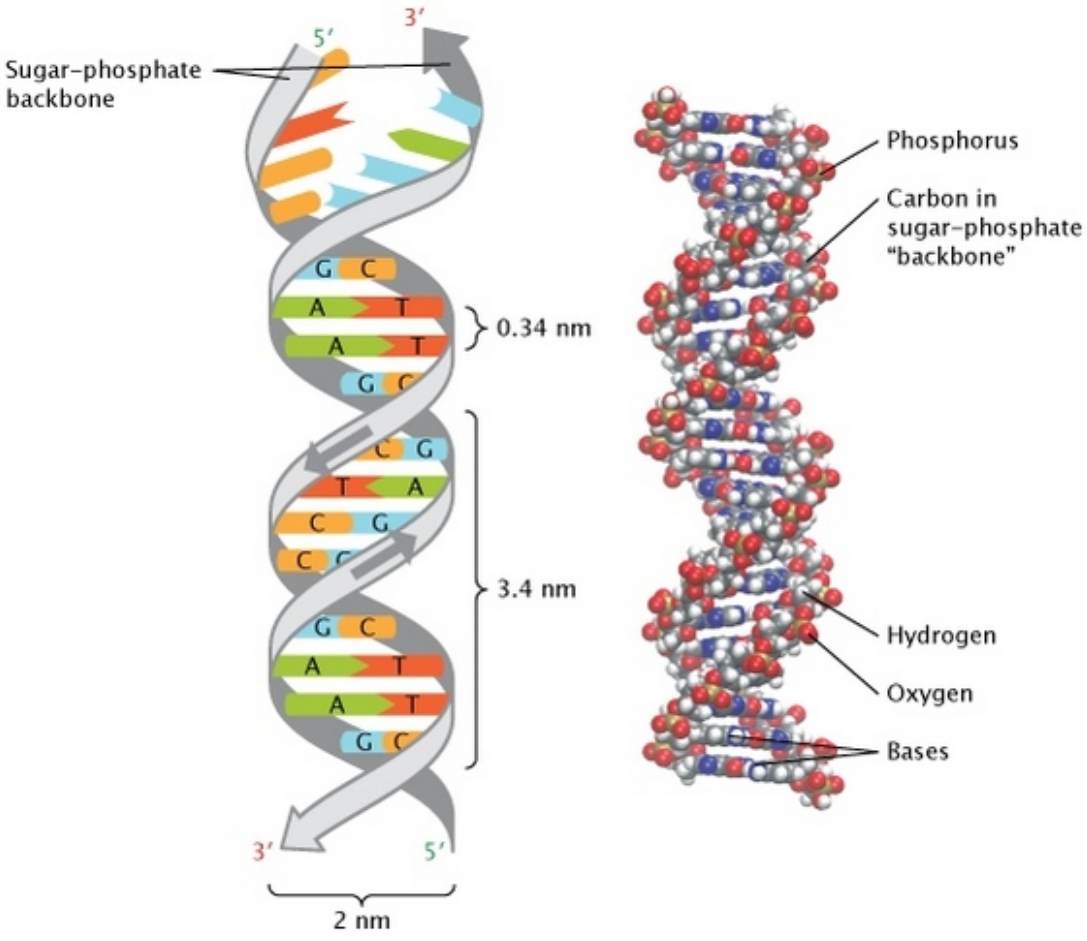

Figure 1.1 Schematic of DNA double-helical structure [8].

The mechanism of self-assembly of A to T and G to C (due to the lowest free energy upon bonding) makes it possible to utilize and manipulate branched helix structures. The understanding of this nature lead to the emergence of DNA nanotechnology.

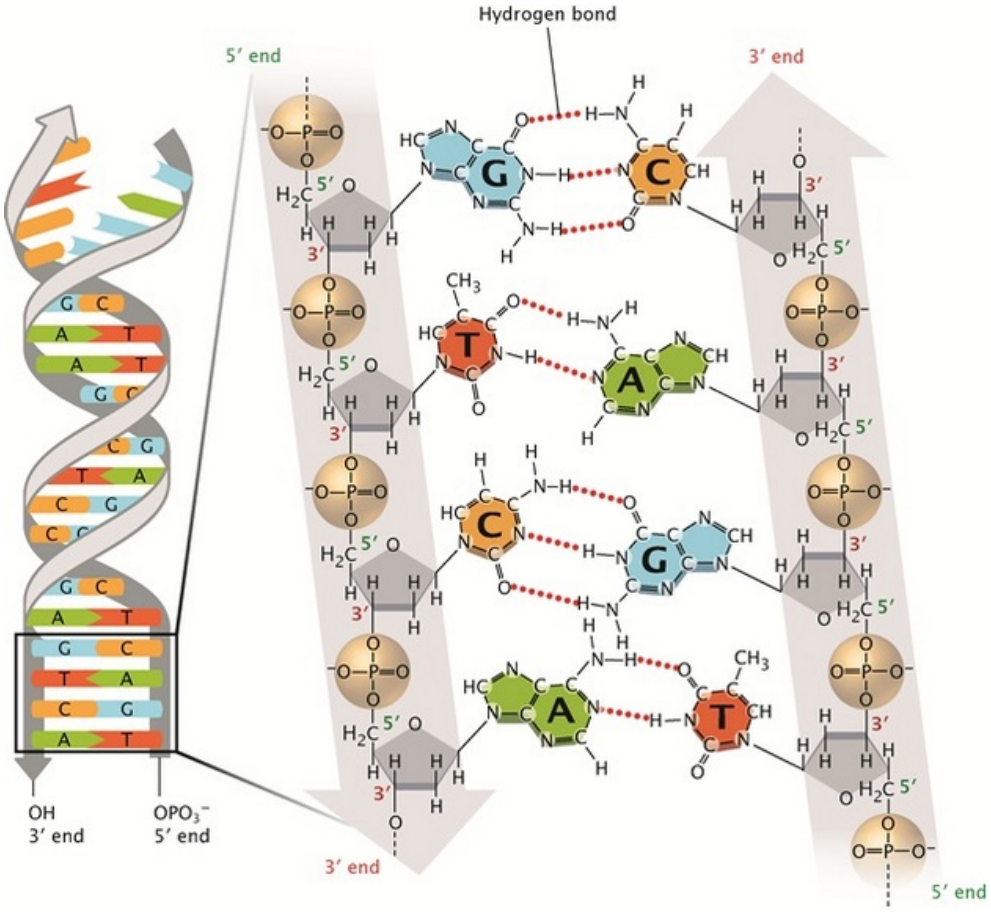

Figure 1.2 Base pairing of DNA [8].

1.2.1 DNA Nanotechnology

DNA nanotechnology is the technology utilising nucleic acid to manufacture nanostructures and investigate their functions at the nanoscale. This is a rapidly

developing field of research after further understanding of DNA structure and advancing of detecting techniques.

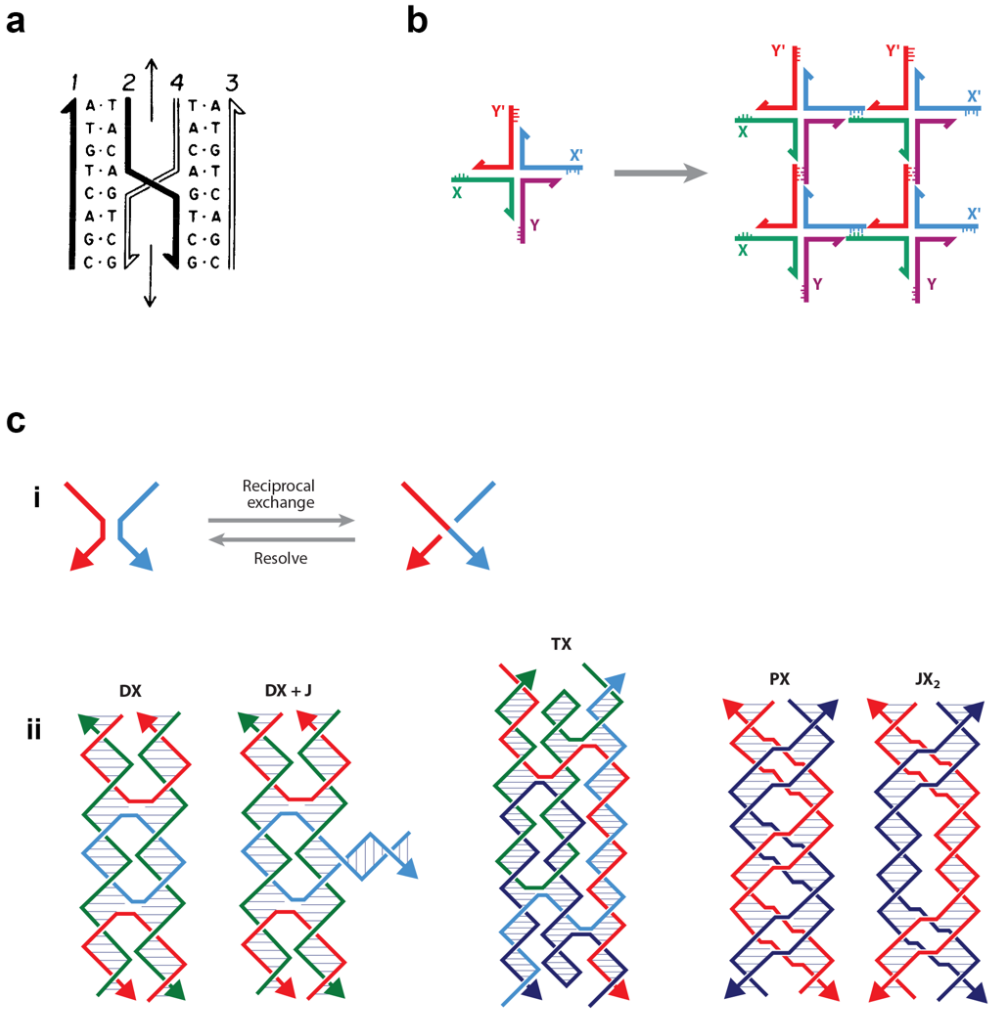

Figure 1.3 Assembly of branched DNA nanostructures. **a)** The Holliday structure. **b)** Assembly of 4-arm branched DNA junction into larger arrangements. **c)** Motif design based on reciprocal exchange [10]. **i)** Reciprocal exchange of DNA structure. **ii)** Examples of different motifs that can result from reciprocal exchange.

During the research on DNA replication, branched structures were found to occur naturally. With the development of DNA sequencing and synthesis, researchers tried to mimic branched DNA structures and explored the potential in utilising brunched

DNA structure as a structural material. Folding oligomeric nucleic acids, various shapes of immobile lattices and junctions such as Holliday Junctions [11] (Figure 1.3 a) were reported during 1960s to 1970s. In 1982, Nadrian Seeman generated larger scale junctions using the technique of sticky-end ligation [12] (Figure 1.3 b). The novel idea of bringing branched DNA junction structures together to form crystalline lattices became fundamental in the design of DNA nanostructures in the following years. The technique of using sticky-end to link DNA junctions with each other was widely applied in constructing various DNA nanostructures. Reciprocal exchange was revealed to be an important part in designing DNA nanostructure motifs [13]. This process switches the connection of two different DNA double helices to form a new cross over connection. This can be achieved by designing the sequence of DNA single strands and apply self-assembly. With the development of DNA nanotechnologies, researcher started to create various nanostructures based on the branched DNA junctions and reciprocal exchange design.

From early 80s' until now, Nadrian Seeman has led the structural DNA nanotechnology for nearly 40 years. Based on the idea of utilising brunched DNA structures to create functional DNA nanodevices, Seeman synthesised two-dimensional DNA crystals via bottom-up self-assemble approach [14], assembled a switchable double-crossover DNA device using B-Z transition [15], created a robust sequence-dependent rotary DNA device controlled by DNA hybridisation [16], and fabricated a biped molecular walking motor built from DNA [17]. These DNA based nanostructures explored the programmability and switchable properties of DNA. More and more researchers have developed these DNA nanostructures by recognizing DNA as a polymer with well-defined structural and chemical properties.

Moreover, the functional modification ability of DNA nanostructures has been well studied by different researchers. Functional proteins [18, 19], metal nanoparticles [20, 21], or quantum dots [22, 23] can be precisely placed on DNA nanostructures. An interesting work in 2006 [24] showed how selected proteins can be arranged on the surface of a DNA nano-structure surface in the shape of the letters 'D', 'N', and 'A'. This work demonstrated the precise control ability on DNA nanostructures and introduced the proper strategy to do so.

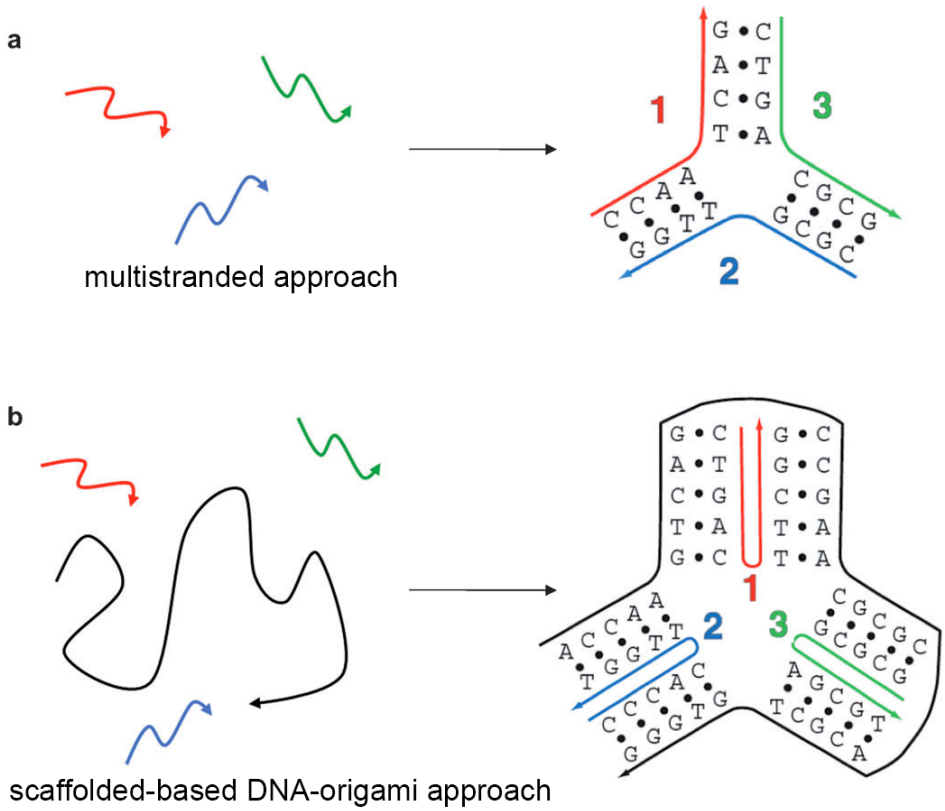

Figure 1.4 Schematic of two main DNA nanostructure construction approaches [25]. **a)** Brunched DNA are self-assembled in multistranded approach to form finite or infinite tiles. **b)** A long single-stranded scaffold can be fold into a desired finite nanostructure via several short single strands.

In the previous DNA nano-structure constructed approaches, the branched DNA were assembled to form tiles structures with mainly infinite theoretical boundary. These structures may be non-uniform in size and shape, also lack of orientation control. A unique assembly strategy was developed by Yan in 2003 for the construction of an aperiodic DNA lattice by the direct nucleation of DNA tiles around a long scaffold strand [26]. Another strategy using a similar 'folding' approach was reported by Shih in 2004 [27]. A long single strand of DNA as a scaffold was folded into an octahedron structure with the help of several short oligonucleotides. These short strands were called staple strands because they grasp the folding structure tightly such as 'staple' them together. Based on this scaffold-based approach, DNA was used to create larger and more complex nanostructures even can up to megadalton scale and into three-dimension. This is the appearance of a large DNA nanostructure family called DNA origami.

As mentioned before, various of DNA based nanostructures has been explored and created for different applications, however, there are still some limitations of these techniques. For instance, researchers need to use a great number of short oligonucleotides to synthesis these nanostructures, which makes the yield of structures synthesis highly sensitive to the relative ratios of strands (stoichiometry). This requires carefully adjustments and numbers of trials. The complex structures also require multiple reaction steps and purifications, which leads to the low yield of structures synthesis. As a result, a technique based on self-assembly procedures with quick and cheap process under mild conditions is required to overcome the limitation of traditional synthesis of DNA nanostructures. Based on the scaffold folding strategy, the nanostructure synthesis is thought to be proceed without many misfoldings and avoid the complications of stoichiometry and purification associated with methods that use

many short DNA strands [28]. Via simply mixture of scaffold sequence and access number of short strands under temperature controlled condition, the synthesis of structures can be easily achieved with a high yield. The DNA nanostructures synthesis via this procedure are call DNA origami.

1.2.2 DNA Origami

DNA origami is a megadalton sized DNA nanostructure with specific designed geometry. In 2006, Rothemund reported a simple but remarkable method to fold long, single-stranded DNA with hundreds of short single-stranded DNA to form arbitrary two-dimensional shapes [28]. This novel approach is an extraordinary breakthrough in the construction of DNA nanostructures. This work opened up the new research field of DNA origami and the followed by numbers of remarkable investigations based on DNA origami structure. Just as the meaning of the word 'origami', the Japanese art of paper folding, the DNA origami technique folds a long single-stranded DNA strand into a desired shape with the help of hundreds of short staple strands (Figure 1.5).

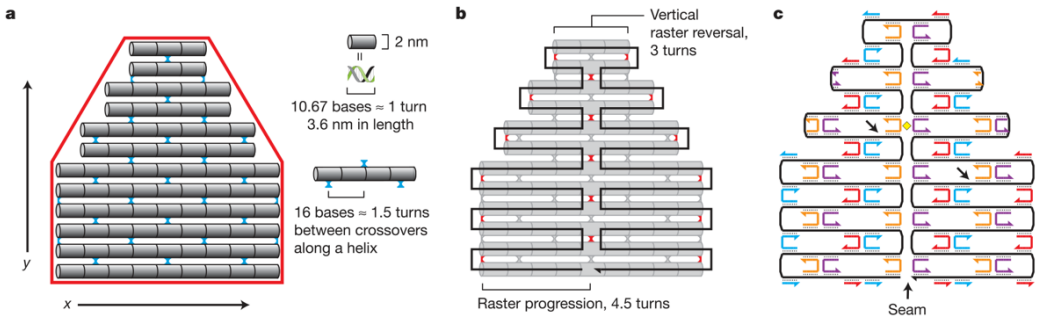

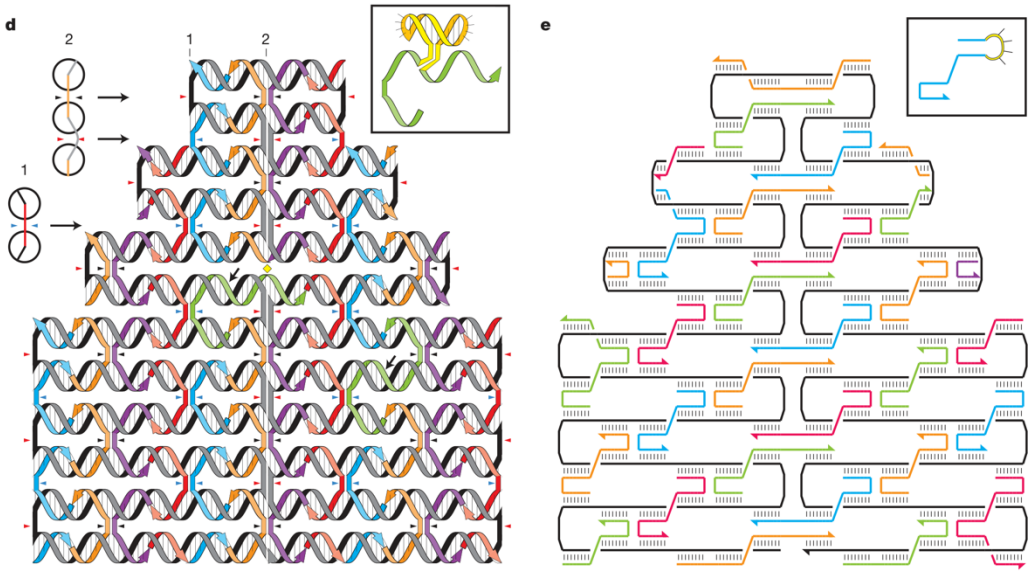

Figure 1.5 Design of DNA origami from Rothemund's work [28].

Although Rothemund's work was based on the similar scaffold-based approach that developed by Yan and Shih, he made up a much more systematic and effective way to synthesis DNA nanostructures. In his study, an efficient way to design a scaffolded DNA nanostructure was instructed. Combining the design on paper and by computer, Rothemund developed a five steps procedure including construction of the geometric model for the desired shape with DNA helical turns and crossover, forming the raster pattern of a long single stranded scaffold to build the folding path, generating the sequences of staple strands, regulation of scaffold crossover twist and merging the adjacent staples across nicks to form longer staple strands for more stable binding condition. This designing procedure is well-organized and then followed up by other researchers. A computer aided software called caDNAno [29] was developed for more complicated DNA origami design. The details of DNA origami design will be discussed in Chapter 3.

In the work of building DNA origami, the self-assembly property of constructed DNA nanostructure was explored. A 7249 bp long single-stranded circular M13mp18 vector DNA was folded with the help of about 220 staple strands into an antiparallel array of helices based on the design. With the aid of Watson and Crick base paring, the scaffold strand can self-anneal under set temperature process (from 90 ℃ to room temperature) with complementary staple strands and assemble the target structure with astonishingly high yields. It is a dexterous and simple procedure that can be accomplished within several hours. The extension of assembly time up to 20 hours when constructed larger scale of DNA origami was also indicated by Rothemund. Recently, Zhao has reported a room-temperature formamide incubation (RTFI) method to overcome the thermal annealing issue [30]. With the aid of formamide, the DNA origami can be assembled in room temperature, avoiding thermal denaturation and multi-step annealing. Stepwise assembly and temperature sensitive component assembly can be allowed utilising this approach.

In the strategy that created by Rothemund, the folding of a long strand of DNA proceeds with reduced errors resulting in final structures with fewer defects and significantly higher yield. The stoichiometry control and oligonucleotides purification was avoided which dramatically reduced experimental errors and synthesis times. It is possible to create more complex shapes and the constructed nanostructures have fixed dimensions and are fully addressable, allowing the attachment of molecules at prescribed positions. The strategy of constructing scaffolded DNA origami can be attributed to several factors: one is the avoiding in adjust the relative concentrations because that staples are only required to bind to the scaffold. Furthermore, the initial attachment of correct staples partially arranges the long scaffold and reduce the

incorrect binding, which leads to eliminate unwanted secondary structure. Combining with ability of design desired shape and efficient in assembly, DNA origami becomes a very powerful strategy to generate robust DNA nanostructures. Various single-layer DNA origami structures were synthesised by Rothemund, including different rectangular shapes, stars, smiley faces, triangles frames and triangular shapes (Figure 1.6 a). These structures were validated under AFM to reveal the details.

Utilising the same idea of constructing single-layer origami, multi-layer of DNA origami was also developed. The adjacent helices were connected via regular pattern of crossover not only in a flat structure, but can applied on three dimensions. In 2009, Douglas extended this method to build custom 3D shapes DNA origami [31]. The nanostructure was formed as pleated layers of helices constrained to a honeycomb lattice. Additionally, another strategy of super-twisting or bending engineered helical axes structures was also reported by Dietz [32]. These works were all developed from Rothemund's concept and applied on 3D platform. The extension of the strategy allows researcher to assemble more complicated and fascinating DNA nanostructures (Figure 1.6 b).

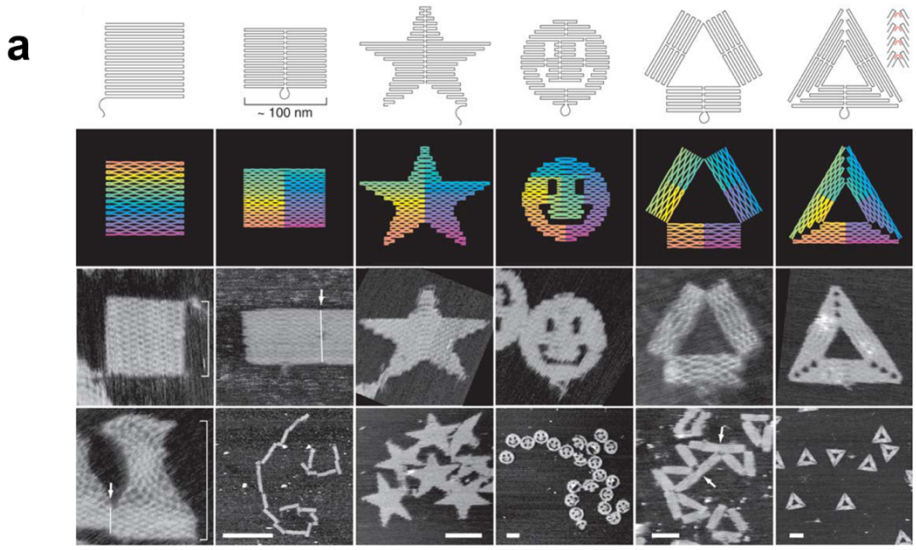

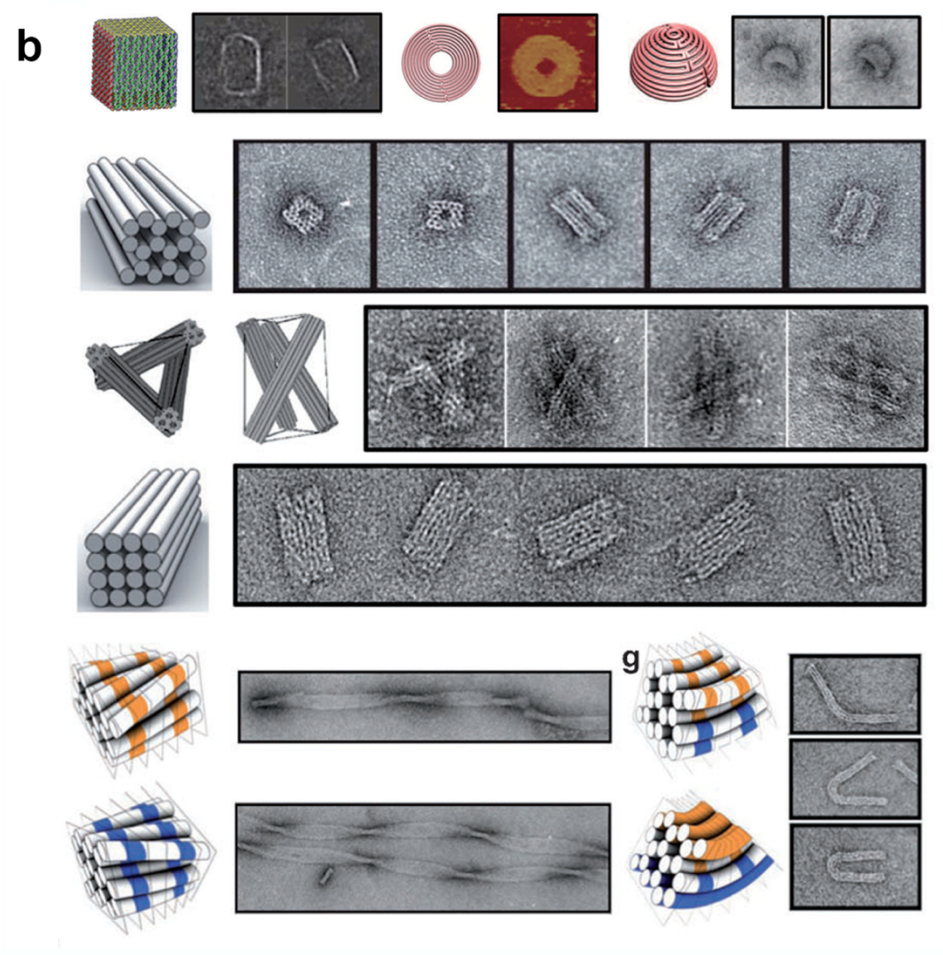

Figure 1.6 Different shapes of DNA origami both in 2D and 3D [28, 25]. **a)** DNA origami shapes assembled by Rothemund, including rectangles, stars, smiley faces and triangles. **b)** 2D and 3D DNA origami structures assembled by various researchers, including vacant, filled, twisted, and curved objects [33, 34, 31, 32].

Utilising DNA as structural materials to construct nanostructures is an important strategy to carry out single-molecule investigation. In addition, another key requirement for achieving single-molecule resolution is the controlled mobilisation of these nanostructures from solution to surfaces. The surface patterning strategies for organising nanostructures will be discussed in next section.

1.3 Surface Patterning and Nanofabrication

A key aspect for single-molecule resolution investigations, is the ability to control and detect individual molecules behaviour. Surface nanofabrication and patterning represent an important way to deposit target molecules and can be employed for a wide range of applications.

Nanofabrication involves the pattering of substrates with nanoscale spatial control. [35]. Following subsequent chemical and biochemical strategies, this can allow the immobilisation of functional nanostructures within a designed pattern on a substrate surface. The Semiconductor industry has pushed the development of nanofabrication in the past few decades. The efficiency of immobilisation and the density of nanodevices on surfaces were increased dramatically with the improvement of fabrication technologies. It was also a breakthrough to achieve a high performance and individual operation per device, which can eventually result in the ability to carry out single-molecule investigations. It is envisioned that new technologies will be developed with applications not only for information technology applications, but also in chemical and biological research fields.

Several technologies were developed for nanofabrication and surface nanopatterning. Photolithography, inkjet printing, electronic or focused ion beam lithography, as well as scanning probe lithography are the main strategies employed to fabricate patterns on surfaces [36]. These methods can achieve a resolution down to the nanometre scale, and deal with complex structures integrated into hierarchic organisation.

The strategies of fabricating or immobilising nanostructures are commonly categorised as "bottom-up" and "top-down" approaches respectively [37]. The bottom-up strategy is based on the creation of new nanostructures which integrate the functions from basic building blocks, such as small molecules, scaffold structures or functional groups. The top-down strategy, on the other hand, utilises various patterning methods to control the nanoscale organization of functional nanostructures on surfaces.

The self-assembly of DNA into nanostructures is an attractive bottom-up strategy. Utilising DNA building blocks to construct functional nanostructures allows the creation of new platforms for various of applications [37]. These strategies were discussed in section 1.2. Another category of bottom-up nanopatterning strategy is polymer based functionalised patterning surfaces. For example, a nanopatterning strategy that generated via bioinspired artificial crystallisation was reported by Joanna [38]. Gautrot et al. reported a controlled immobilisation approach for His-tagged green fluorescent protein (GFP) using polymer brushes [39].

Differently, top-down nanofabrication approaches have drawn attention in chemical and biological research. The molecular interaction/reaction environment and/or the extracellular matrix can be mimicked and manipulated on surface using several nanofabrication techniques such as electron-beam (e-beam) lithography, soft lithography, nanoimprint lithography and scanning probe lithography [36, 40]. Robert et al. reported a density tunable functional DNA structures patterned on PEG coated glass [41]. This strategy opened up a new way to design biophysical environments for further investigations. Cell signalling pathways and cell behaviour investigations can be carried out by immobilising target molecules in a designed pattern on surface and investigating the interactions or behaviour of the molecules or the cell applied on them

[42]. The density or topography of the patterned surface can be modulated in a quantitative way. A platform for the geometric immobilisation of the extracellular matrix (ECM) binding ligand RGD was fabricated by Spatz and et al. to show the preferential distance between peptides on surface for cell-adhesion [43]. Another work was reported by Schvartzman et al. showing that not only spacing but also integrin clustering is important in cell-adhesion. Different cell behaviours based on different geometric and numerical arrangements of ligands were investigated [44]. Figure 1.7 shows examples of different nanofabrication and surface functionalisation approaches.

The main advantages of using nanofabrication techniques in biological studies are the nanoscale mimicking and controllable ability. The combination of nanofabrication processes and controlled surface functionalisation allow researchers to create a physiological mimicking environment for various chemical and biological processes. The size, shapes and the nature of components on the surface are tunable to generate a precisely predictable pattern for monitoring different processes. For example, Cai et al. developed an on-chip measurement protocol to monitor the occupancy of nanodots using nanolithography strategies[45]. Employing similar patterned and functionalised nanodot arrays, Wang et al. showed how one dimension DNA nanostructures could be precisely tethered on dot pairs and how the binding strength of the interaction depends on the number of hybridizing base pairs employed to drive their organization on surface [46]. Moreover, the same approach can be employed to control the assembly of single wall carbon nanotubes (SWCNT) on lithographically-defined nanoscale anchoring dots on surface [47].

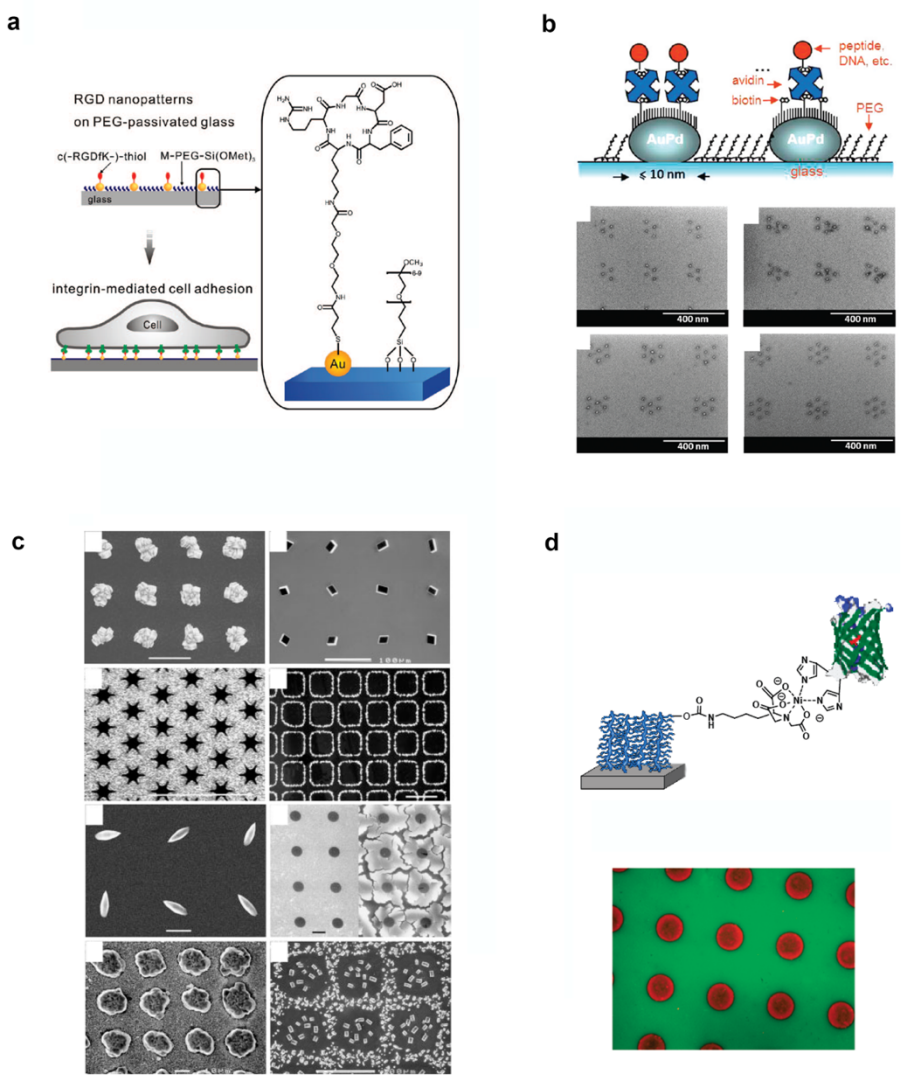

Figure 1.7 Examples of nanofabrication works. **a)** Fabrication of RGD ligand nanopatterns by Spatz et al. [43]. **b)** Biofunctionalised clustering on patterned surface, by Schvartzman et al. [44]. **c)** Bioinspired artificial crystallisation created by Joanna [38]. **d)** Polymer brushes for GFP patterning on surface, by Julien et al. [39].

Based on the development of surface fabrication and patterning strategies, the size of individual devices and patterned components are dramatically decreased to nano-meter level. As a result, nanoengineered substrate can be applied as biochips to

study several biological reactions and mechanism. One of the most important study is focused on the spatial dependence of cell adhesion binding investigations. Using the modern nanofabrication technology, engineered artificial extracellular environment, which components are spatially positioned with the nm scale control can be achieved to perform a platform in the study of interaction of cytoskeletal proteins with ECM. Recently, some research of mimicking ECM in vitro to reveal the spatial distribution of integrin binding sites were done via developed surface fabricated substrate. The possible influence of the spatial distribution on cell-ECM interaction can be examined on these artificial environments. The cell behaviour as well as the parameters of the spatial arrangement of binding sites were studies for the better understanding of the focal adhesion mechanism.

One of the major question correlated to the cell adhesion binding sites is the minimal density. Since RGD domain in ECM was recognised as a crucial part in the focal adhesion, the surface RGD concentration was demonstrated to reach down to 1 fmol/cm^2 with an average spacing of binding sites of 440 nm for cell spreading using a synthetic peptide substrate. However, the density was revealed to be variability in the cell response and peptide specificity [48]. The model of precise control with single molecule level resolution on the distribution of integrin binding ligands on biomimetic surfaces for the study of integrin ECM interactions was pioneered by Spatz et al [43]. The study was carried out on the patterned substrate by block-copolymer micelle lithography and demonstrated the spacing in the range between 58 nm to 73 nm to be ultimate for effective focal adhesion mediated by integrins. Meanwhile, clustering of integrins was shown to be necessary for the formation of adhesion, and the minimal

size of such clusters, as well as the spacing between them have been studied [44] using e-beam lithographic substrate.

All these different examples highlight how it is possible to control the assembly of biomolecules and nanostructures on surface via the development of nanofabrication approaches and surface functionalisation strategies. By controlling the size, shape, and density of nanopatterns, and designing chemical and biochemical recognition elements, it is possible to study and control chemical and biological processes at the nanoscale, towards single-molecule resolution.

1.4 Goals of This Study

In this project, we present a novel platform based on the controlled immobilisation of DNA nanostructures on surfaces for single-molecule investigations. We applied DNA origami as a platform to display a high degree of positional order and precise binding sites, allowing for complex arrangements and the assembly of different nanoscale architectures. In particular, semiconductor quantum dots (QDs), fluorescence molecules, linear small peptides and structural protein were modified at the scale of individual molecules on DNA origami for single-molecule investigations: this will be discussed in chapter 3.

Additionally, chapter 4 will present a strategy for the controlled immobilisation of DNA nanostructures on Focused Ion Beam (FIB) nanofabricated surfaces. This strategy combines the programming ability of DNA as a scaffolding material, with a one-step lithographic process. Moreover, the platform developed is reusable after a

simple cleaning process and can be designed to exhibit different geometrical arrangements.

Chapter 5 will then discuss how combining the two strategies together, extracellular cell matrix mimic substrates were fabricated for cell adhesion investigations with single-molecule resolution. Finally, chapter 6 will present a general conclusion and discussion future research and challenges in the field.

Chapter 2

Techniques, Materials and Methods

This chapter presents the techniques and methodologies that have been used in this project including Atomic Force Microscopy (AFM), Focused Ion Beam (FIB), and surface fabrication technologies. DNA origami assembly strategies and relevant chemical, molecular and cellular biological approaches are also discussed.

2.1 Techniques

Controlled immobilisation and functionalisation of DNA nanostructures with single-molecule resolution were investigated in this project. AFM is important in the validation of the formation of nanostructures and patterned surfaces with single molecular resolution. FIB combined with surface fabrication techniques allowed the development a patterned platform for the controlled immobilisation of different nanostructures. These are advanced and progressive techniques and played a key role in this project.

2.1.1 Atomic Force Microscopy (AFM)

Atomic Force Microscopy (AFM) is a label-free imaging technique for the investigation of sample surfaces with atomic scale resolution. Compared to other surface imaging methods such as Scanning Tunnelling Microscope (STM) or Scanning Electron Microscopy (SEM), AFM has strength in investigating non-conducting samples [49]. As a result, AFM is capable of imaging soft samples such as a biological membrane or a surface-attached biomolecule. It is also very powerful in revealing functional modifications and micromechanical properties of a sample [50].

The principle of AFM is using a sharp probe to scan along the sample surface to generate a topographic image based on the signal generated from the interaction between probe and sample surface molecules (Figure 2.1). The probe scans across the sample surface in a raster-fashion step-by-step. Via monitoring the magnitude of interaction between the probe and surface, these responses can be plotted according to the (X, Y) position of the probe to generate the topographic images of the sample surface [49].

Binnig et al. developed AFM in 1986 [49]. A typical AFM is constructed by a cantilever, a piezoelectric actuator, a four-sectional photodiode, a laser and generator and a laser path guided mirror set (Figure 2.2). In the simplest mode, contact mode of AFM, the sharp tip on the spring cantilever is the part that contacts the sample surface. The applied contact force makes the bending of cantilever which is monitored by the four-sectional photodiode via collecting signals of laser that shined on the back of cantilever and deflect on to the photodiode. The piezoelectric actuator controls the movement of sample from/to the tip to keep the cantilever bending (applied force) constant based on a feedback system. As a result, when the sample is scanned under

AFM, (X, Y) position information and the Z position details that calculated from the piezo movement are combined together to form the topography of sample surface (Figure 2.2).

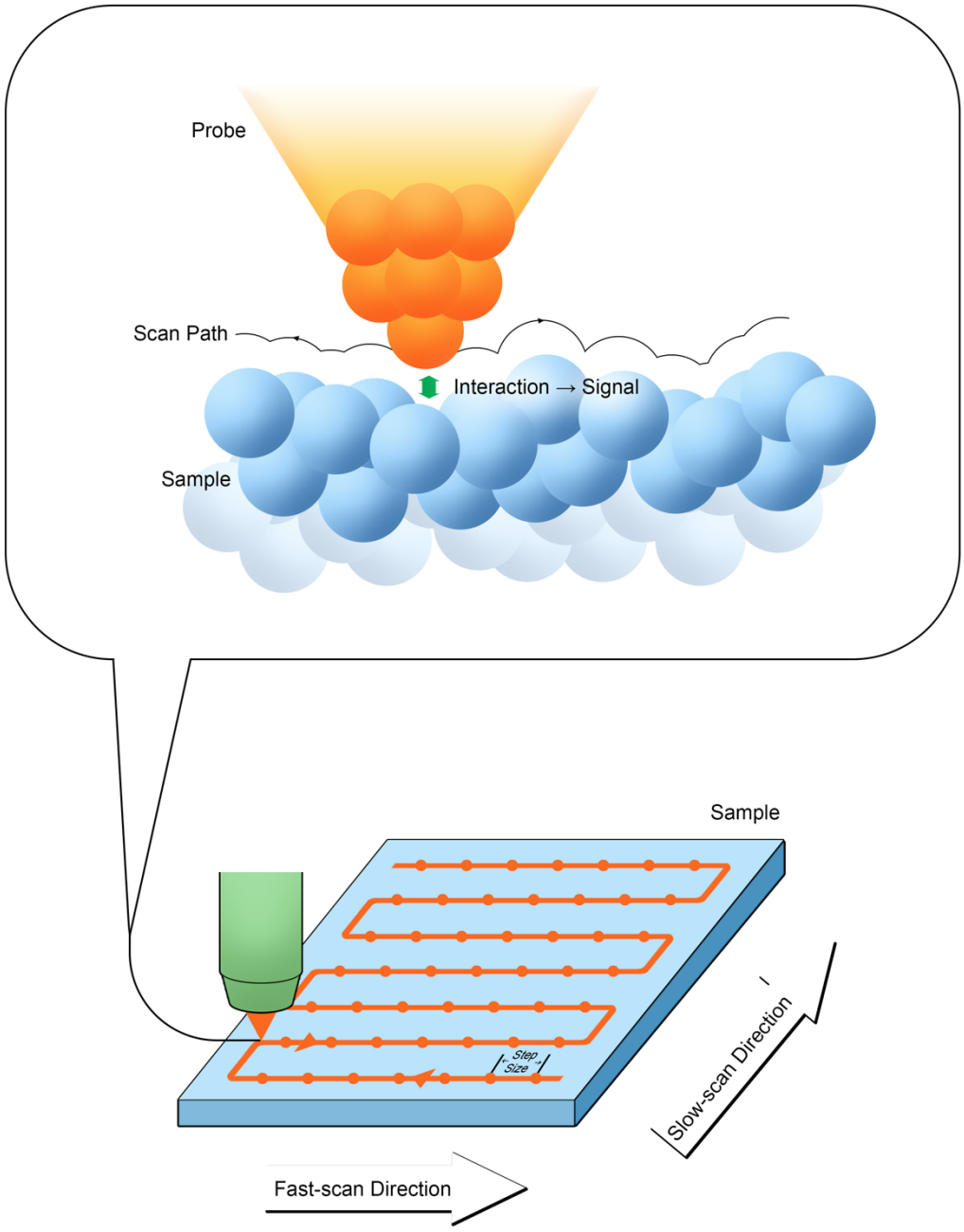

Figure 2.1 Schematic of the principle of AFM.

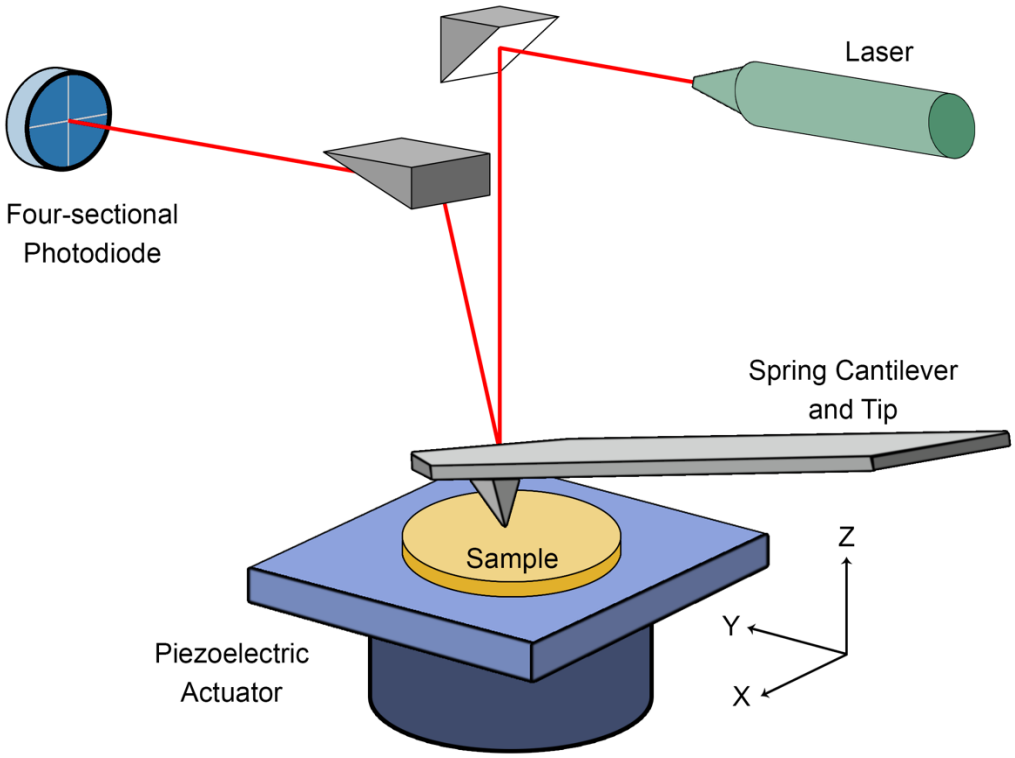

Figure 2.2 Schematic of a typical AFM system.

The sharp end of tip has a radius of approximate 10 nm and the cantilever is normally about 100 µm long with an elastic modulus range from few to tenths of Newton per metre. The scanning resolution can be down to atomic scale due to the sensitive detectability to small changes of the tip-sample interaction, and precision control of piezoelectric actuator in X, Y, and Z directions. It is possible to achieve a horizontal resolution of down to 1 nanometre and a vertical resolution of down to 0.1 nanometre in AFM. The scanning probe is moving at equally spaced intervals across a scan line (Figure 2.1), so the resolution of images from AFM is also based on the

numbers of data points that collected per line. The AFM images captured in this project are normally at a 512 data points per line resolution. It is also possible to apply AFM scanning in liquid environments [51].

The Van der Waals attractive forces and the inter atomic repulsive forces mainly contribute to the deflection of cantilever. These forces can be approximated by Lennard-Jones potential function [52]:

$$V = 4\varepsilon\left[\underbrace{\left(\frac{\sigma}{r}\right)^{12}}_{repulsion} - \underbrace{\left(\frac{\sigma}{r}\right)^{6}}_{attraction}\right]$$

where ε is the depth of the potential well. It indicates a measure of how strongly the two particles attract each other. σ is the equilibrium distance at which the intermolecular force between the two particles is zero. r is the separation between the particles. The $\left(\frac{\sigma}{r}\right)^6$ represents the van der Waals attractive interaction and $\left(\frac{\sigma}{r}\right)^{12}$ comes from the repulsive force between two atoms. The Lennard-Jones potential is a total potential of attractive and repulsive interactions [53]. Based on this, the interaction force vs. tip-sample distance can be plotted to show a curve (Figure 2.3).

The curve includes contact and non-contact regimes which indicate the different conditions when tip interacts with the surface. With the tip moving close to sample surface, there are also four types of tip-sample interactions including tip not bended and not in contact with the sample, tip bended by attractive forces but not in contact with the sample, tip bended and in contact with sample, and tip bended by repulsive forces. Based on these different conditions of tip-sample interaction, AFM can be carried out

via different modes. The contact mode is operated in the repulsive regime with the tip in "contact" with the surface. The tapping mode operates the vibrating cantilever-tip moving into and out of contact with sample that it 'taps' the surface [54]. Non-contact mode operates at larger distances between the tip and the surface and operates in the attractive regime of force interaction.

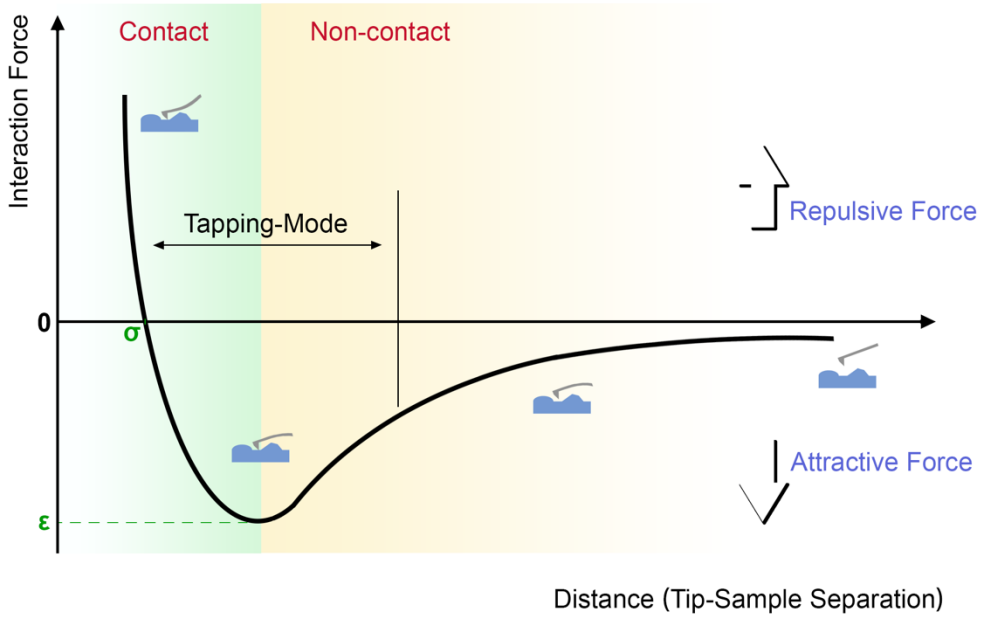

Figure 2.3 Interaction force vs. distance curve.

Normally, DNA origami structures are nanoscale in dimensions, and therefore cannot be observed via traditional imaging techniques. With the development of Scanning Probe Microscopy, especially Atomic Force Microscopy, DNA nanostructures can be investigated based on surface imaging. In our laboratory, a Bruker Dimension® Icon™ Atomic Force Microscopy was used to carry out the sample scanning (Figure 2.4) under ScanAsyst™ mode.

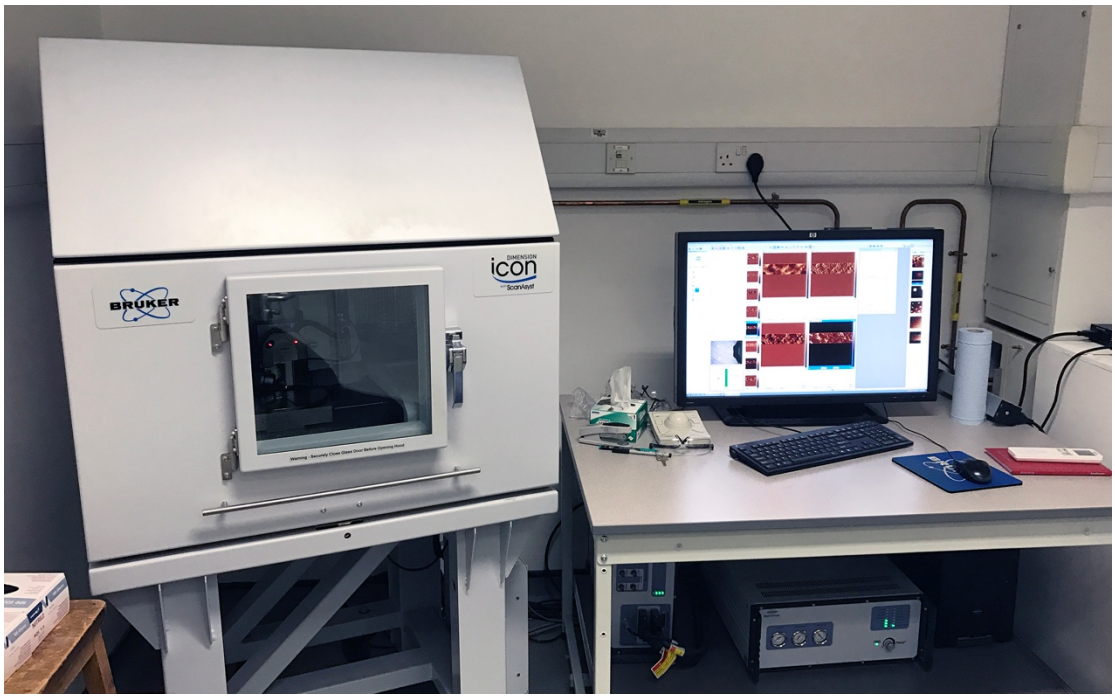

Figure 2.4 Bruker Dimension® Icon™ Atomic Force Microscopy.

ScanAsyst™ mode is developed by Bruker based on the PeakForce Tapping® technique in order to achieve high resolution AFM images [55]. In PeakForce Tapping, the scanning probe continually taps the sample surface with an oscillatory rate below the resonance of the probe. The pico Newton level interaction force between sample surface and probe is measured via detecting the deflection of the cantilever. The peak force of each tap is monitored and controlled through feedback loop to maintain a constant imaging force based on superior force control. In this sense, PeakForce Tapping® controls the instantaneous interaction force instead of monitoring the average interaction of the amplitude and phase which is used in Tapping Mode. The imaging peak force constant in PeakForce Tapping® is down to 10 pN, which is significantly lower than other mode, for instant that around 1 nN in Tapping Mode. This low interaction force is ideal for biological and delicate samples measurement. With the

superior force control techniques, the real-time force interaction pattern analysis algorithm can remove parasitic deflection and the signal-to-noise ratio is dramatically reduced. Through these sensitive controlled procedures, the tip shape and sample integrity are maintained and allowed to generate high-resolution images. Combined with the patent-pending intelligent algorithms improved in ScanAsyst™ mode, the image quality is spontaneously and constantly monitor and the appropriate parameter adjustments are made represent to the sample surface properties, these make it possible to achieve very small structures measurement such as revealing the structure of double helix DNA. As a result, ScanAsyst™ mode is an ideal AFM technique to use in this project.

2.1.2 Focused Ion Beam (FIB)

Focused Ion Beam (FIB) is an advanced technology ideal for surface nanofabrication. Samples are scanned by a focused beam of ions to machine structures or patterns on surfaces. FIB is similar to scanning electron microscope (SEM) in terms of the actual instrument, but uses an ion beam instead of an electron beam [56]. It can provide high resolution images as well as perform nanofabrication for several applications.

FIB was developed in 1980s and then industrialised as a commercial instrument during the following years [57]. The use of FIB as a nanofabrication technique was dramatically improved by the semiconductor industry for chip design and fabrication. FIB allows controlled milling of sample surfaces with high precision down to a few

nanometres. This enables nanodevice modification and meticulous surface patterning with programmable control [58, 59].

FIB employs a focused active ion beam to hit the solid sample surface (Figure 2.5). The energy of the ion is lost to the sample atoms and electrons upon hitting. The material from the substrate sample will sputter out of the sample surface as neutral and ionized atoms; this allows the milling of the substrate. The image of a sample surface can then be generated via collecting the emitted electrons. The ion hitting sample surfaces enables the dissociating molecules and breaking of chemical bonds by which the surface modification can be achieved on a sample surface [56].

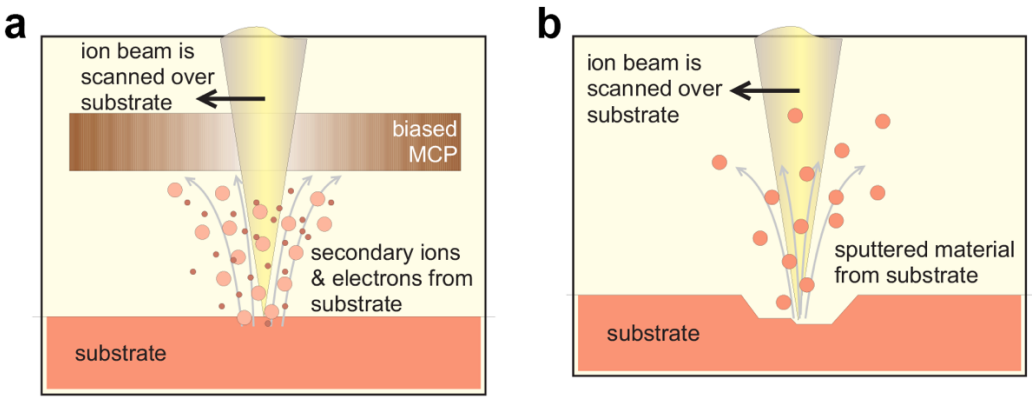

Figure 2.5 Schematic of the principle of FIB [60]. **a)** FIB for imaging sample. **b)** FIB for milling sample surface.

A focused ion beam can generate a high ion current in order to remove part of the substrate materials. The position of the applied focused ion beam can be controlled to fabricate patterns on surface [61, 62]. Compared to conventional e-beam lithography, ion beam offers a maskless solution which employs fewer steps and lower cost. The patterning processes can be carried out on various solid substrates such as gold, metal

oxide, graphene or silicon, for a wide range of applications [63, 64, 65, 66]. FIB enables patterning from micro to nanoscale, and the pattern details can be precisely controlled based on the nature and position of the focused ion beam. The size and shape of the beam intensity applied on the sample determines the basic imaging resolution and micromachining precision. Generally, the smaller the beam diameter, the better the achievable resolution and milling precision.

A typical FIB instrument includes several components: an ion column, a work chamber with vacuum system, and the stage controlling part with user interface (Figure 2.6).

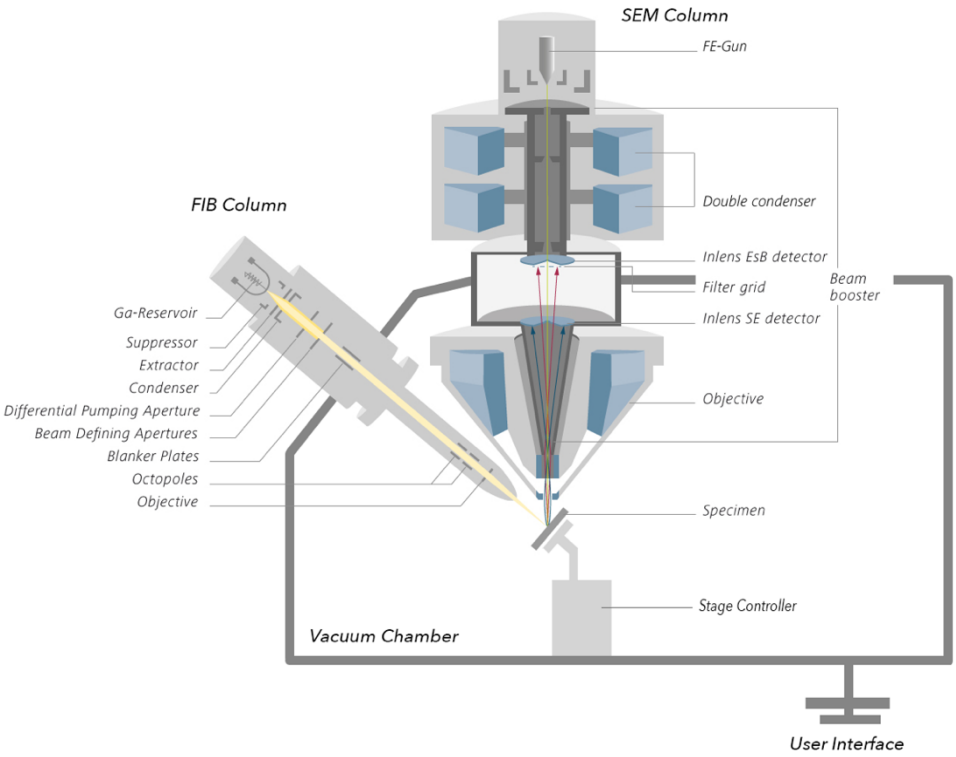

Figure 2.6 Schematic of FIB instrument (ZEISS Crossbeam FIB-SEM System).

The ion column is the most important part in a FIB instrument. FIB column and SEM column are normally integrated within one system to perform both functions.

Gallium ion (Ga^+) is generally stored in the Ga-reservoir; this liquid-metal ion source (LMIS) enables the generation of the Ga^+ ion beam via applying a strong electric field. Gallium is used because of its properties of low vapour pressure, low melting point, high stability and long life time [67]. A high voltage of around 7000 V is employed to extract ion as 'focused' beam. The beam can be further condensed via electrostatic lens and condenser to focused to a fine spot with a resolution of down to around 10 nm. Octupole allows the moving of the ion beam to a defined pattern. The multichannel plate (MCP) objective enables the imaging function by collecting signals of sputtered secondary particles. The blanker plate and apertures can help in controlling the ion beam and avoiding long term shadowing on the sample surface.

The ion beam milling and imaging is carried out in a stainless-steel working chamber. A vacuum environment down to 10^{-7} mbar is normally required and maintained in the working chamber. The vacuum environment reduces the diffusion of ion beam and increases the accuracy in positioning the point that the ion beam shadows on. The sample is usually placed on a motor-powered stage and the stage can move on up to 5 axes including X and Y across sample surface, rotation of the sample, in Z of the distance between column and sample for focusing and tilling function for facing e-beam column or ion-beam column. Altogether the controlling operations can be carried out via a user interface software.

A Quanta™ 3D FEG FIB system was used for nanopattern fabrication in this project. Figure 2.7 shows the appearance of this FIB system, including operating appliance, vacuum appliance, detectors, sample chamber, electron column, ion column, and etc. This is a SEM and FIB dual beam system (both electron beam and ion beam) which allows high-resolution material characterization for 3D nanofabrication of large

samples over a wide range of materials as well as high-quality imaging of the sample surface down to the nanoscale.

Figure 2.7 Quanta™ 3D FEG FIB System.

2.2 Materials

2.2.1 DNA Origami

DNA origami is synthesised via M13mp18 single strand backbone and staple single strands with presence of Tris-acetate-EDTA (TAE) buffer and magnesium salt. A

temperature controlled step cooling down system including Polymerase Chain Reaction (PCR) machine and water bath are applied.

1. Tris-Acetate-EDTA buffer (TAE) 50× (2 M Tris-Acetate; 0.05 M EDTA, pH 8.0), (VWR), store at room temperature (RT).
2. Deionized (DI) Millipore water (resistivity of 18 MΩcm).
3. Magnesium chloride ($MgCl_2$), anhydrous, ≥98%, (Sigma).
4. M13mp18 single-stranded DNA, 1.0 μg/μL, (Affymetrix), store at -20℃.
5. Oligonucleotides (IDT): 220 staple strands (include modified strands), see appendix i and ii, store at -20℃.
6. Amicon® Ultra-0.5 mL Centrifugal Filters, 100 kDa MWCO (Millipore).

2.2.2 DNA Origami Modification

The modifications of DNA origami were carried out via modifying staple strands. Part of modified staple strands were purchased from IDT.

1. Oligonucleotides for extended staple strands and sticky ends (IDT).
2. Oligonucleotides for biotinylated staple strands and sticky ends (IDT).
3. Oligonucleotides for fluorescently labelled staple strands and sticky ends (IDT).
4. Oligonucleotides for amino anchors staple strands (IDT).
5. Oligonucleotides for maleimide modification (Cambio).
6. A20FMDV2 peptide with Cysteine modification (PeptideSynthetics).
7. Biotinylated EGF recombinant human protein combine with streptavidin (Thermo Fisher).
8. Qdot® 525, 565, 605, 655, 705, 800 Streptavidin Conjugate (Thermo Fisher), store at 4 ^{o}C, no allow freeze.

9. BamHI-HF® Restriction Enzyme (NEB).
10. HindIII-HF® Restriction Enzyme (NEB).
11. 1× CutSmart® Buffer (NEB).

2.2.3 FIB Nanopattern Fabrication

In our Laboratory, we have employed the Thermal Evaporator for metal deposition, and FEI™ Quanta™ 3D FEG Scanning Electron Microscope (SEM) and Focused Ion Beam (FIB) system for FIB nanopattern fabrication.

1. Glass coverslips, Ø 13 mm, No. 0 (Thermo Fisher).
2. Silicon slide (InterQuest), cut into 10 mm×10 mm square slides.
3. Sulfuric acid (H_2SO_4), concentrated.
4. Hydrogen peroxide (H2O2), 30% concentration. Store at 4℃.
5. Ethanol, 200 proof.
6. Deionized (DI) Millipore water (resistivity of 18 MΩcm).
7. Teflon mini-rack (Invitrogen).
8. Gold (Au), 1.0 mm wire, 99.999% high purity (Goodfellow).
9. Chromium (Cr), grit, 99.95% coating quality (Sigma).
10. Diamond tipped pencil (Agilent).
11. PELCO Tabs™, Carbon Conductive Tabs, 12 mm OD (Ted Pella).
12. 3M™ Copper Conductive Tapes, Single Adhesive Surface (Ted Pella).
13. Standard SEM Pin Stub Mount, Ø 12.7 mm×8 mm pin height (Ted Pella).
14. Tweezers, tick, stainless steel (Rubis).

2.2.4 DNA Origami Immobilisation

A Harrick PDG-32G-2 plasma cleaner was used in our laboratory.

1. Muscovite mica sheets (Agar Scientific), freshly cleaved immediately before use.
2. Trizma® base, 2-Amino-2-(hydroxymethyl)-1,3-propanediol, ≥99.9% (Sigma).
3. MOPS, 4-Morpholinepropanesulfonic acid, ≥99.5% (titration), (Sigma).
4. Carboxyethylsilanetriol di-sodium salt, 25% in water, (Fluorochem), store at 4℃.
5. EDC, 1-Ethyl-3-(3-dimethylaminopropyl) carbodiimide hydrochloride, purum, ≥98.0% (AT), (Sigma), store at -20℃, avoid moisture.
6. Sulfo-NHS, N-Hydroxysulfosuccinimide sodium salt, ≥98.0% (HPLC), (Sigma).
7. Gibco™ Dulbecco's phosphate buffer saline (PBS) 1× (no magnesium, no calcium, 2.7 mM potassium chloride, 0.14 M sodium chloride, 1.5 mM potassium phosphate, and 8 mM sodium phosphate, pH 7.4), (Invitrogen), store at room temperature (RT).
8. Sodium Chloride (NaCl), BioXtra, ≥99.5% (AT), (Sigma).
9. Parafilm.
10. 6-Well plates (Falcon).

2.2.5 Atomic Force Microscopy

In our laboratory, Atomic Force Microscopy (AFM, Bruker Dimension Icon) was performed under the ScanAsyst™ mode.

1. Compressed air.
2. ScanAsyst-Air tips (silicon tip on Nitride lever, f_0: 70 kHz, k: 0.4 N/m), (Bruker).

2.2.6 Fluorescence Microscopy

Confocal laser scanning microscopy (CLSM) was performed on an inverted microscopy, Leica TCS SP5 equipped with a HCX PL APO lambda blue 63 1.4 oil objective lens.

1. Microscope Slides, 1.2 – 1.5 mm (Thermo).
2. Fingernail polish.

2.2.7 Cell Adhesions

Human cutaneous melanoma cell lines A375P (Giard *et al*, 1973) was used in this project. The A375P Puro and A375P β6 cell lines were created in John Marshall's group in Bart's Cancer Research Institute. Retroviral infection was carried out in the A375P line with human integrin β6 cDNA and resistance gene for β6 cell line, and the puromycin-resistance gene only for Puro cell line.

1. Dulbecco´s modified eagle medium (DMEM), (Lonza).
2. Foetal bovine serum (FBS), (Sigma).
3. Bovine serum albumin (BSA), (Sigma).
4. Trypsin-Versene® (Lonza).
5. Tissue culture plastics (Falcon).
6. Dimethyl sulphoxide (DMSO), (Sigma).

2.3 Methods

2.3.1 Synthesis of DNA Origami

DNA origami is assembled by combining M13mp18 (5 nM) and staple strands (50 nM) in 50 μL TAE buffer with 12.5 mM Mg^{2+} (See both DNA sequences details for rectangular and triangular DNA origami in appendix i and ii, they are synthesised in the same way with different sets of sequences). M13mp18 is a bacteria phage vector strand with 7249 bases long. An appropriate quantity of ions, such as magnesium here or sodium in the DNA hybridisation approach, are demanded to equilibrate the electrostatic repulsion between highly negatively charged DNAs molecules. An amount of 12.5 mM Mg^{2+} was chosen based on balancing the increase of the yield and reduction of the aggregation. In presence of more than 50 mM Mg^{2+}, DNA will form big clusters instead of proper DNA origami structures. The mixture solution is heated to 94 ^{o}C to completely dehybridise all of dsDNA. Temperature step controlled cooled down approach is carried out in a PCR machine. From 94 ^{o}C to 65 ^{o}C, cooling rate is about at 0.3 ^{o}C per minute. A cooling rate of 0.1 ^{o}C per minute is employed from 65 ^{o}C to room temperature. This is based on the average of annealing temperatures of staple strands around 60 ^{o}C. A slower cooling rate when mixture solution is close to annealing temperature will increase the self-assembly efficiency and reduce the defects of mispairings.

The self-assembled DNA origami is purified with Millipore Amicon Ultra 100 kDa spin columns in a centrifuge at 13000 rpm for 2 minutes, 3 times, to get rid of access staple strands. Residues in the spin column is adjusted to a concentration around 20 nM by regulating the volume to about 50 μL. This is based on the calculation of

estimating nearly a hundred percent yield from the concentration of M13mp18. The self-assembly of DNA origami is a high-efficient process with an extremely high yield. A NanoDrop Spectrophotometer is used to detect the rough concentration of DNA origami products based on the constant of a molecular weight of 330 g/mol per base and an extinction coefficient = 33 mg/ml for A260 = 1. The actual result is normally close to the estimated numbers.

DNA origami can be stored in Eppendorf tubes. Long term storage is recommended in -20 ^{o}C freezer. For short term routine, 4 ^{o}C fridge is normally used instead of storing in room temperature. Heating up to 70 ^{o}C or higher will deconstruct the origami structure. The DNA origami nanostructure is stable for several months based on standard storage conditions. The whole procedure requires a DNase-free environment. Restriction enzymes will not affect the main structure unless the origami is modified with enzyme cutting regions.

2.3.2 AFM Characterisation of DNA Origami

AFM was used to image the DNA origami structures. DNA origami is cast on either silicon dioxide, glass or mica surfaces for imaging. The DNA origami solution is diluted by TAE buffer with 30 mM Mg^{2+} to around 1nM in order to get a good separation of the DNA nanostructures once immobilised on surface. Magnesium is required in the procedure as an ion charged bridge, immobilising DNA origami to the substrate surfaces. Mica is a common used as a substrate based on its easy cleavage property. Mica samples were cleaved twice by solid scotch tape immediately prior casting. 5 μL of diluted DNA origami solution was directly deposited on freshly cleaned

mica and left to adsorb on the surface for 2 min. Subsequently, the substrate was washed by distilled water to remove non-absorbed origami and then blown dry by compressed air. ScanAsyst-Air tips with 0.4 N/m spring constant were used to scan the sample by AFM under ScanAsyst™ Mode. A resolution of 512 pixels per line with 1 Hz scan rate was chosen for appropriate imaging of the DNA nanostructure. The AFM topographic images of DNA origami nanostructures on surface will be shown in the following chapters and the cross-section function was carried out to characterise the height of the nanostructures.

2.3.3 Modifications of DNA Origami

2.3.3.1. QD(s) Modification

For the modification on DNA origami with single or multiple QDs of the same type (CdSe/ZnS, core-shell), the QD(s) were directly assembled to the biotinylated sticky end(s) on the DNA nanostructures. Staple strand R75 in the rectangular DNA origami and A19 in the triangular DNA origami were chosen for single QD modification. Staple strands A56, B56 and C56 in the triangular DNA origami were chosen for the modification with 3 QDs. These staple strands are extended by 16 bases in 3' end with biotin (see Appendix iii), purchased from IDT. A mixture of M13mp18 and the staple strands were prepared by standard DNA origami synthesis as described in section 2.3.1m employing a PCR machine. After removing the excess staple strands and modifiers, the DNA origami with different numbers of biotinylated sticky ends were ready for QDs conjugation.

Streptavidin-conjugated QDs were mixed with biotinylated DNA origami solutions in a 5:1 ratio (the ratio is based on the numbers of QDs versus numbers of sticky ends on origami) in TAE buffer with 12.5 mM Mg^{2+}. The mixture was incubated at 37 ^{o}C for 5 minutes and then cooled down slowly over 2 hours to room temperature. Excess QDs were removed by dialysis with 50 nm pore cellulose membranes. Millipore Amicon Ultra 100 kDa spin column can be also used for purification. However, the spin column requires high speed centrifugation which might affect the delicate structure of streptavidin coating layer of QDs, it is recommended to use a slow but mild membrane dialysis for purifying ssDNA-QDs conjugation. QD(s) conjugated DNA origami solution were then cast on surface and could be characterised by AFM.

Multiple different types of QDs modified DNA origami were assembled in a different way. In detail, the chosen staple strands (A37, B37 and C37 for 3 different QDs modification on triangular DNA origami, and R1, R101, R110, R139, R211 and R220 for 6 different QDs modification on rectangular DNA origami: see Appendix iii) were extended by 16 bases with different sequences. Complementary ssDNA was designed to be complementary to the extended sequences with biotin modification at the ends. The specific type of QDs were mixed with definite complementary ssDNA in a ratio of 5:1 and then cooled down to room temperature over 2 hours after incubating at 37 ^{o}C for 5 minutes. Excess ssDNA was removed by dialysis with 25 nm pore cellulose membranes. Different types of ssDNA conjugated QDs were then formed. Extended staple strands replaced the ordinary strands and mixed with M13mp18. DNA origami with different sticky ends were constructed using standard procedures (section 2.3.1). A mixture of ssDNA conjugated QDs with sticky ended DNA origami in a 5:1 ratio was heated up to 47 ^{o}C and then cooled down slowly to room temperature to carry

out the DNA hybridisation. AFM could then be employed to characterise the constructed nanostructures, once the solutions were cast on solid substrates.

2.3.3.2. Fluorophore Modification

The fluorophores were modified on DNA origami using similar procedures employed the modification with multiple QD of the same type described above. In detail, the chosen staple strands (R57 and R184 for rectangular DNA origami, Appendix iv) were extended and modified with fluorophores at the end by design and purchased from IDT. DNA origami with fluorophore modified sticky ends were synthesised as described in the last section. Fluorophore that linked to sticky ends was assembled on DNA origami with these extended and modified staple strands (fluorophore modified sticky ends) involving the DNA origami construction.

The fluorophores modified DNA origami for restriction enzyme cleavage were synthesised in a similar procedure to the constructing of DNA origami modified with multiple QDs of different types. Fluorophore modified ssDNA strands were ordered from IDT. These strands contain a restriction enzyme cutting region in design. Extended staple strands that are complementary to these ssDNA was also designed and ordered (IDT). DNA origami with complementary sticky ends were synthesised at first as described before. Then origami solution was mixed with fluorophore modified ssDNA for DNA hybridisation via cooling down from 47 ^{o}C to room temperature. The fluorophores modified DNA origami were characterised under AFM and fluorescence microscopy. The procedure of fluorescence microscopy characterisation will be represented in section 2.3.4.6.

The extended staple strands were designed with restriction enzyme cutting regions (BamHI  and HindII). For dynamic enzymic control in solution, 5 μL DNA origami, 14 μL CutSmart buffer and 1μL enzyme were mixed and incubated at 37 ^{o}C for 1 hour. The digested products were purified by spin centrifuge filters to get rid of cleaved fluorescent strands.

For enzymic digestion on surface, the fluorophores modified origami was covalently immobilised on surface at first (see section 2.3.4.4). The substrate with a droplet of 19 μL of CutSmart buffer and 1 μL enzyme on top was incubated in a thermal incubator at 37 ^{o}C for 1 hour. The cleaved fluorescent strands were removed by DI water washing for several times.

2.3.3.3. Amino Anchors Modification

Amino anchors were assembled onto DNA origami for surface covalent immobilisation. The modification of amino group is achieved by simply assembling target functional groups at the end of sticky end. The chosen staple strands (A05, A13, A33, A42, A50, B05, B13, B33, B42, B50, C05, C13, C33, C42 and C50, all positioned in the inner edges of triangular DNA origami) were designed with an amino group at the 3'end and ordered from IDT. Ordinary staple strands are replaced by these modified strands in the mixture with M13mp18 and synthesised into DNA origami structures using standard procedures (section 2.3.1). These amino anchors provided the binding sites to the carboxylic silane treated substrate surface.

2.3.3.4. Peptides Modification

Peptide A20FMDV2 was assemble on DNA origami using the same method of assembling multiple different QDs on DNA nanostructures. The numbers of peptides on a single origami depends on how many complementary sticky ends that origami has. Up to six positions were chosen in this study (namely at A32, B32 C32, A37, B37, and C37 of a triangular DNA origami).

Peptide-ssDNA conjugation was constructed via maleimide-thiol conjugation (see section 3.1.3.3 in chapter 3). Commercially available protected maleimide modified ssDNA need to be deprotected before conjugation. 50 nmoles of the protected maleimide modified ssDNA was freeze dried at first. Deprotection and conjugation will inefficient in the presence of water. Freeze dried samples were washed adding 2 mL of anhydrous acetonitrile, and the solvent was evaporated by a rotary evaporator. 2 mL of anhydrous toluene was added to the vial, mixed and then evaporated. The rinsing procedure was repeated for 3 times. In the third time, toluene was kept in vial and incubated at 90 ^{o}C for 4 hours to deprotect the maleimide-modifier. After incubation, toluene was evaporated. The vial containing the deprotected maleimide modified ssDNA was immediately mixed with the reduced peptide. The thiol group on the cysteine of the peptide needed to be reduced from the oxide form right before conjugation. The conjugation reaction occurs after the mixing. This can happen in TAE buffer or PBS buffer with a pH range between 6.5 and 7.5. The mixture was put on a shaker for 1 hour to complete the conjugation.

Peptide-ssDNA conjugation was validated and purified by reversed phase HPLC. Purified products were freeze dried, resuspended in TAE buffer, and stored in a

-20 ^{o}C freezer. Peptide-ssDNA conjugation was mixed with staple strands and M13mp18, and standard DNA origami synthesis was carried out.

A20FMDV2 is a linear peptide with 21 amino acid. Heating up to 94 ^{o}C will not affect the structure and function of this peptide. After origami synthesis procedure, peptide-ssDNA conjugates were assembled on the DNA origami via hybridising to the complementary sticky ends via heating up to 47 ^{0}C (based on the basic T_m of ssDNA sequence as 41 ^{o}C) and cooling down to the room temperature. The numbers of peptides on the DNA origami is determined by the numbers of sticky ends designed on the origami.

Epidermal growth factor (EGF) was modified on DNA origami via streptavidin-biotin conjugation. The EGF was biotinylated and assembled with streptavidin which is commercial available. By the similar approaches of QDs modification, EGF was attached on origami structure via recognise the biotinylated sticky ends that already modified on DNA origami nanostructures.

2.3.4 FIB Nanofabrication

2.3.4.1. Preparation and Substrate Cleaning

It's important to carry out proper cleaning procedures before carrying out the surface passivation. Any contamination, even nanoscopic, not removed prior to patterning will result in defects in the surface passivation. First, piranha solution (1/3 volume of H_2O_2 plus 2/3 of H_2SO_4) was prepared to remove all ironic and organic impurities on the substrate. Substrates were place (glass cover slip or silicon wafers) on

Teflon mini-rack, immersed in piranha solution and let soaking for 5 min. Then the slides were taken out of the piranha solution and immersed in the DI water for 2 min. Sonication is required for the slides in ethanol and DI water for 15 min for each. Cleaned substrates were blown dry with a stream of inert gas (Ar or N2), then applied in a plasma cleaner under high power for 5 min. Now the substrates are clean enough and possible to proceed to metal deposition.

2.3.4.2. Metal Deposition

A thermal evaporator was applied to deposit gold and chromium layer on the substrate surface. Using high purity of metal source is crucial for the metal coating layer quality and avoid any potential contaminations. A hot plate was heat up to 180 ^{o}C and the pre-cleaned substrates were incubated on it for 5 min to force off any adsorbed water molecules. Then the slides were put on the Thermal Evaporator holder with cleaned sides face down. The thickness of metal evaporation was monitored by the thickness detector crystal and achieved 1.5 nm adhesion layer of Cr and 3 nm thick of Au on top of the Cr. The Cr layer is necessary for the adhesion of the Au to the glass/silicon surfaces and avoiding peeling off from substrate during the following procedures. At the end, metal coated substrates were annealed on a hot plate at 300 ^{o}C for 1 hour which will form a flat clean surface for the further procedures.

2.3.4.3. Ion-Beam Pattern Writing

We used FIB to fabricate nano-apertures arrays on the metal coated substrates. The arrays pattern was 7 μm by 7 μm consisting of 200 nm by 200 nm apertures spaced

every 1 μm (64 squares in total). This ensured that each individual aperture is optically resolvable and discrete once functionalized and imaged with a fluorescence microscopy. Previous to applying FIB, a diamond pencil was used to make visible mark on sample slides, which would help in tracking the location of pattering area in the future. The metal coated substrate slide was stuck on the specimen stub mount via using carbon conductive tab. A copper conductive tape was attached to bridge over slide surfaces and mount. The prepared sample was then put into FIB working chamber with vacuum pressure level. The sample surface was focused properly under electron beam channel and the sample stage was tilled by 52° to face the ion beam column. Further focusing was required under ion beam channel to overcome the spacing drift. Diamond pen pre-marked label was found to be in the scan area and the ion-beam milling was carried out around this area. Preloaded patterns (arrays that drawn manually and saved in system compatible format) were imported into the system and the ion-beam milling was carried out according to the pattern. Ion beam milled the surface under 30 kV/50 pA conditions. Various milling depth parameter were set for covering all the different thickness of metal layer and then need to be checked under AFM. After the milling program finished, the patterned surface was validated under electron beam channel. Patterned slides were removed from working chamber after vacuum vent. The fragile slides were carefully apart from specimen stub mount using pre-heated blade. Carbon tab and copper tape were cleaned off using acetone.

2.3.4.4. Functionalization of Nanopatterned Surfaces

Standard amide coupling was carried out to covalently immobilise DNA origami on the patterned area. Briefly, the DNA origami solution was cast on the

patterned substrate in the presence of Mg^{2+} (to induce initial physisorption). Carboxyethylsilane was then cast on the surface to form carboxylic terminating monolayers on the exposed patterned nanoapertures and amide coupled to the amino anchors on DNA origami under the activating agents (NHS and EDC). Other uncovalently immobilised DNA origami would be washed away and covalently bonding ones would remain on the surface according to the patterned apertures.

Here are the details of controlled immobilisation of DNA origami step by step. Firstly, we placed the patterned substrates on a microscope slide with the pattern facing up. An O_2/plasma cleaning at high power for 5 minutes was applied to clean and activate the exposed silica surface. Plasma treatment would not affect the structure of metal layers. The cleaned substrates were placed in a 6-well plate for carry out solution included procedures. QD(s) modified DNA origami solution were diluted by 20-folds in Tris buffer (5 mM; pH 8.2) with 30 mM Mg^{2+} and 60 μL of the diluted solution were cast on the patterned substrate. A small piece of Kimwipe was roll up and wet with DI water, then placed in the well beside the substrate. This procedure enabled a moisture environment in the plate wells when incubation taken place. Parafilm was used to seal the wells. The 6-well plate carried substrates was placed on a shaker for 90 minutes at room temperature for physisorption of origami. After incubation, substrates were washed using Tris buffer by pipetting 60 μL of the buffer up and down several times. The washing approach were repeated of 8 times. A solution of carboxyethylsilane (0.6 mM) in the Tris buffer was prepared and used to wash in 8 times by the same method as previous. The plate was resealed by Parafilm and put on the shaker for 2 minutes. Carboxyethylsilane were immobilised on to the exposed silica surfaces during shaking incubation. Silane treated substrates then were washed by MOPS buffer (10 mM; pH

8.1) with 30 mM Mg^{2+} for 8 times (same pipetting method as previous). An activating solution with EDC (1-ethyl-3-(3-dimethylaminopropyl)-carbodiimide; 50 mM) and sulfo-NHS (N-hydroxysulfosuccinimide; 100 mM) in the MOPS buffer were prepared and added (60 μL) on to the substrate which doubles the volume on the surface while halving the concentration of EDC and sulfo-NHS. The solution on substrate surfaces were mixed well by pipetting several times up and down. The 6-well plate were sealed again with Parafilm and placed on the shaker for another 10 minutes. The amide bonds were forming during the incubation. After incubation, the 60 μL of the liquid was removed from the surface with a pipette. The surfaces with remaining solution were washed by 8 times with the MOPS buffer followed by another 8 washes with 100 μL DPBS (Dulbecco's phosphate buffered saline) with 125 mM Na^{+}. Additional wash with DI water was employed to finally remove the non-specific immobilisation and clean the surface for imaging. The surface functionalization approach was completed after wash and ready for characterization after suitable sample preparation approaches (drying approaches for AFM and wet procedures for confocal microscopy, see in following sections).

2.3.4.5. Atomic Force Microscopy

AFM was applied on investigating the surface geometry of nanofabricated apertures and controlled placement of DNA origami. AFM can achieve down to nano scale to reveal DAN origami structure with functional modification and its immobilisation in the patterned area. The origami immobilised substrates after approaches from last section were blown dry with a stream of inert gas (Ar or N_2). ScanAsyst-Air mode with ScanAsyst-Air tip was used to scan the sample surface. The

patterned area can be chased following the diamond pen scratched mark. Scanning was carried out around the marked area and then zoomed in to reveal the detail structures in nanoapertures.

2.3.4.6. Fluorescence Microscopy

Fluorescence microscopy was applied for further confirmation of controlled immobilisation of DNA origami. We verify the functionalised patterned coverslip based on the presence of QD-labelled DNA origami controllably immobilised in the nanoapertures. An inverted confocal microscope Leica TCS SP5 that capable of epifluorescence microscopy was used to image the sample. An Oil immersion lenses with 63× magnification is suitable for imaging the nanopatterns (as they are spaced at least 1 μm apart, hence optically resolvable).

The functionalised patterned slides were placed face down on top of a glass microscopy slides. The liquid environment between the glass slides and the coverslips was kept in an enclosed environment by sealing the edges of the coverslips using fingernail polish. The optics were aligned and the patterns could be found in white light (natural light) channel. A Leica TCS SP5 confocal microscopy system with a 63 × oil lens was used here.

Properly focusing on the target area were required. Under the fluorescence channel (based on the various emission of different fluorophores) the clear fluorescence dots array and enzyme digested result were investigated.

2.3.5 Cell Culture Techniques

2.3.5.1. Growth and Passage of Cell Lines

Cells were grown at 37°C and 8% (v/v) carbon dioxide/air condition in a humidified incubator. Cells were maintained as adherent monolayers on tissue culture plastic. Growth medium contained of DMEM accompanied with 10% FBS. Cells were sub-cultured approximately every three days. After incubation with 0.25% (w/v) trypsin/EDTA solution, adhered cells were removed from culture plastic and neutralised by adding three folds of growth medium. Cells were then suspension to fresh tissue culture flasks with fresh growth medium.

2.3.5.2. Storage of Cell Lines

Cells were removed from tissue culture plastic by trypsin when in logarithmic-phase and then neutralised by addition of growth medium. The cell solution was pipetted well to generate a single-cell suspension. 5 minutes of centrifugation at 3000 RPM was carried out to pellet the cell. The pellet then was resuspended in growth medium added with 10% dimethyl sulphoxide (DMSO), and transferred to 2ml cryovials (Falcon). The cell was stored overnight in insulated polystyrene boxes at -80°C at first, and then transferred to liquid nitrogen for long-term storage. Vials were subsequently defrosted at 37°C and the cells were washed once in warm growth media before further approaches.

2.3.5.3. Cell Adhesion on Patterned Substrates

Cells were removed from tissue culture plastic by trypsin, and neutralised, pelleted and resuspended as described before. The cells concentrations were counted using cytometer for both Puro and ß6 cell lines. Same numbers of cells for both cell lines were applied on different pattern modified substrate in 24 wells plate. The substrates were blocked with 1% BSA before cells plating. 2 mL of growth medium were added to each well and then incubated for 1.5 hours. The substrates were carefully washed by PBS for 2 times to remove non-adhered cells. The patterned area with cells were imaged using differential interference contrast microscopy (DIC) to observe the cell adhesion behaviours.

Chapter 3

DNA Origami and Functional Modifications

This chapter presents the synthesis of DNA origami nanostructures and their different chemical modification/functionalisation. In order to carry out single-molecule investigations, DNA nanostructures play a key role throughout the work due to the properties of controllable shape and geometrically precise functional modification. Utilising the coding structure of DNA, multi-functional modification was achieved for various investigations, as discussed in the following sections.

3.1 Introduction

3.1.1 Design of DNA origami

DNA origami is a DNA nanostructure synthesised from a long backbone and hundreds of staple DNA single stands. The staple strands in DNA origami can be

designed to construct different shaped structures. Meanwhile, the modifications designed on the staple strands are the key of DNA origami functionalisation.

The idea of designing a DNA origami structure contains several steps. First, a shape plan of DNA origami structure is decided for a specific investigation/application. The scaffold strand then is routed to a raster style and reveal the designed shape. The choice of the scaffold sequence needs to be made after the confirmation of routing plan of the scaffold.

Single-stranded M13mp18 is the most commonly used scaffold strand. M13mp18 is a M13 lac phage vector from E. coli ER2738 within the gene encoding β-Galactosidase [68]. Phenol is applied to extract the single-stranded M13mp18 from the double-stranded vector. It contains 7249 bases and has a derivation of 8064 bases long. The scaffold sequence defines the sequences of staple strands because these staple strands will be designed so to be complementary to the scaffold strand. Once the scaffold sequence and routing plan are decided, the staple strands will be designed to cross over the helix of the scaffold route to 'staple' the scaffold folding structure. The cross over design is based on the Holliday junction structure of DNA and makes the structure stable (Figure 3.1) [69].

The Holliday junction structure is important in the design of DNA origami structures. These cross-over structures connect antiparallel double helixes together. Large number of Holliday junctions construct the whole DNA origami structure to make it strong and stable [28, 31]. The bowing of scaffold strands can be formed as designed via the electrostatic repulsion effect generated by these double helical cross-overs and the proximity of base paring throughout the neighbouring helices.

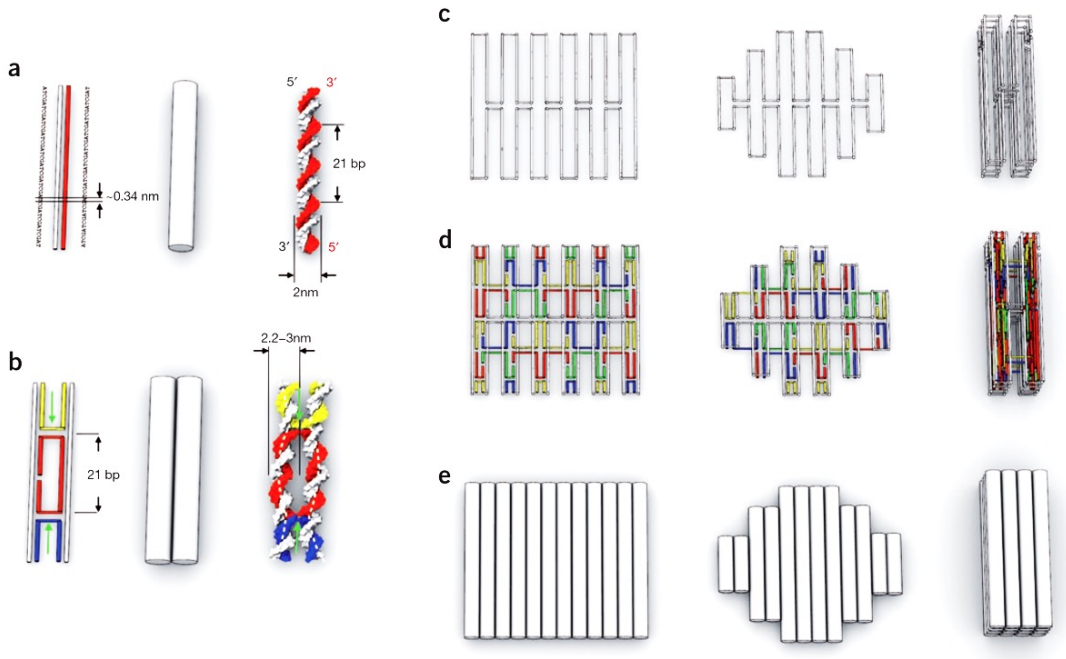

Figure 3.1 The DNA origami design concept [69]. **a)** Individual double-helix structure of DNA. **b)** Interhelix cross-over structure of DNA. **c)** Folding route design of scaffold strand. **d)** Staple strands are designed complementary to the scaffold strand. **e)** Cylinder representation of DNA origami.

There are large amount of information and data contained in the shape design of DNA origami. With the development of computational techniques and CAD software, caDNAno was presented by S. M. Douglas in 2009 [29] to help design DNA sequences to fold into desired nanostructures. The software can process the request of designed motifs to generate the sequences of staple strands. In this way, the work of designing DNA origami is dramatically reduced and the accuracy is improved significantly as well. 2-D and 3-D structures can be designed using this software, while the location of cross-over structures and connections of neighbouring of antiparallel helices can be defined to control the layout of DNA origami structure (Figure 3.2).

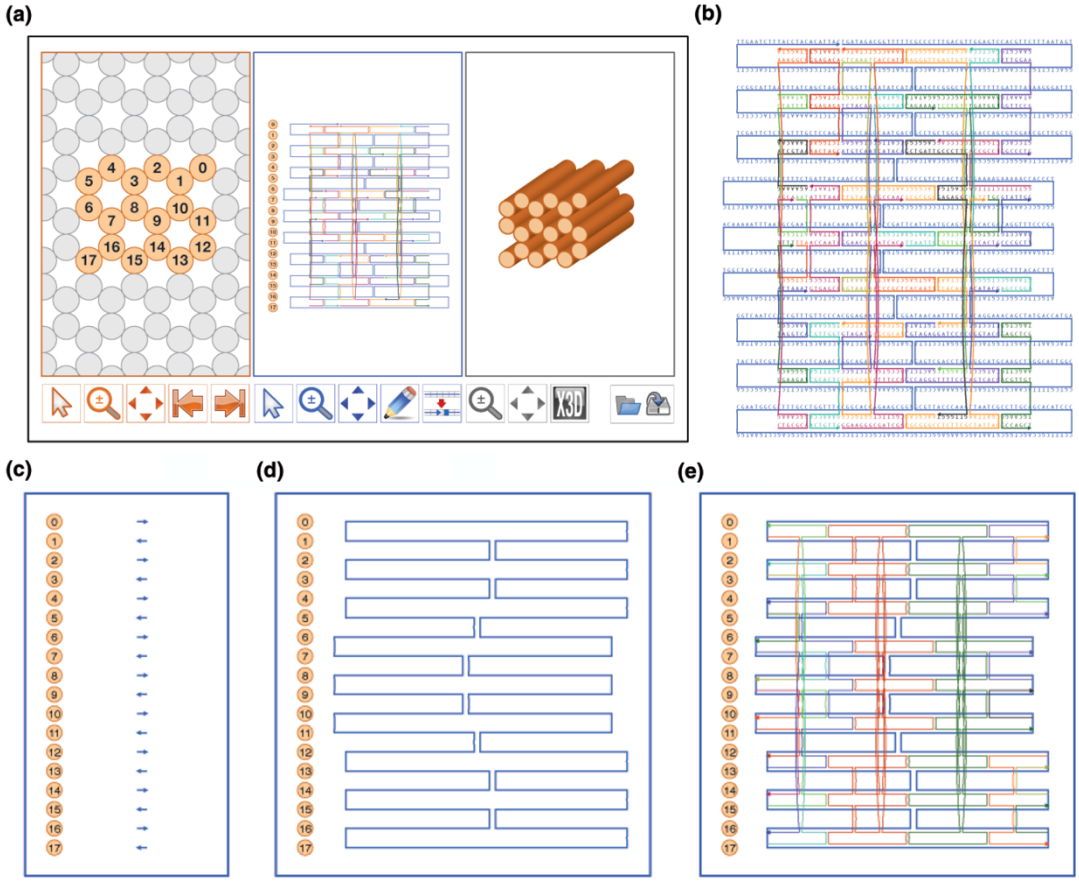

Figure 3.2 caDNAno interface and designing approach [29]. **a)** caDNAno interface. **b)** Schematic of the design of DNA origami. **c) d) e)** Design path using caDNAno interface including path panel design, scaffolding folding path, and auto-staple stands generation.

For specific investigation using DNA origami, staple strands can be designed to assemble with functional groups, form specific structures, or employing sticky ends out of origami surface, and even create dynamic structures for alterable functional approaches. In theory, every staple strand has potential modifiable regions for designing functionalised structures. For example, fluorescence molecules can be synthesised on either end of arbitrary or chosen staple strands via conjugation reaction in order to label the DNA origami structure for molecular sensing [70]. Extension of staple strands allows

forming sticky ends on DNA origami to interact with other oligo probes [71]. Using the placement strategy, dynamic structures can utilise the flexibility and encoding property of DNA to create nanomachines or nanotools [72, 73]. Under controlled condition, the partial complimentary DNA strands can be replaced by the fully complimentary one due to the thermodynamic equilibrium. Via regulating the reaction environment, DNA nanostructure can be design to perform 'on' or 'off' conformations for applied as a dynamic machine. As a result, designing the extension sequences or modifications of staple strands are key in forming functional DNA origami structures.

The design of DNA origami combines the knowledge of synthetic chemistry, molecular biology, understanding of dynamic mechanism and conjugation technologies. DNA origami have various of advantages and potential applications which I will discuss in the following section.

3.1.2 Advantages and Applications of DNA Origami

DNA origami have some distinctive advantages over conventional DNA nanostructures which make it a strong platform in various of fields.

A key advantage of DNA origami is stability. DNA origami is founded on the base paring rules which provide a stable structure. It is less sensitive to temperature, salt concentration or pH changes than many other nanostructures in biological investigations. They can be involved in many chemical and biological reactions with a broad range of conditions. Their robustness is quite convenient for expanding to apply on harsher conditions.

Reversibility is a very important advantage of DNA origami, especially in the functionalisation process. It is easy to construct or deconstruct DNA origami: you can form or reform origami to control the process, or assemble or detach reacted regions by simple approaches without destroying the primary DNA origami structure. This property can also be exploited to use DNA origami as a template for specific recognition in a mixture of analytics [74, 75], which would also reduce the analytic concentration, increasing the sensitivity of detection.

The flexibility in size and shape makes DNA origami suitable for many processes. Based on the simple construction rule, DNA origami can be formed into different sizes and shapes, 2D or 3D. This flexibility makes DNA origami of a widely usage from the tissue to cell scale, and even down to the single molecule approach. As a result, DNA origami can behave as a nanodevice or a nanorobot [76, 77] in the mechanical or pharmaceutical investigations.

Multiple modifications ability allow DNA origami explored its potential in various fields. It is possible to assemble different types of molecules on DNA origami. The positions of modification can be precisely controlled. This property makes it possible to construct more complicated structures with compound functionalisation, and to mimic a complex organisation within one molecular platform for achieving systematic studies at single molecule resolution. Another important strength of DNA origami is that each individual position on the 2D structure contains different sequence information. This allows us to place specific functional molecules or nanoparticles at precise positions on the DNA origami. This approach combined with sequence-selective ligands [78] provides enormous potential for applications in materials science and biotechnology.

Researchers have already sought out many applications of DNA origami such as single-molecule investigations, selective incorporation and controlled placement of DNA origami. Based on Atomic Force Microscopy (AFM) studies, DNA origami is used as a scaffold on single-molecule investigations. One of the most remarkable works using 2D DNA origami was reported by Voigt who demonstrated that single-molecule chemical reactions can be performed on a DNA origami scaffold [79]. The ability to study events at the single-molecule level using DNA origami extends beyond chemical reactions. Rinker showed that distance-dependent multivalent binding effects could be systematically investigated by incorporating multiple affinity ligands into DNA origami [80]. Most recently, a work by Ngo using a protein based adaptor by utilizing the sequence-specific DNA binding zinc finger protein to locate a monomeric protein of interest at specific positions on DNA origami [81] strongly shows that single enzyme reaction detection is possible employing DNA nanostructure. In addition, Castronovo *et. al* demonstrated that a DpnII restriction enzyme cleaved all dsDNA in a nanopatterned array within 20 minutes of adding the enzyme [82].

Another application of single-molecule detection of DNA origami relies on the visualization of DNA structural changes. One of the first work was reported by Rinker that represented the use of DNA origami to construct rectangular nucleic acid probe tiles for label-free RNA hybridization, molecular analogise of macroscopic DNA chips [80]. To the most upcoming field of microRNA, Zhu reported that they developed a novel approach based on streptavidin and quantum dots binding complex (STV-QDs) labelled single strand displacement reaction on DNA origami to quantitatively detect the concentration of miRNAs [72], which plays important roles in post-transcriptional gene repression as well as many other biological processes such as cell growth and

differentiation. In this study, the detection limit of RNA molecules was so small, which means that the target RNA could be directly detected from a single cell without using polymerase chain reaction (PCR) amplification.

DNA origami was also applied on molecular machine fabrications. Using artificial DNA platform to control molecule movements is an emerging application of DNA nanotechnology. DNA molecular machines are operated by adding and removing specific DNA strands for complex movements and the thermodynamic stabilization energy works as "fuel" during hybridization to provide the mechanical motion of DNA machines. Using this strategy, DNA tweezers that perform close–open motions were constructed [77]. Also, two remarkable DNA origami machines ware reported: a DNA walker with two legs that can control its direction of motion and a DNA motor that can move forward autonomously by the cleavage of a DNA-nicking enzyme [83]. Another strategy for the fabrication of a molecular machine utilises the transportation ability of DNA origami. A method of combining DNA origami structures with glass nanocapillaries to reversibly form hybrid DNA origami nanopores in order to control DNA translocation was reported by Hernández-Ainsa [84]. Differently, Sørensen recently reported the use of terminal deoxynucleotidyl transferase (TdT) for direct enzymatic ligation of DNA origami to nucleotide triphosphates coupled to proteins and other large macro-molecules [85]. These strategies reveal the transport ability of DNA origami, and indicate that we can use DNA origami to transport different molecules in a desired biological process.

DNA origami have already been extended to cellular studies and shown its huge potential in intracellular signal triggering and pathway monitoring [76]. It was also indicated as resistant to various types of enzymes, especially of endonucleases or

exonucleases [69]. In this case, DNA origami was widely used as a structural or functional component in nanoscale self-assembled structures, antisense therapeutics, microarray diagnostics, and biosensors [85]. An interesting work on using DNA origami for optimal delivery of the anthracycline doxorubicin (Dox) to human breast cancer cells [86] was reported recently, highlighting an upcoming research direction of great potential: DNA origami will be a strong utility for cellar or extracellular study, especially of the human diseases concerned research.

3.1.3 Quantum Dots

Nanoscale materials exhibit different properties and behaviours compared to bulk materials [87]. Quantum dots (QD) are a good example of this[88]. A QD is a type of semiconductor nanoparticle that has discrete electronic states [89]. The size and shape of QDs can be precisely regulated by the duration, temperature, and ligand molecules used in the synthesis. Different types of QD will emit light with specific frequency which is tunable by material, size and shape [90]. The fluorescent properties come from the absorption of a photon with energy above the semiconductor band gap energy results in the creation of an electron-hole pair (or exciton). The different material, size and shape of QDs result in different band gap. The absorption has an increased probability at bigger gap which leads to the shorter wavelengths. The radiative recombination of an exciton leads to the emission of a photon in a narrow, symmetric energy band. As a result, the fluorescence of QDs have long lifetime which is suitable for many detection targets. Normally, QD is synthesised from CdSe as the core and ZnS as the shell. It can be conjugated with many functional units such as carboxylic group

or streptavidin proteins [91]. Both optical and probe scanned microscopy can be applied on detecting QD. Single QD can be observed and tracked over an extended period of up to a few hours using confocal microscopy. The sizes of QDs from few nano-meters enable them to be detected under AFM. These properties of QD make it an ideal material to evolve in single-molecule resolution investigations.

3.1.4 Conjugation Techniques

DNA origami is a strong platform for several applications once modified by various of functional molecules. The procedures of modification are mainly based on conjugation techniques which attach a target molecule to another structural molecule. With the proper choice of reagents, reactions, and conditions, controllable and specific binding can be achieved; this in turn allows for the creation of new functional supramolecular structures [92].

Covalent conjugation and noncovalent conjugation are two main types of conjugation strategies. Covalent conjugation is usually achieved using specific crosslinking agents to bridge two molecules together. These conjugations sometimes require activating agents and solvent environments. Meanwhile, noncovalent conjugation is based on the affinity interaction between ligands and its substrate molecule, via supramolecular interactions. These ligands are mainly proteins such as antibodies and demand mild reaction conditions. The proper selection of the most suitable strategy is the key to accomplish an effective conjugation for the desired nanostructures.

3.1.4.1. Modification of Oligonucleotides and Peptides

Modifying crosslinking agents or ligand binding domains on structural molecules is the fundamental step in forming conjugations. Based on the development of synthetic chemistry and molecular biology, a comprehensive range of reactions are available to couple target functionalities on to another molecule.

Modification of oligonucleotides is a key part in synthesis of probe and label. As discussed earlier in Chapter 1, nucleotide, the unit of a DNA structure, contains a five-carbon sugar group (deoxyribose), a phosphate group and a nitrogenous base. There are several available modification sites on oligonucleotides such as the sugar group, bases, or the phosphate group on the back bone. For the pyrimidine bases and purine bases, there are several unsaturation points to be modified on the nitrogenous ring and imidazole ring [93]. Modifications on the phosphate group are more common and widely used. Using condensation agents such as EDC it is possible to easily couple amine groups and phosphate groups to form a phosphoramidate linkage. Biotin can be modified on oligonucleotides using this strategy with the help of PEG linkers. The modification of biotin on oligos is fundamental in carrying out the streptavidin-biotin conjugation for several biological investigations. Maleic acid imides (maleimide) can also be coupled to a phosphate group with an incorporation reaction using a 5'-maleimide modifier phosphoramidite (Figure 3.3) [94]. This procedure makes it possible to link oligonucleotides with peptides via maleimide-thiol linkage immediately after deprotection of 5'-maleimide modifiers (this will be discussed more in detail in section 3.1.3.3). The deprotection procedure is easy to carry out by incubating in anhydrous toluene under 90 ^{o}C for about three hours.

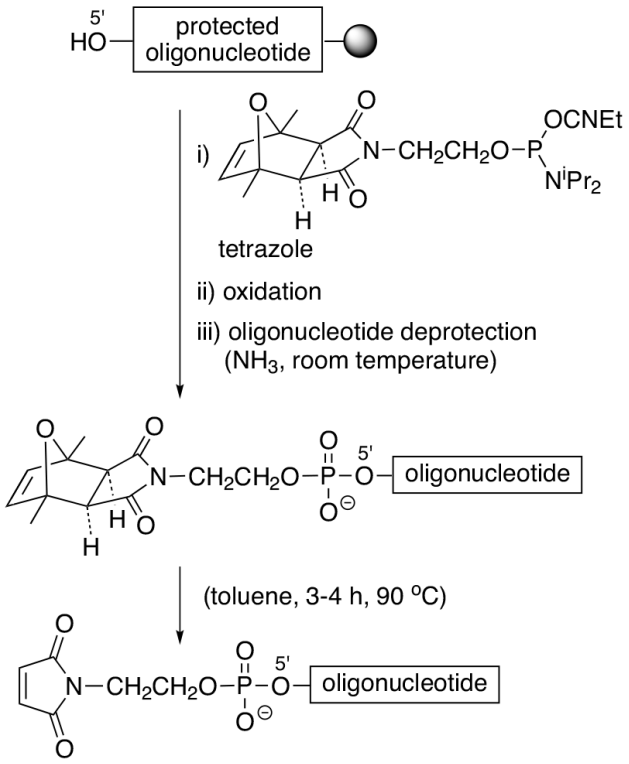

Figure 3.3 Schematic of 5'-maleimide modifier incorporation and maleimide modifier deprotection [94].

Peptides are another important family of target molecules that have been modified in this project. There are a number of different synthetic strategies for forming peptide conjugates, with each strategy integrating controlled techniques to produce well-defined bio-inspired molecules. Synthetic control of the sequence of peptide and adding functional group at the side-chain or terminal are two major process of functionalising peptides. Artificial peptide sequence construction can be carried out via expression (via designing specific genetic sequences as well as the mutation control, for generally more complex proteins), N-carboxyanhydride polymerisation, solid-phase amino acid coupling or solution-phase coupling (both for sequence specific chains). This strategy is suitable to form the required peptide with specific side-chain. For

instance, cysteines provide thiol groups on the peptide side-chain, and can be incorporated without changing the functional sequence of the peptide. While synthesis of cysteine on the target peptide, it makes the sequence available in conjugating to the thiol sensitive substrates. Another strategy is chemical synthesis of functional group on the side-chain or terminals of the peptides via linkers or click chemistry reactions. The sulfhydryl group, carboxylate group, or primary amine group are main sites for modification [92]. Coupling the terminal carboxylate group on a peptide with an amine group on another molecule via condensation reactions such as EDC/NHS coupling is wildly used based on the mild condition and easy approach.

3.1.4.2. Streptavidin-Biotin Conjugation

Streptavidin-biotin conjugation is a popular noncovalent method utilising the natural robust binding of streptavidin and biotin. Streptavidin is a bacterial origin protein which has the binding ability to small molecule biotin [95]. Streptavidin has four subunits to form a tetramer structure. Each subunit can provide a biotin binding site. As a result, streptavidin has a maximum of four biotin binding sites (Figure 3.4).

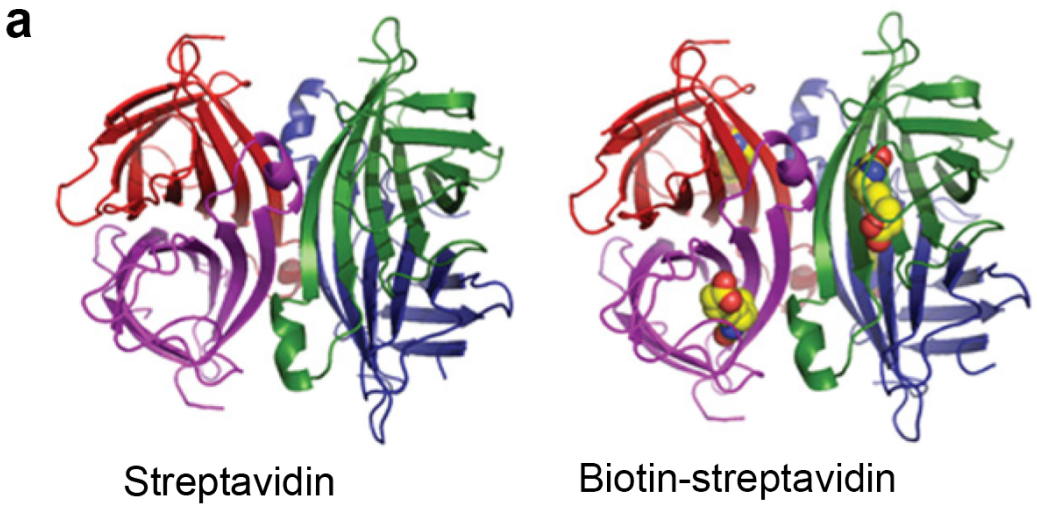

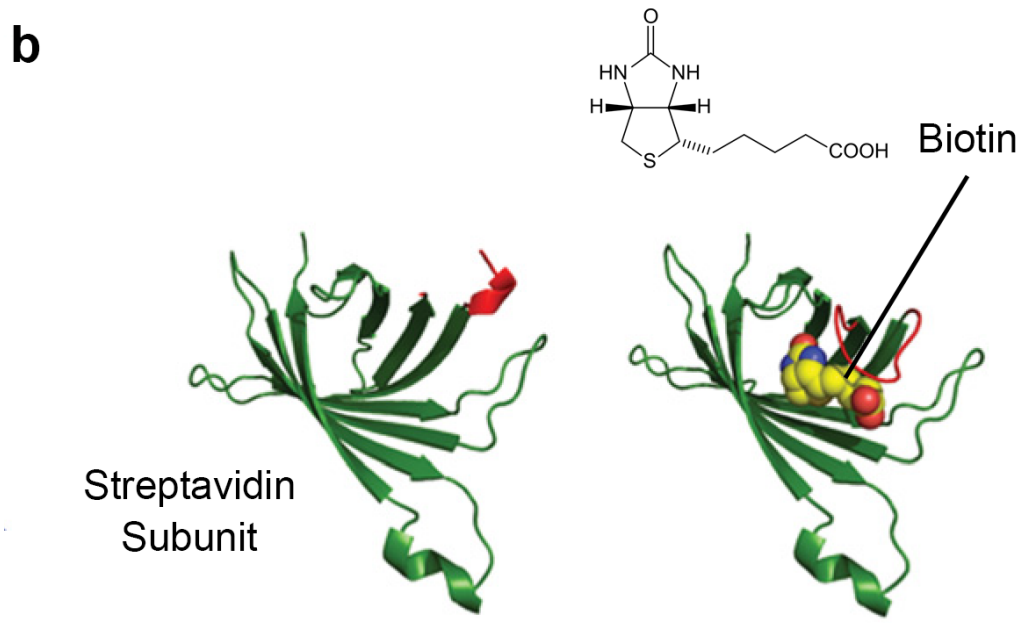

Figure 3.4 Structure of streptavidin [96]. **a)** Structures of streptavidin tetramer and biotin bound streptavidin. Each subunit of the tetramer is presented as different coloured ribbons (red, purple, green and blue). Streptavidin can have up to four biotin binding on it, because of one biotin binding site per subunit of the tetramer. **b)** Streptavidin subunit structure. The Molecular formula of biotin is shown. Biotin is presented as space-filling molecule bound in the binding pocket of streptavidin subunit.

Streptavidin has an isoelectric point of 5 to 6 which moderates the charge over the structure. Comparing to the isoelectric point of around 10 for avidin (another biotin-binding protein), the property of streptavidin dramatically reduces the ionic interaction for nonspecific binding. The structure of streptavidin is strong. This allows streptavidin to involve in various of chemical or biological modification processes with a broad range of conditions [92]. In addition, streptavidin cannot bind to carbohydrate receptors because it is not a glycoprotein. Compared to avidin, which binds to carbohydrate

content, streptavidin avoids these nonspecific interactions to achieve higher sensitivity in binding.

Streptavidin binds to biotins with extremely high affinity of $K_d \sim 4 \times 10^{-14}$ [97, 98]. Hydrogen bonds and van der Waals interactions mainly contribute to the formation of the strong streptavidin-biotin complex, as demonstrated via X-ray crystallographic investigations [98]. Other interactions including oriented dipole arrays, hydrogen-bond dipole networks to alter charge distribution, and disorder–order transitions [99] can also be found in streptavidin-biotin conjugation.

Streptavidin can be modified with several different molecules utilising terminal amines on the polypeptides chain of this protein. Amide bond can be formed to link streptavidin with other carboxylate-containing molecules such as Quantum Dots (QDs) using EDC/NHS reaction [100]. Biotin can be modified with many molecules via biotinylation techniques. One of the important biotinylation approaches employed is based on the assembly of biotin on the phosphate group of oligonucleotides to form biotinylated oligo probes. In this project, streptavidin coated QDs and protein were used to conjugate with biotinylated DNA nanostructures (see results part of this chapter, section 3.2.2 and 3.2.4).

3.1.4.3. Maleimide-Thiol Conjugation

Maleimide is an important unsaturated imide that is widely used in synthetic chemistry. It is formed from the maleic anhydride and ammonia as a derivative of the reaction. Notably, a stable thioether bond can be formed between the double bond of maleimide and thiol group via alkylation reaction. The reaction has selectivity for the

thiol group in the pH range of 6.5 - 7.5 (Figure 3.5) [101]. The mild reaction conditions make it popular in coupling peptides to oligos.

Figure 3.5 Schematic of maleimide-thiol reaction

Additionally, there is a hydrolysis side reaction of the maleimide group in the presence of water. A maleamic acid will be formed as an open ring structure that is then unable to react with a thiol group (Figure 3.6) [92]. As a result, protected maleimide is normally used in functionalising target molecules, and it is linked with a thiol group immediately after deprotection (Figure 3.3).

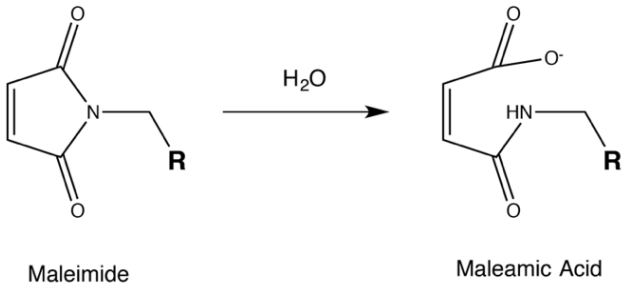

Figure 3.6 Hydrolysis of maleimide

The thiol group in this conjugation approach can be from the functional side chain of protein. A cysteine can bring in a thiol group for carrying out maleimide-thiol

conjugation on protein. A maleimide modified DNA strands were conjugated with a cysteine contained peptide to form a functional DNA-peptide probe in this project.

3.1.4.4. EDC/NHS Conjugation

Amine-containing molecules are popular in modification and crosslinking. It can be applied in protein or peptide molecules as well as oligos [92]. It is a common natural reaction that an amino group binding with carbonyl group in many chemical and biological processes [102].

The EDC/NHS coupling is a typical conjugation method to link carboxylic acid group to amine [92] (Figure 3.7). EDC (1-Ethyl-3-(3-dimethylaminopropyl)-carbodiimide) is a zero-length crosslinker used for activating carboxyl groups. NHS and Sulfo-NHS are applied to prepare amine-reactive esters. The molecule with carboxylic acid group is active to form a o-Acylisourea intermediate. Then The unstable intermediate can be attacked by amine group to form amide bonded conjugation. A NHS or Sulfo-NHS (water soluble analog) is commonly used to increase the efficiency of this reaction. Once the o-Acylisourea intermediate was formed, Sulfo-NHS can attack to form amine-reactive sulfo-HNS ester which can be easily replaced with amine group to form the conjugation. The conjugation approach can be carried out in solution or on surface. In this project, EDC/NHS coupling was employed to immobilise DNA nanostructure with amino anchors to the carboxylic silane treated surfaces.

The use of EDC/Sulfo-NHS is not only because of the ability to increase the reaction efficiency but also based on the advantages of water solubility of the reaction reagents. This allows directly carrying out the coupling without any organic solvent,

which is superior in bioconjugations. In addition, the access reagents can be easily washed away by water and other buffer solution when reacting on surface.

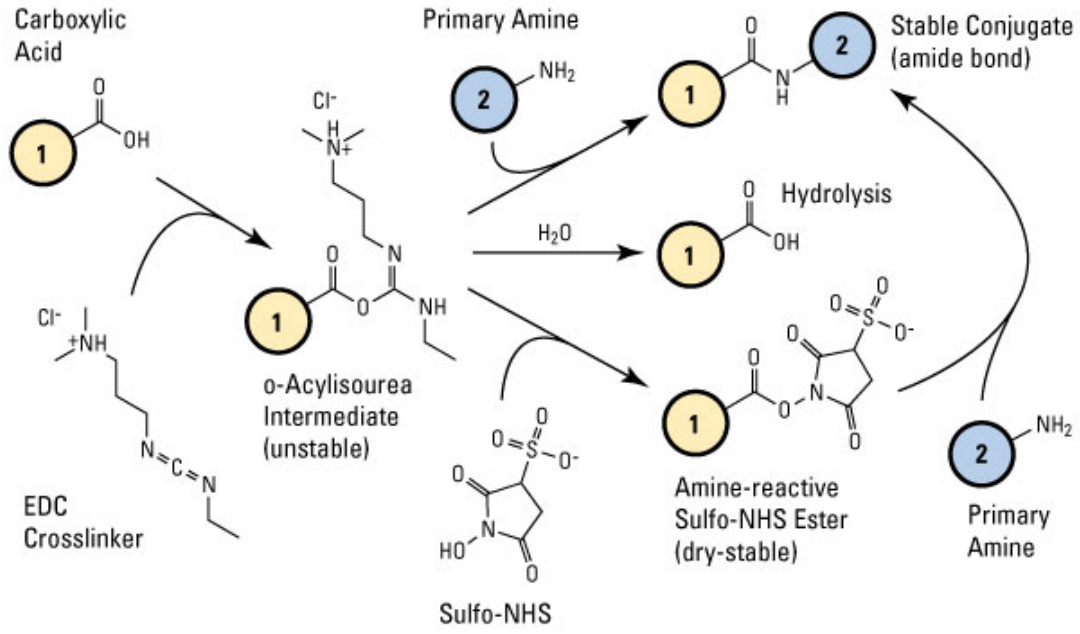

Figure 3.7 Schematic of EDC/Sulfo-NHS coupling reaction [92].

3.2 Results and Discussion

3.2.1 DNA Origami

DNA origami is an ideal platform to achieve single-molecule control. Based on several requirements for detecting methods and functional analysis, DNA origami of various shapes and sizes were synthesised in this project. The long single stranded DNA backbone (M13mp18) is the same for the different DNA origami employed. But the shape and size of the DNA origami changed via selecting different sequences of staple

strands. Synthesised DNA origami were cast on mica and imaged under AFM (Figure 3.8) in order to verify their assembly.

Rectangular DNA origami and triangular DNA origami were synthesised via M13mp18 and different sequences sets of staple strands (Figure 3.8 a and b, also see Appendix i and ii). AFM images demonstrate that rectangular DNA origami is a flat rectangular shape nanostructure with 120 nm in length and 60 nm in width, while the triangular DNA origami has three 120 nm edges and a triangular shape hole in the middle. The triangular DNA origami can be also recognized by its triangular frame (Figure 3.8 c and d). From the cross-section of each type of DNA origami, these flat nanostructures have a depth of around 1.5 nm ~ 2 nm (Figure 3.8 e and f), in line with the height of dsDNA.

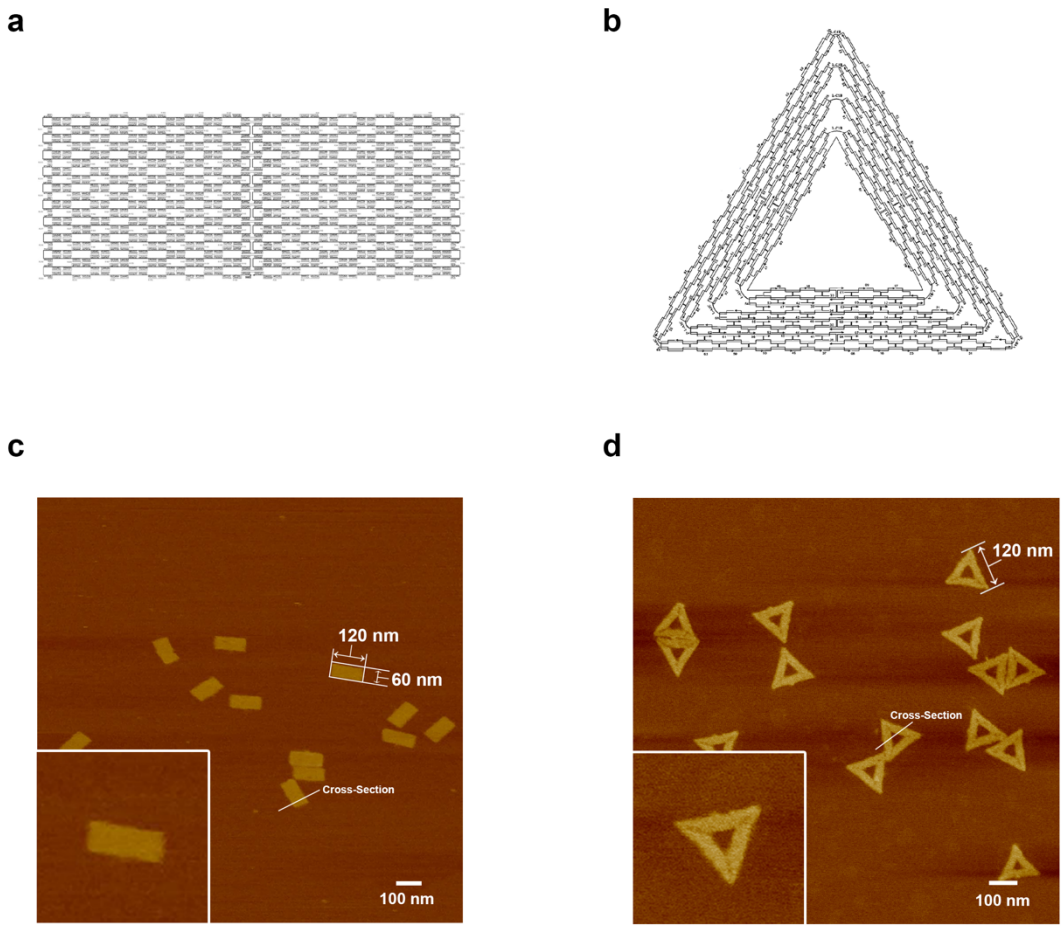

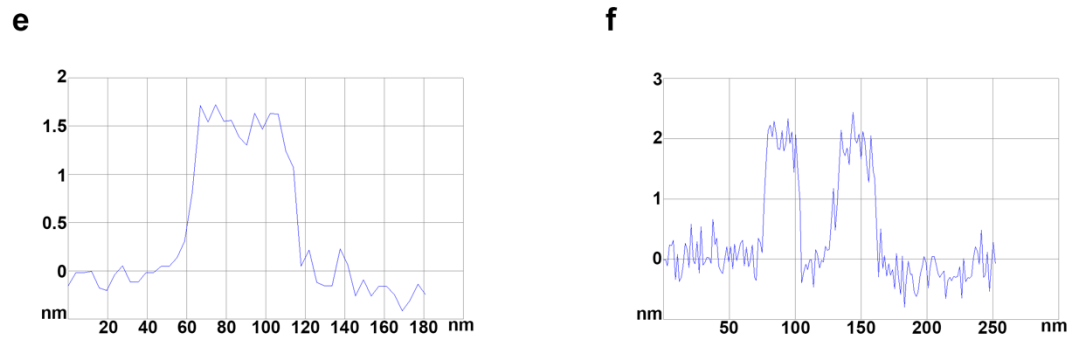

Figure 3.8 DNA origami and analysis. **a)** Schematic of rectangular DNA origami. **b)** Schematic of triangular DNA origami. **c)** AFM image of rectangular DNA origami, showing the size of DNA origami with 120 nm in length and 60 nm in width. **d)** AFM image of triangular DNA origami, showing the size of DNA origami with 120 nm edges. **e)** Cross-section of rectangular DNA origami shown in the inset of c), which demonstrates the depth of DNA origami is around 1.5 nm. **f)** Cross-section of triangular DNA origami shown in the inset of d), which demonstrates the depth of DNA origami is around 2 nm.

The microscopy results meet the theoretical calculation of DNA origami shape and size. As designed the rectangular DNA origami is 350 base pairs in length and 160 base pairs in width. Considering each nucleotide base pair is 0.34nm in length, the rectangular DNA origami is 119.0 nm in length and 54.4 nm in width, in theory. There is no major difference between calculation and analysis from the recorded AFM images. The triangular DNA origami has 368 base pairs for each edge which would be 125.1 nm in length, and this is not far from the 120 nm results from AFM images as well. In addition, the double helix structure of DNA has a diameter of approximately 2 nm, and

DNA origami is a one flat layer structure with depth similar to the double helix diameter: the AFM analysis data show this to be between 1.5 nm and ca. 2 nm.

Magnesium is required in the self-assembly synthesis of DNA origami. Typically, the moderate concentrations of Mg^{2+} ions help in screening the electrostatic repulsion between neighbouring double helices. Different concentrations of Mg^{2+} ions in presence of DNA origami synthesis were carry out as preliminary experiments (Figure 3.9). When no magnesium presences in the synthesis, extremely low yield of DNA origami indicated that the Mg^{2+} ions are important in constructing nanostructures. Comparing to the normal condition of Mg^{2+} (12.5 mM), DNA origami represented cluster structure under high magnesium concentration (30 mM).

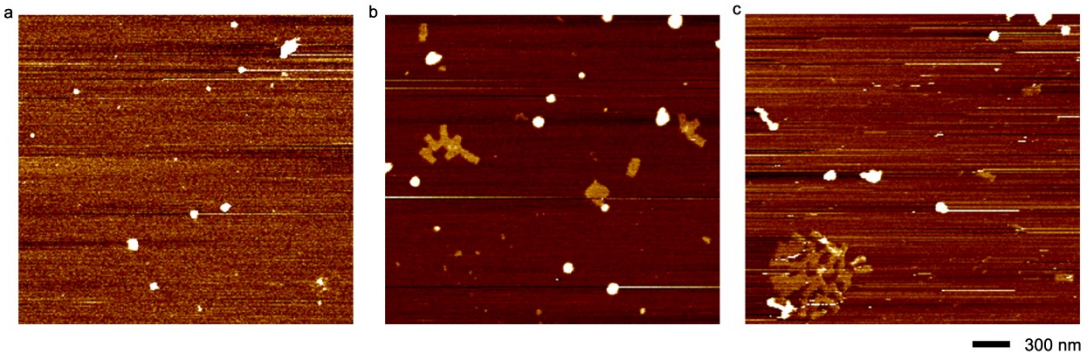

Figure 3.9 Different concentrations of Mg^{2+} in DNA origami synthesis. DNA origami were synthesised with **a)** no magnesium, **b)** 12.5 mM Mg^{2+}, and **c)** 30 mM Mg^{2+}.

The magnesium concentrations for casting DNA origami on mica surface for AFM imaging were also examined to ultimate a suitable casting procedure (Figure 3.10). DNA origami were found well deposited with a clean surface when applied 25 mM of magnesium. While increasing the concentration of Mg^{2+} to 50 mM, clear images can still be obtained, but several salt dots can be found on surface as well. However, when the magnesium concentration increased up to 75 mM and 100 mM, 'dirty' images were

shown with huge salt clusters. The results indicate that 25 mM to 50 mM is the suitable range of Mg^{2+} concentration for casting DNA origami on mica surface. Clear and well separated origami structures can be found, as well as reducing the unwanted salt crystal structures on surfaces.

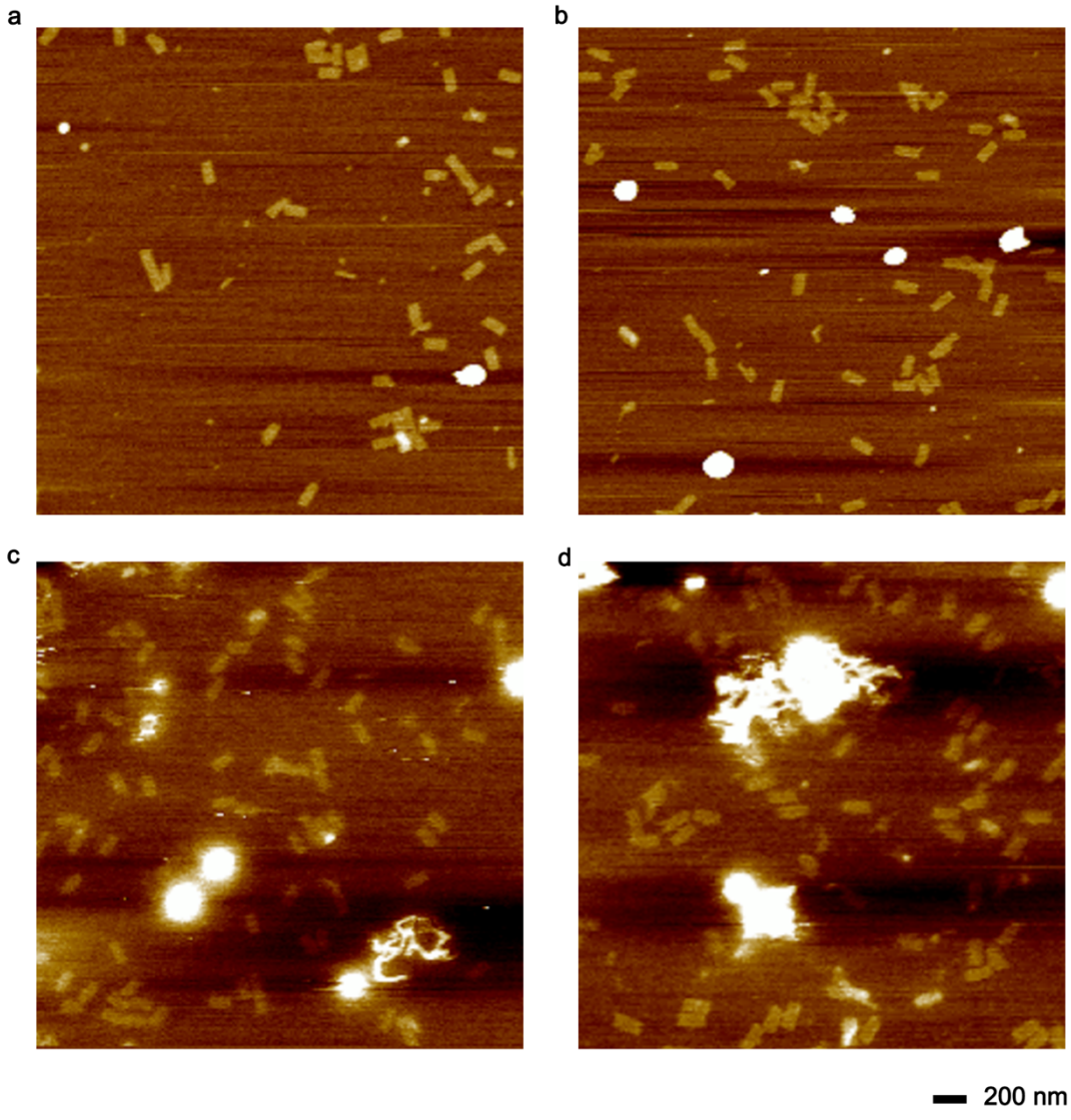

Figure 3.10 Different concentrations of Mg^{2+} in casting DNA origami on mica surface. DNA origami were cast with the magnesium concentrations of **a)** 25 mM, **b)** 50 mM, **c)** 75 mM, and **d)** 100 mM.

DNA molecules have flexibility in their morphology under different conditions including buffer type, in dry and in liquid. The AFM scanning mode and scanning probes can also affect the morphometries of DNA origami during imaging. Different casting, drying and buffering conditions were carried out as well as different AFM scanning modes (Figure 3.11).

The sizes of DNA origami do not exhibit significant differences under different conditions. From AFM scanning results, DNA origami reveal broader morphologies in liquid than under dry conditions. The interaction between buffer and DNA molecules, and the loose structure of DNA molecules in liquid environment, are one plausible explanation for the different morphometries [103, 104]. Another result displayed more compact structure of DNA origami (Figure 3.11 b-iii) when cast right after centrifuge purification. This might be due to the force from the employed centrifuge and the interaction between DNA molecules and filter membrane.

DNA origami after suspension in buffer for few minutes or stored within buffer in freezer and then defrosted, display more flabby structures (Figure 3.11 b-iv). The blowing dry technique also impacts the AFM scanning results. This mostly gives rise to cleaner surfaces when blown dry with Argon or Nitrogen, than via self-drying in air. Surface dust and salt deposition are largely reduced when applying a blowing dry technique. Overall, the surface casting condition, mica cleavage technique, environment humidity and temperature have influence on morphometries of DNA origami as well. This might also due to the scanning conditions varies from every time. However, the influence is asymmetric and minor.

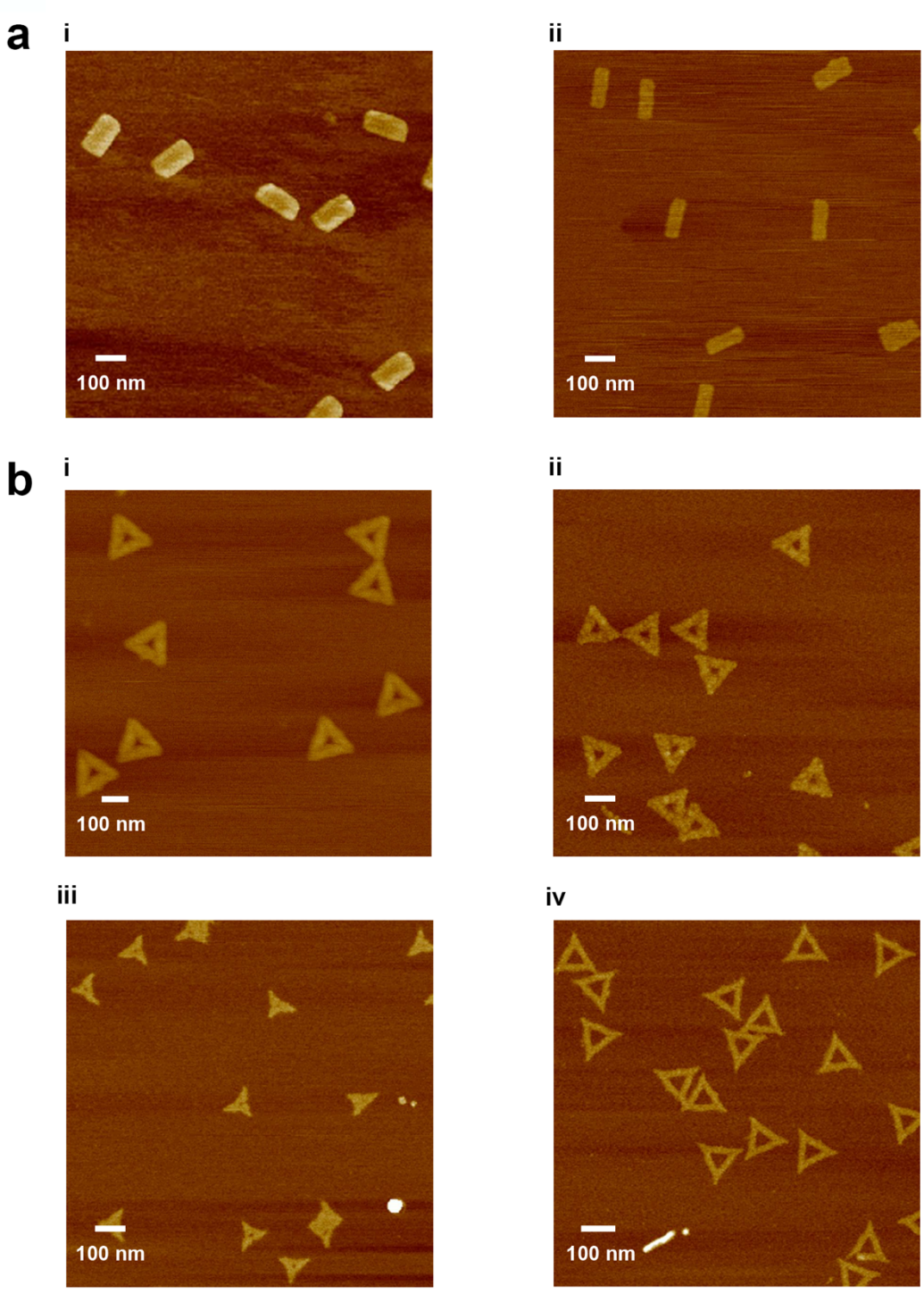

Figure 3.11 AFM images of DNA origami under different conditions. **a)** Rectangular DNA origami **i)** scanned in liquid; **ii)** scanned under dry condition. **b)** Triangular DNA origami **i)** scanned in liquid with TAE buffer; **ii)** scanned in liquid with water; **iii)** scanned in dry right after purification; **iv)** scanned in dry after stored within TAE buffer.

3.2.2 Quantum Dots Modification

The multi-modification property of DNA origami makes it a strong platform for various applications. Quantum Dots (QDs) modified DNA origami becomes an ideal material for new generation nanoelectronic and nanoplasmonic devices based on the tunable emission, efficient broadband light harvesting capability, and solution processability of semiconductor quantum dots (QDs), and their controlled positioning on DNA origami [105]. There are several different strategies to attach QDs onto DNA origami.

Covalently conjugation and noncovalent conjugation are the two main types of procedures employed to tether QDs to DNA origami. Based on the requirement of controlled modification on DNA origami, the conjugation procedures demand specific binding for controlled positioning of the QDs, and mild reaction conditions to avoid deconstructing the DNA nanostructures. The noncovalent conjugation employing a Streptavidin-Biotin interaction strategy was chosen for QDs modification on DNA origami based on its specific targeting property and high efficiency (Figure 3.12).

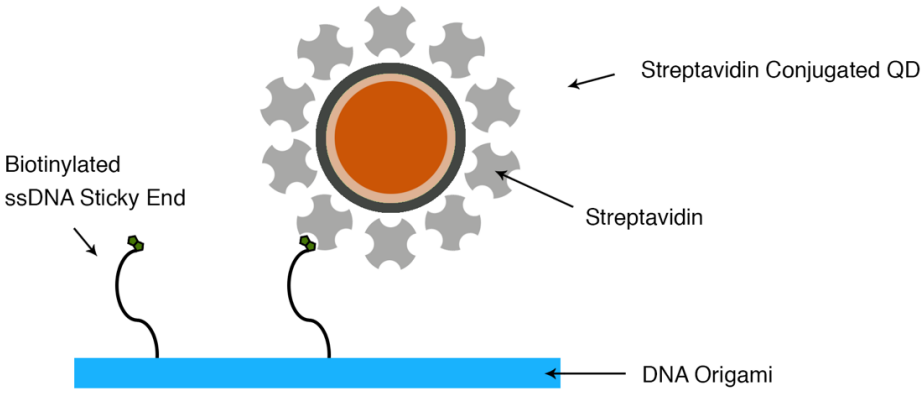

Figure 3.12 Strategy of binding Streptavidin Conjugated QD on DNA origami.

The strategy of binding streptavidin conjugated QDs on DNA origami is based on the highly selectivity of Streptavidin-Biotin interaction [100]. The staple strands on the chosen position of the DNA origami were extended and biotinylationlised to form biotinylated sticky end. QD were coated by streptavidin which would selectively bind to the aforementioned biotinylated sticky ends. We have employed this strategy in the functionalisation of both rectangular and triangular DNA nanostructures with individual Quantum Dots.

3.2.2.1. Single QD Modified DNA Origami

The single QD modified structures were synthesised at first to confirm the procedure of streptavidin-biotin interaction system on the DNA origami platform. One of the arbitrary staple strand was chosen (R75 of the rectangular DNA origami and A19 of the triangular DNA origami was chosen, see appendix iii) and extended 16 bases long for achieving enough spacing for the subsequent QD attachment, hence minimising steric-hindrance effects. These strands are commercially available with biotinylated modification at the end. The non-modified staple strands were replaced by these extended biotinylated staple strands in the stock mixture. The DNA origami structures were then assembled via standard procedures. Streptavidin conjugated QDs would then bind to the biotinylated sticky ends when mixed with DNA origami. The binding rate of streptavidin-biotin interactions is high and quick in mild conditions which leads to the self-assembly of QD on DNA origami. The so constructed QD modified DNA origami were validated by AFM.

QD modified DNA origami were cast on mica and scanned under AFM. QDs can be observed as bright dots under AFM. The height of QD is approximate 7 nm

shown on the control image of only QD on the surface (Figure 3.13 g and h). The DNA origami with QD on the designed position can be observed as bright dots in the right place on the origami structure (Figure 3.13 c and d). From AFM images, QDs can be found on the corner of origami structures which is the designed modification position with the right height shown via the cross-section. This indicates the successful assembly of QD modified DNA origami.

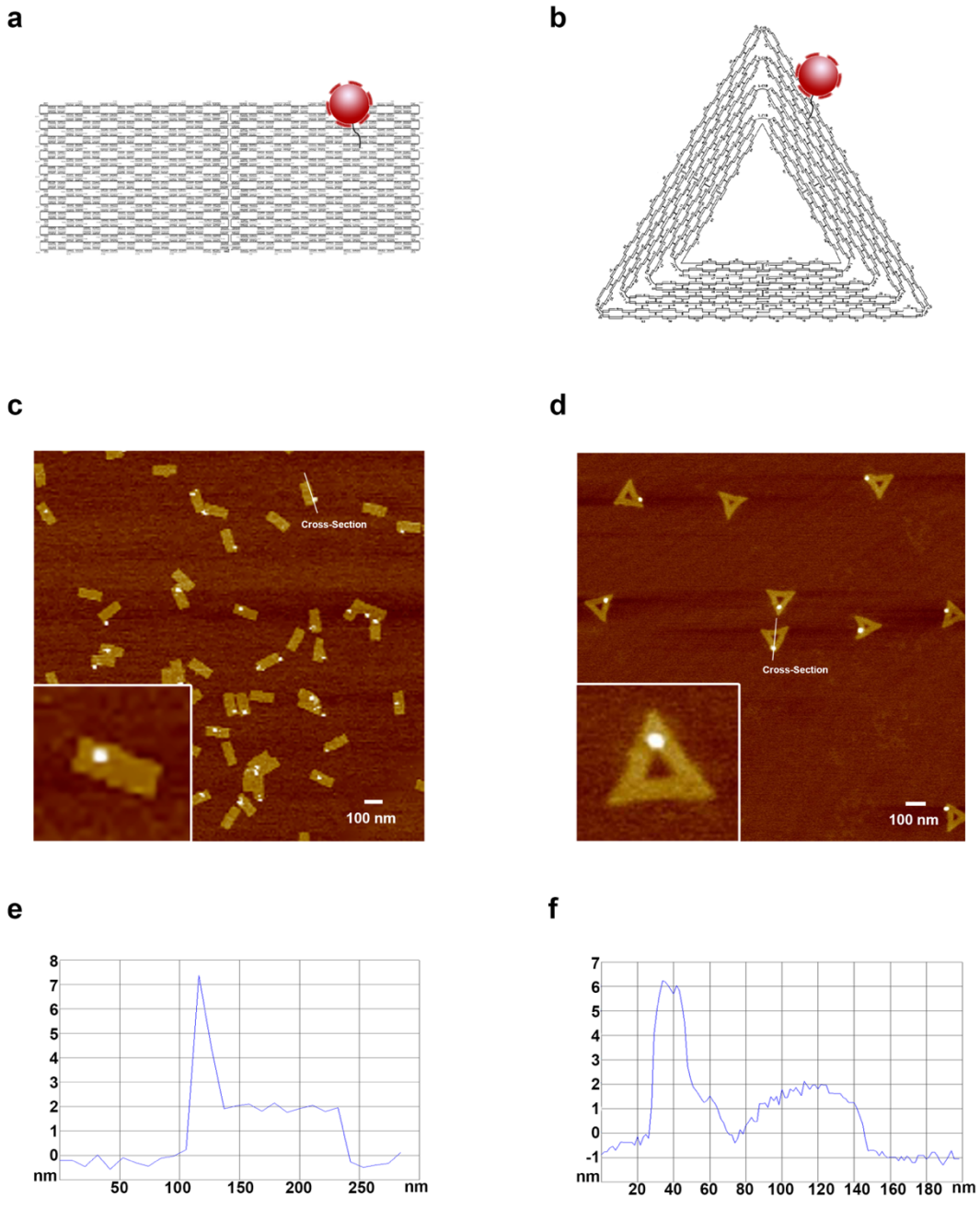

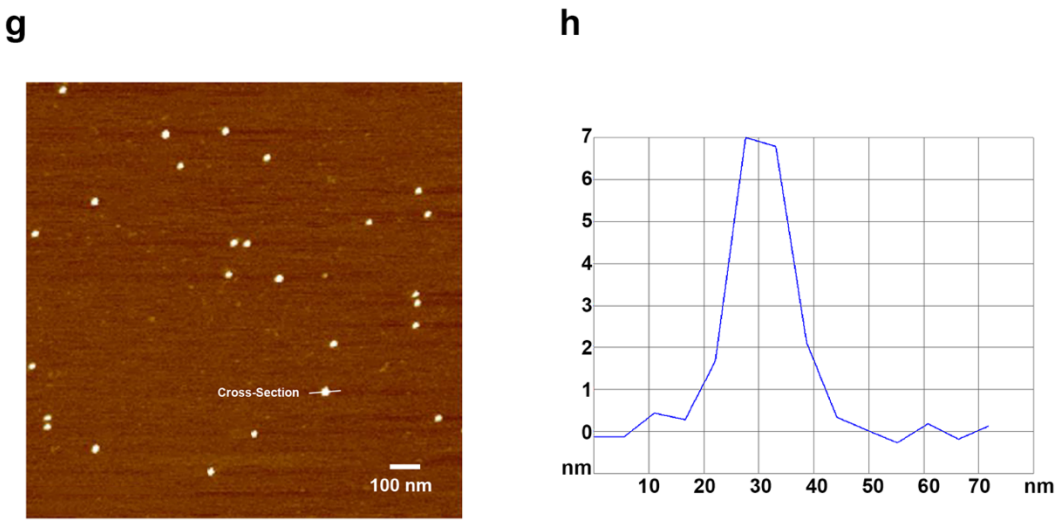

Figure 3.13 Single Quantum Dot modified DNA origami. **a)** Schematic of rectangular DNA origami modified with single QD. **b)** Schematic of triangular DNA origami modified with single QD. **c)** AFM image of single QD modified rectangular DNA origami, showing QD as bright dots on the designed position of DNA origami (close to the corner of rectangle). **d)** AFM image of single QD modified triangular DNA origami, QDs (bright dots) are attached to one corner of the triangles. **e)** Cross-section of single QD modified rectangular DNA origami shown in the inset of c). **f)** Cross-section of single QD modified triangular DNA origami shown in the inset of d). **g)** AFM image of Quantum Dots. **h)** Cross-section of QD shown in the inset of g).

The section analysis of QD indicates a similar height result (7 nm) comparing to the dots that on DNA origami (7 nm), which confirmed the modification of QD. The sticky ends are 16 bases extended staple strands (approximately 5 nm) and stretch out of the flat origami surface. When the origami was cast on mica surfaces, the QD position would be varying but close to the corner area. This explains the slight differences of QD positions shown on the AFM images (Figure 3.11 c and d).

The extension of the staple strands is not only for the spacing of QD attachment, but also for the potential in multi-modifications on one DNA origami which will be discussed in the following sections.

3.2.2.2. Multi-QDs (same) Modified DNA Origami

The available modifications on DNA origami can be multiple. In theory, functional groups can be attached to arbitrary staple strands by design; various modifications can be assembled on one DNA origami to mimic a multi-molecule interaction system for several investigations. There are different approaches to achieve multi-modifications, for both the same or different modifications.

Single QD modification was revealed to be an efficient approach. Based on the same procedure, multi-QDs modification can be carried out using streptavidin-biotin interaction. Instead of having only one biotinylated sticky end per DNA origami, two, three or even more biotinylated sticky ends can be assembled on the origami structures. These functionalised sticky ends provide the multi attachment points for QDs. As a result, multiple (of the same) QDs can assembled on one DNA origami with a one-step approach.

Figure 3.14 shows AFM images of the successful organization of one, two and three QDs on the DNA scaffold. These are same type of QD that modified on around one, two or three angles of DNA origami. The bright dots shown on AFM images indicate the QDs were well assembled on the designed position. The adjustments of ratio of DNA origami and QDs (increase the QDs amount when synthesis of multi-QDs) lead to the high yield.

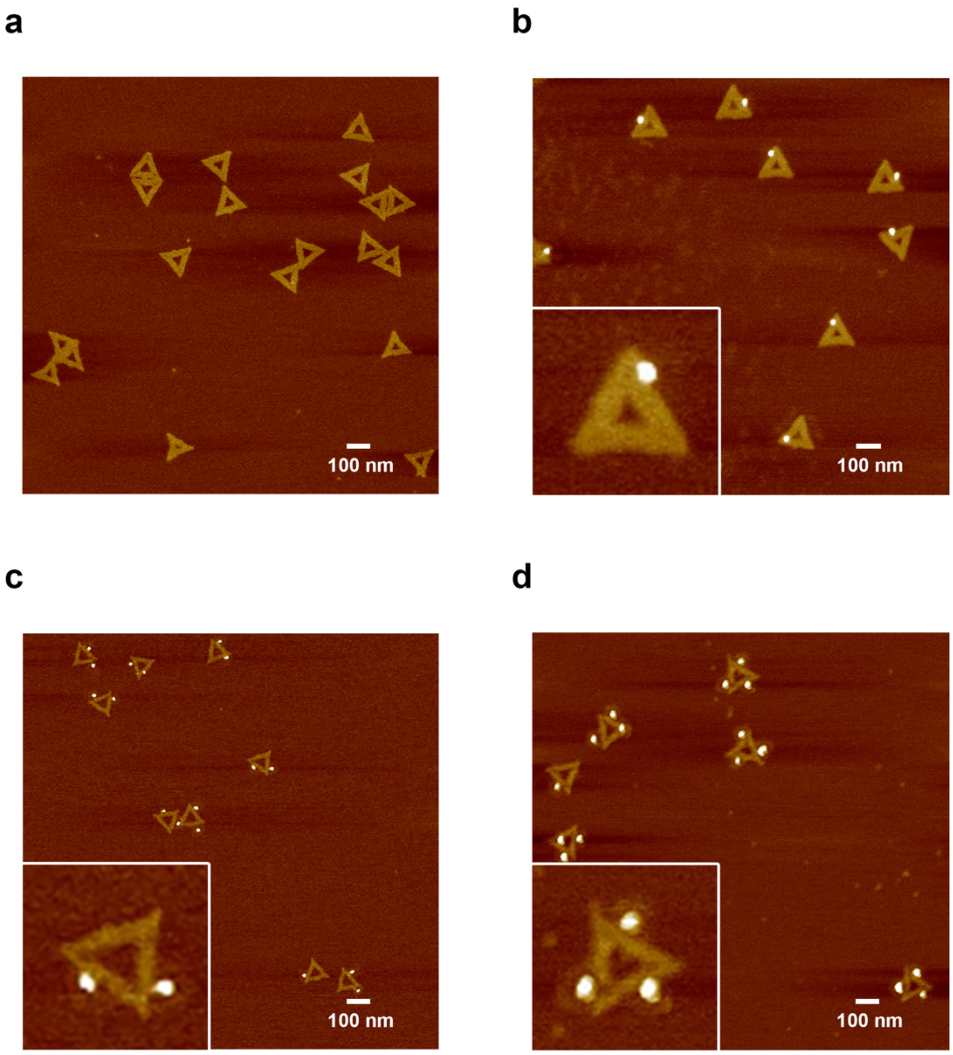

Figure 3.14 Multi-QDs modified triangular DNA origami (same QD). **a)** AFM image of pristine DNA origami without any modification. **b)** AFM image of single QD modified DNA origami. **c)** AFM image of two QDs modified DNA origami. **d)** AFM image of three QDs modified DNA origami.

The yield of QD attachment on this triangular DNA origami platform was found to be of 86% for three QDs, 89% for two QDs, and 91% for one QD per origami. The

yield can be counted from the numbers of modified and non-modified DNA origami based on the AFM images of the surfaces cast samples. An example of the statistic can be seen from Figure 3.15.

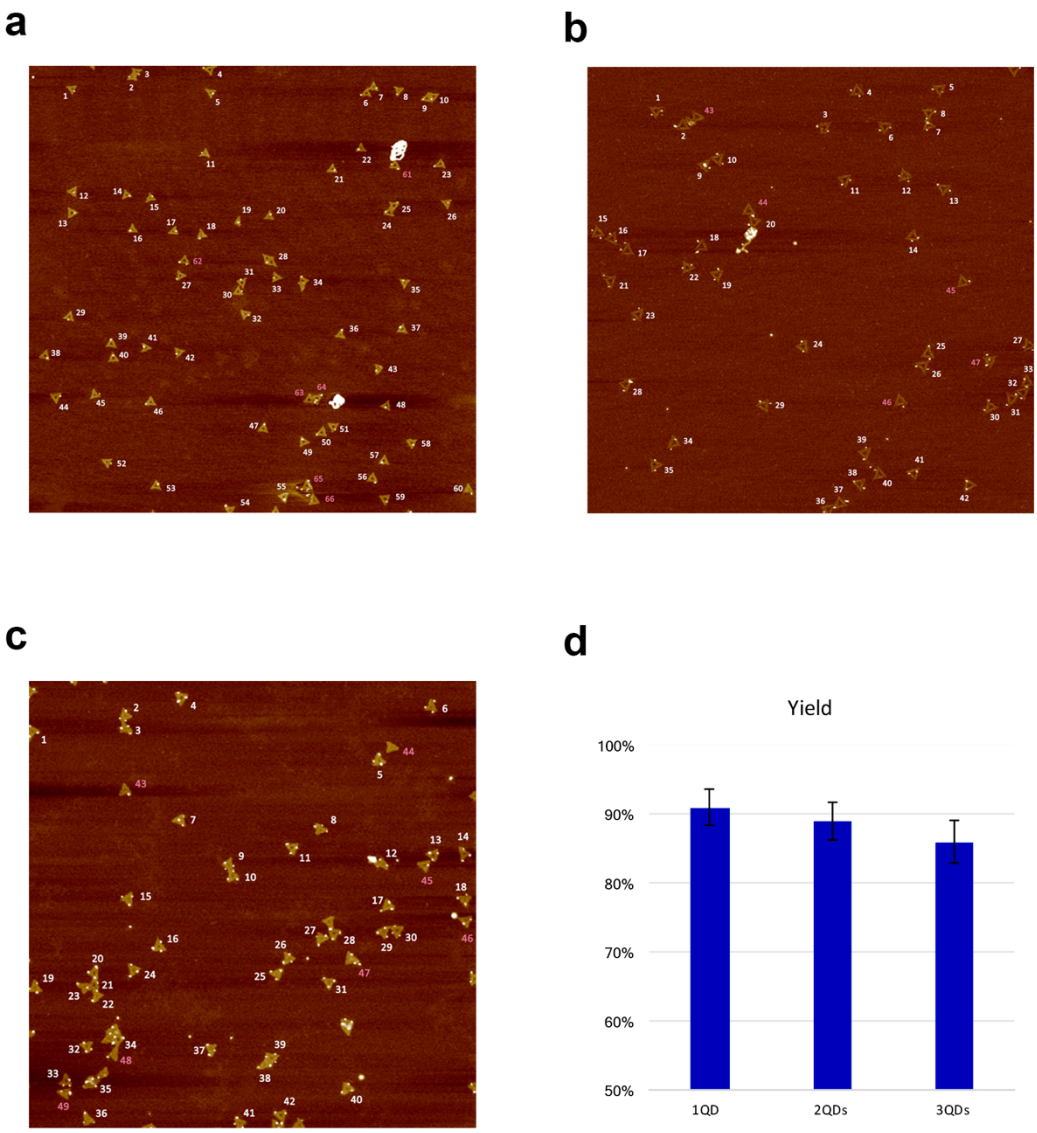

Figure 3.15 Yielding Statistics of QD(s) modified DNA origami. **a)** Sample of counting for one QD modified DNA origami. **b)** Sample of counting for two QDs modified DNA origami; **c)** Sample of three QDs modified DNA origami. **d)** Statistics from five cast samples per type of DNA origami, the yields are 91% for one QD modified origami, 89% for two QDs modified origami, and 86% for three QDs modified origami.

3.2.2.3. Multi-QDs (different) Modified DNA Origami

From single QD to multiple QDs, increasing modifiable abilities can be achieved with simple approaches. Moving forward, multiple different QDs can also be assembled on to one DNA origami utilising the coding nature of DNA. This strategy is based on the multiple modifications available on a single DNA origami platform.

The idea of assembling different QDs on one origami structure is crucial for creating a multi-functional platform for several investigations. Multiple and different QDs (streptavidin conjugated) can assemble on origami. Because that different QDs are using the same streptavidin conjugate coating, via direct biotin linkage approach, the type of QDs on origami would be random and not controllable. Fortunately, the nature of DNA coding property indicates an approach of controlled organisation for different QDs on origami. Base paring is a selective binding approach which can be easily carried out on DNA origami platforms. Once QD is conjugated with a specific biotinylated ssDNA strand, this QD can be assembled to DNA origami specifically designed with a sticky end complementary to the biotinylated ssDNA on the QD, via DNA hybridisation. As a result, specific sticky ends would only hybridise to the complementary biotinylated ssDNA which is bound to the specific QD of interest. Via this strategy, selected numbers and type of QDs can assemble on origami utilising the design of different sequences of sticky ends and complementary biotinylated single strands (Figure 3.16).

This is a two-steps approach consisting in a biotinylated ssDNA-QD conjugation and DNA hybridisation between DNA functionalised QD and the sticky end on origami. One QD is coated with 10 to 14 streptavidin, which means DNA modified QDs have more than one ssDNA. This increase the efficiency of QD binding to sticky end on the DNA origami.

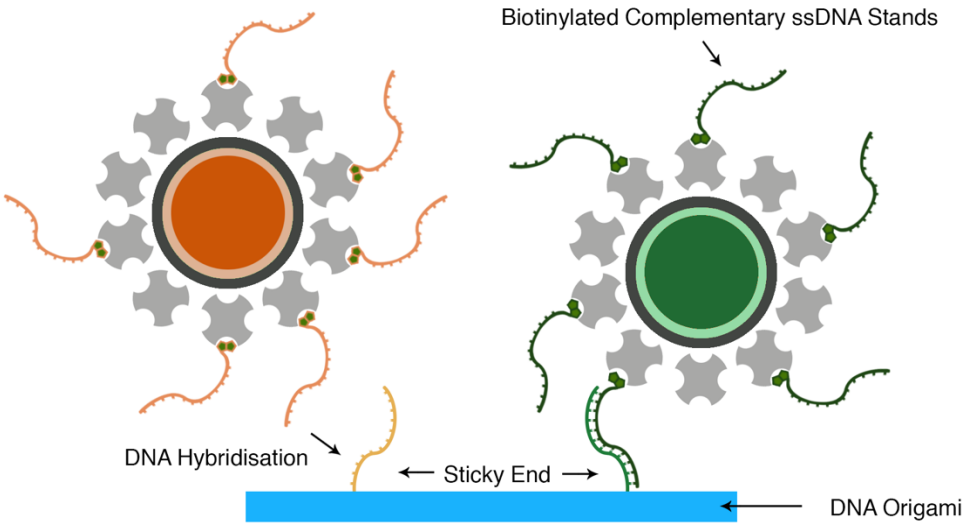

Figure 3.16 Strategy of binding different Streptavidin Conjugated QDs on DNA origami. Different sticky ends have specific sequences which will hybridise with biotinylated ssDNA that already linked to definite QDs.

Three different QDs modifications on a single triangular DNA origami was carried out in this project. Three different sequences of sticky ends were synthesised on three angles of the triangular structure via extending certain staple strands into designed sequences. Three types of streptavidin conjugated QDs with different wavelengths were attached with specific biotinylated ssDNA via streptavidin-biotin interactions and purified using dialysis to get rid of the excess of biotinylated ssDNA in solution. The DNA modified QDs cold then hybridise to the DNA origami platform. The complementary sticky end dictates the position of the QDs on the DNA origami. The QDs modified with certain ssDNA sequence would only hybridise to the complementary sticky end on the specific position of the DNA origami. The

hybridisation was carried out in solution. Once the solutions were cast on the mica surface, AFM validated the successful formation of the hybrid structures.

The different QDs modified DNA origami nanostructures were observed under AFM to reveal the details of the multi-modification approaches based on DNA base paring hybridisation (Figure 3.17). Three types of QDs were assembled on DNA origami, one QD, two QDs and three QDs modified structures can be observed. The yield of origami with all three different QDs is 38%, which is lower than 80% yield of origami with two QDs. The yield of one QD modified DNA origami is the highest with 96%. The lower yield of three QDs modification indicates the steric repulsion would affect the multiple hybridisation. This is a DNA hybridising based approach which is effected by the hybridisation temperature. When DNA modified QDs and DNA origami mixture were annealed at room temperature, the yield (43% for one QD, 27% for two QDs and 9% for three QDs) was found to be much lower than the yield achieved cooling down from 47 ºC to room temperature. Higher annealing temperature may increase the yield but would denature the streptavidin tetramer structure.

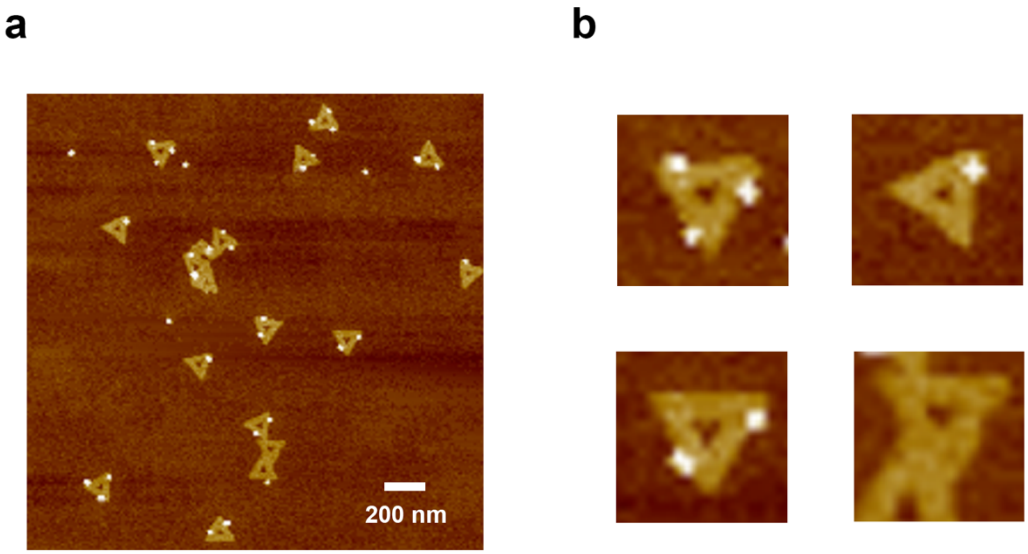

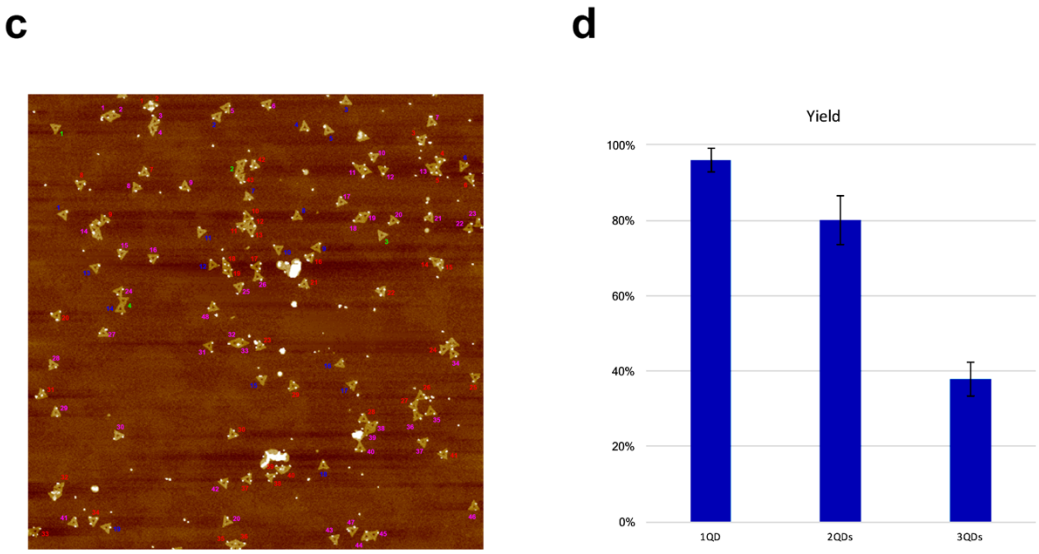

Figure 3.17 Different QDs modified DNA origami. **a)** AFM images different QDs modified DNA origami, including one, two and three different QDs. **b)** Zoom in AFM images of three, two, one and none different QDs modified DNA origami. **c)** Example of yield statistics, green number indicates non-QD modified origami, blue numbers indicate one QD modification, purple numbers indicate two QDs modification and red numbers indicate three QDs modification. **d)** Statistics from five cast samples, the yields of different QDs modified DNA origami are 96% for one QD modified origami (counted all one, two and three QDs modified origami), 80% for two QDs modified origami (counted all two and three QDs modified origami), and 38% for three QDs modified origami.

Since the different QDs (with different emitting wavelengths of 525, 606, and 655 nm) appeared to be similar under AFM, super-resolution images for the fluorescent signals of QDs were carried out by our collaborators in the School of Physics (Kemal

Keseroglu in the group of Dr Andrei Sapelkin). This allowed us to distinguish the different types of QDs and their position on the DNA nanostructures. A new method called Quantum Dot-based Optical Spectral Separation (QDOSS) was developed by utilising the size-dependence of the peak emission wavelength of semiconductor nanoparticles, instead of commonly used QD blinking effect, to achieve super-resolution imaging. The fluorescent images were captured from confocal microscopy with spectroscopic signal separation function. Then an ImageJ fitting plugin, GDSC-SMLM (v3.1) was applied to generate super-resolution (SR) images [74]. The SR images reveal the spacing and position of each QD fluorescent signal. AFM images were compared with reconstructed SR images to validate the different types of QDs and their positions on DNA origami (Figure 3.18) *. The resolution down to at least 60 nm can be achieved using a mixture of quantum dots with distinct emission wavelengths.

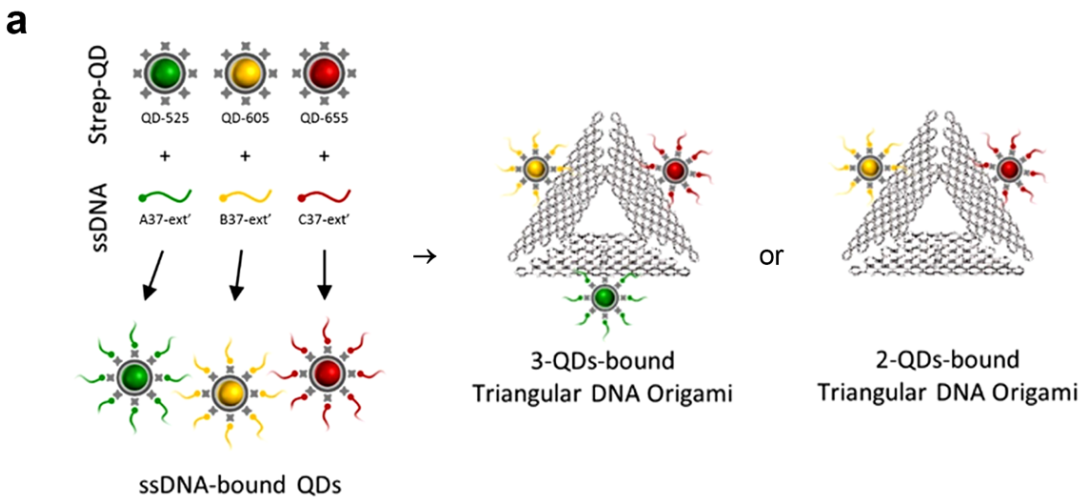

* This is a collaboration work with Kemal Keseroglu and Andrei Sapelkin in School of Physics and Astronomy, Queen Mary University of London. A script of co-authored paper named '*Super-Resolution Imaging via Spectral Separation of Quantum Dots*' had been submitted.

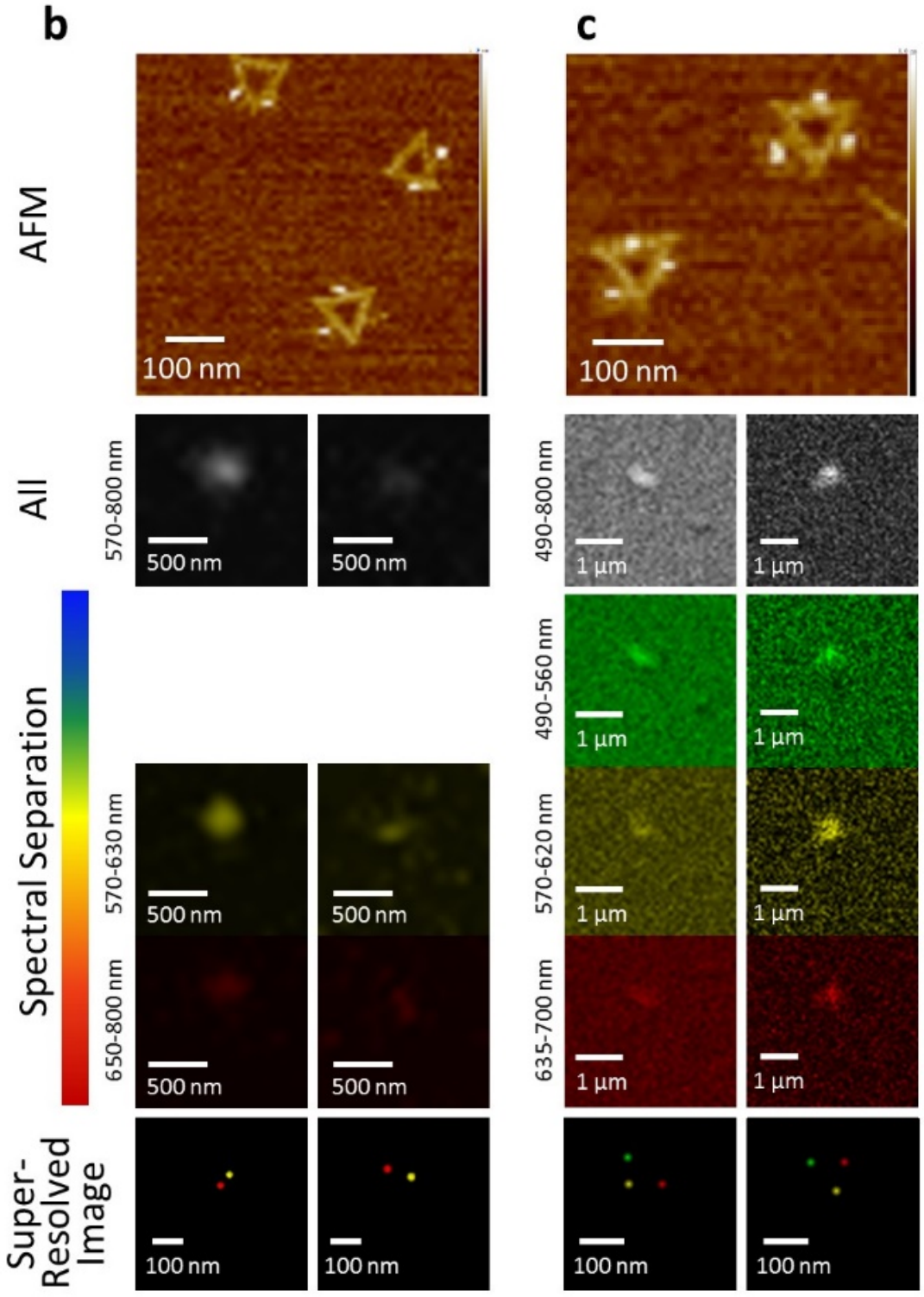

Figure 3.18 Super-resolution imaging of different QDs modified to triangle DNA Origami. **a)** Schematic of 2-QDs and 3-QDs modified DNA origami assembly. Each

side of triangular DNA origami has a sticky end complementary to the ssDNA bound to QDs. 2-QDs-bound origami has QD-605 and QD-655 on two different sides of the triangular structure. 3-QDs-bound origami has in the QD-605, QD-655 and QD-525 on the all three edges of triangular structure. **b** and **c)** AFM, Confocal Microscopy, and reconstructed images of b) 2-QDs and c) 3-QDs-bound DNA origami. To give an illustration, two spots were spectrally separated and localisation images were reconstructed for each system. Sums of all images (grey) represent the confocal images of the spots without spectral separation (the emission wavelength ranges from 570 nm to 800 nm in b and 490 nm to 800 nm in c). Spectrally separated images and the localisations in the reconstructed images were recoloured as green for QD-525, yellow for QD-605 and red for QD-655.

Triangular DNA origami were programmed for the assembly of three different streptavidin conjugated QDs with a maximum emission at 525 nm, 605 nm and 655 nm. Each of these QDs was functionalised with a different biotin modified single-stranded DNA, complementary to the sequences which extended from the sides of the aforementioned triangular DNA origami. Two or three different types of QDs were then attached to DNA origami. In this arrangement, the distance between positions of different QDs is approximately 60 nm, by design.

From AFM images. it was found that the distance between the QDs varies between 60 nm to 90 nm, due to the flexibility of the DNA strands anchoring the QDs to the Origami. The same sample for AFM imaging were then used to collect confocal images. After a spectral separation approach, signal and the positions of each distinct QDs were clearly revealed. Comparison of the AFM and the reconstructed SR images

shows consistency in the patterns and distances of QDs attached to DNA origami, thus confirming optical resolution down to at least 60 nm (with localisation precision of 6nm), i.e. well below the diffraction limit. The spectral separation method helps validate the multiple different QDs modification on DNA origami.

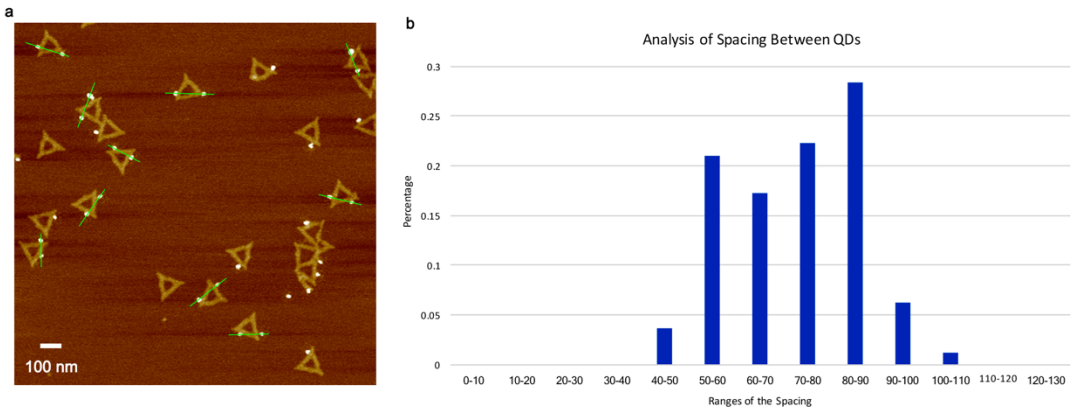

Figure 3.19 Analysis of spacing of QDs on DNA origami. **a)** AFM image of sections for analysis the spacing between QDs. **b)** Analysis of numbers of different spacing of QDs. The spacing of QDs were found to be around 60 – 90 nm.

The successful assembly of three different QDs modified DNA origami reveals the capability of functionalising multiple types of nano-objects on this platform. More types of QDs modifications were achieved using the same strategy (Figure 3.20).

Rectangular DNA origami with 6 different sequences of sticky ends were designed to assemble 6 different types of QDs. Along two long sides of the rectangular shape, three QDs were designed on each side. From the AFM validation images, rectangular DNA origami with multiple types of QDs modification were represented. Up to 4 types of QDs on one origami structure can be achieved. The yield of 4 QDs modification is lower than 10% which may be due to the steric repulsion from the closer distance of the modifications on this design. However, the constructed of 4 or 3 QDs

modified DNA origami indicate the multiple modification ability based on modifying selected staple strands.

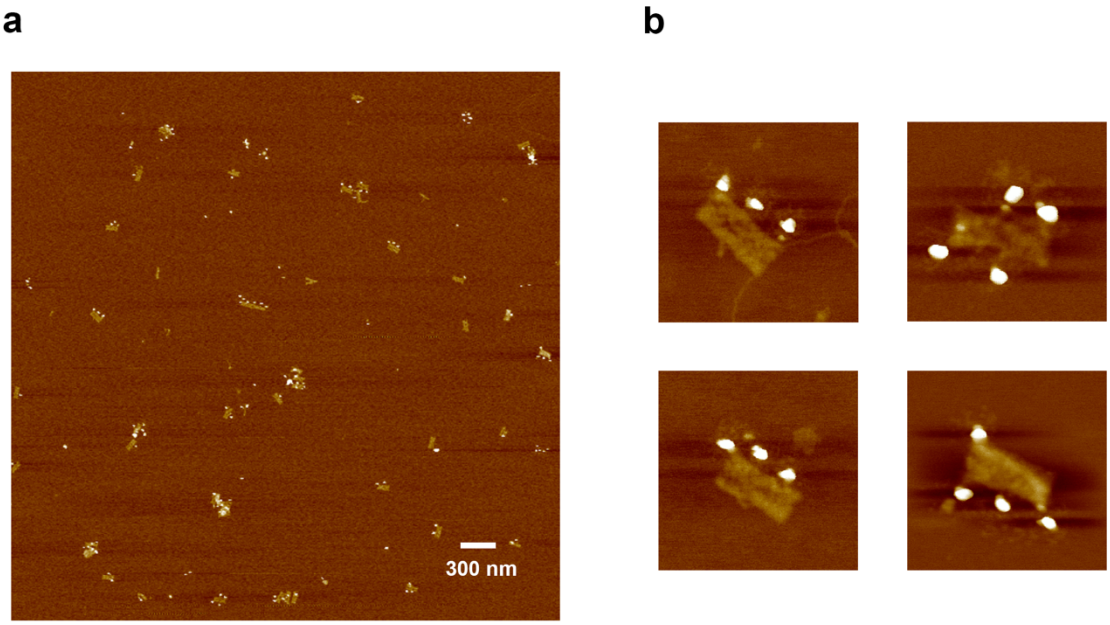

Figure 3.20 Different QDs modified rectangular DNA origami: **a)** AFM images of multi-QDs modified DNA origami; **b)** Zoom in AFM images of DNA origami with up to four different types of QDs.

The successful assembly of different types of QDs on one DNA origami helps in exploring the multiple functional modifications possible with DNA nanostructures. The idea of utilising modified staple strands to control the modification types and positions indicates the potential of using the similar complimentary sticky end approach for different types of molecules other than QDs.

3.2.3 Fluorescent Modification

DNA origami is a DNA based nanostructure without fluorescent capability by itself. It is hard to track DNA origami in many biological investigations. Although we already discussed the QDs modified origami which have brought in fluorescent capability in the last section, a QD is big molecule and sometimes hard to control. Modification of small fluorescent molecules on DNA origami could help in exploring the capacity of this platform.

3.2.3.1. Multi-fluorophore Modified DNA Origami

Fluorophores can be assembled on DNA origami via modifying fluorescent molecules on chosen staple strands. R57 and R184 of our rectangular DNA nanostructure (see section 2.3.3.2) were extended to form two sticky ends with different sequences. Fluorophore modified ssDNA (commercial available from IDT synthesised with designed sequence) that are complementary to the extended sequences were employed in the construction of multi-fluorophore DNA origami. As a result, two different types of fluorophores were assembled on position R57 and R184 of our rectangular DNA origami. Position R57 was modified by Rhodamine Red™ and position R184 was modified by Alexa Fluor® 488. AFM validation images show the successful construction of the origami structures (Figure 3.21 a). However, the fluorophore molecules are too small to be displayed in AFM images. The validation was also carried out by casting the same sample on glass coverslips and observing these under epifluorescence microscopy. The DNA origami carrying two different fluorophores, were cast on the surface for fluorescence imaging, and the signal from

Alexa Fluor and Rhodamine Red dyes were captured. The same pattern of random immobilisation for two different fluorophores indicates the successful construction of DNA origami with two types of fluorescent molecules. Comparison of images from the two channels demonstrate the co-localization of the two fluorophores within the same pixel of the captured image (Figure 3.21 b). There is no binding interaction between these two fluorophores that links them together: the green and red signals are located in the same places only if these two types of fluorophore molecules are assembled on the same DNA structure.

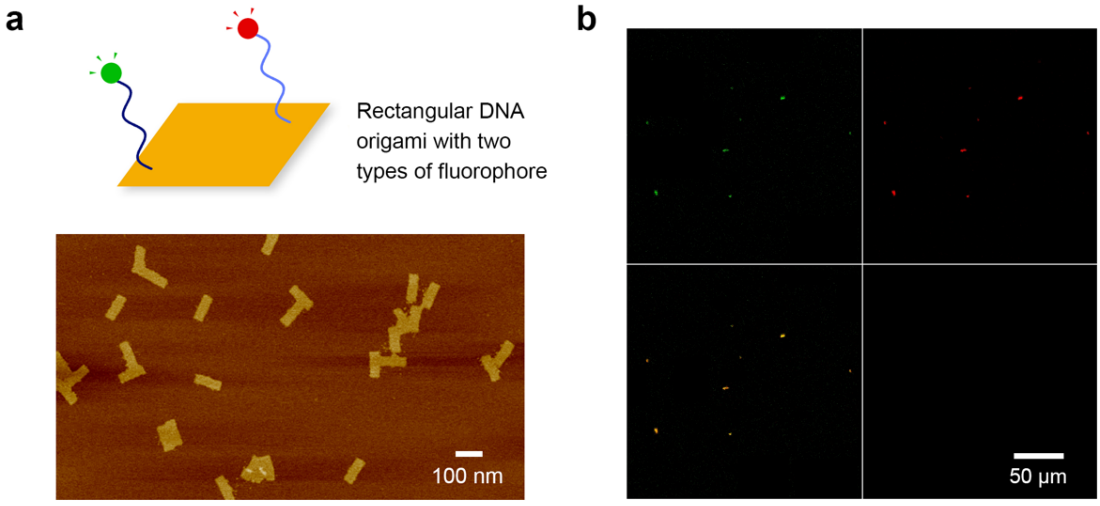

Figure 3.21 Fluorophore modified DNA origami. a) Schematic and AFM image of rectangular DNA origami with two types of fluorophore. Alexa Fluor® 488 (green dot) and Rhodamine Red™ (red dot) were assembled on origami. The fluorophore cannot be represented under AFM. b) Confocal image of fluorophore modified DNA origami. The green (top left), red (top right), and merge (bottom left) channel represent the Alexa Fluor and Rhodamine Red signals to be localised in the same position.

3.2.3.2. Dynamic Control on Origami by Restriction Enzyme

Based on the detectable capability of tracking fluorescent signals, the fluorophore modified DNA origami can be applied for several dynamic investigations. Here we developed DNA origami to form a platform for monitoring cleavage events by restriction enzymes. The idea is to modify a fluorophore molecule on DNA origami based on a sticky end strand containing a restriction enzyme cutting region. A restriction enzyme will catalyse the cleavage of the phosphate back-bone of specific DNA sequences. The fluorescent signal would be then removed from the DNA origami structure upon the interaction with a specific restriction enzyme. Figure 3.22 displays a schematic of this surface approach. This experiment is a proof of principle to show DNA origami can be employed in enzyme recognition events, with single-molecule control.

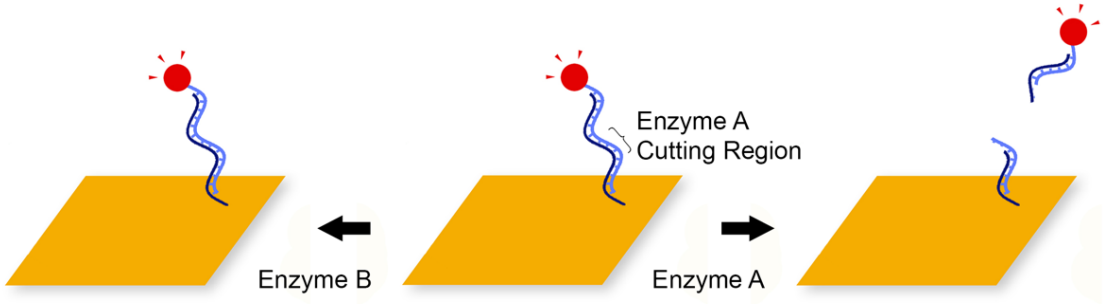

Figure 3.22 Schematic of restriction enzyme single cleavage on DNA origami.

The experiment was carried out on Cy3 modified DNA origami. The Cy3 fluorophore was conjugated to a ssDNA that complementary to the sticky end on DNA origami. The employed sequence contains the restriction enzyme BamHI cutting region with the sequence GGATCC. Enzyme BamHI and HindIII were both added to solutions

of Cy3 modified DNA origami at 37 ^{o}C (that is the physiological temperature for enzymes' activity). Centrifuge filters were employed to remove any cleaved strands from the solution. The solutions were than cast on cover slips and total internal fluorescence (TIRF) investigations were carried out.

The comparison of TIRF microscopy images for the origami before and after cleavage shows that Cy3 were removed from the origami by BamHI but nothing changed when HindIII was added to the same solution in control experiments (Figure 3.23). The use of HindIII represents a control because HindIII does not recognise any portion of the sequence in the origami structure. The significant reduction of fluorescent signal in BamHI cleaved sample indicates that single restriction enzyme cleavage can be carried out on DNA origami nanostructures.

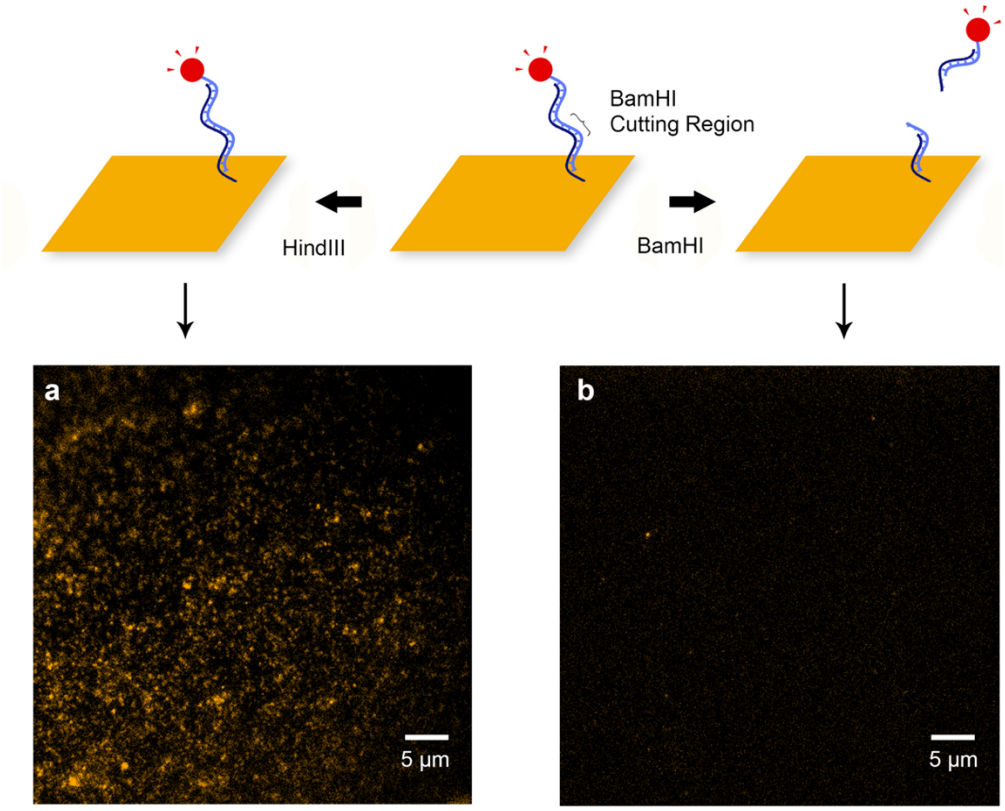

Figure 3.23 TIRF images of restriction enzyme cleavage. **a)** HindIII applied sample. No cleavage was found from image. **b)** BamHI applied sample that cleavage removed

the Cy3 signals. c) AFM images of Cy3 bound DNA origami before and after enzyme cleavage. This indicates that enzyme does not affect the whole origami structure.

The restriction enzyme cleavage was then carried out directly on surface. In this new set of experiments, first the Cy3 bound DNA origami were covalently immobilised on surface (the approaches of this immobilisation were discussed in chapter 2, section 2.3.4.4; DNA origami with amino anchors were covalently linked to the carboxylic silane treated surface via EDC/NHS coupling).

The covalently bound strategy reduces the non-specific interaction of origami with the substrate surface. DNA origami are not stable when only physisorbed on surface with the presence of magnesium. During carrying out covalently bonding strategy, silane molecule was introduced on substrate surface. As a result, the cleaved DNA strands will not attach to the surface when magnesium presences as an integrant reagent in enzymatic digestion. The tail structure of silane molecule prevent the physisorption of DNA strands on surface. From this strategy, the results show only enzyme interaction events.

On the other hand, magnesium is not needed in the covalent immobilisation approach. When enzyme cleavage happens, the DNA origami will stay on the surface, while the cleaved strands with the Cy3 fluorophore will move into the solution that can be washed away. This will show the reduction of fluorescent signal only due to the enzyme cleavage but not affect the DNA structure.

The BamHI cleavage and HindIII control were carried out on surface at 37 ^{o}C and room temperature for one hour. The significant reduction of Cy3 signal can be observed between the HindIII control sample and BamHI cleavage sample at 37 ^{o}C (87%

cleavage). This indicates the cleavage occurred on DNA origami. Meanwhile, a smaller reduction of Cy3 signal were observed on the samples at room temperature (64% cleavage) which indicates the lower efficiency of restriction enzyme at not suitable temperature ranges (Figure 3.24).

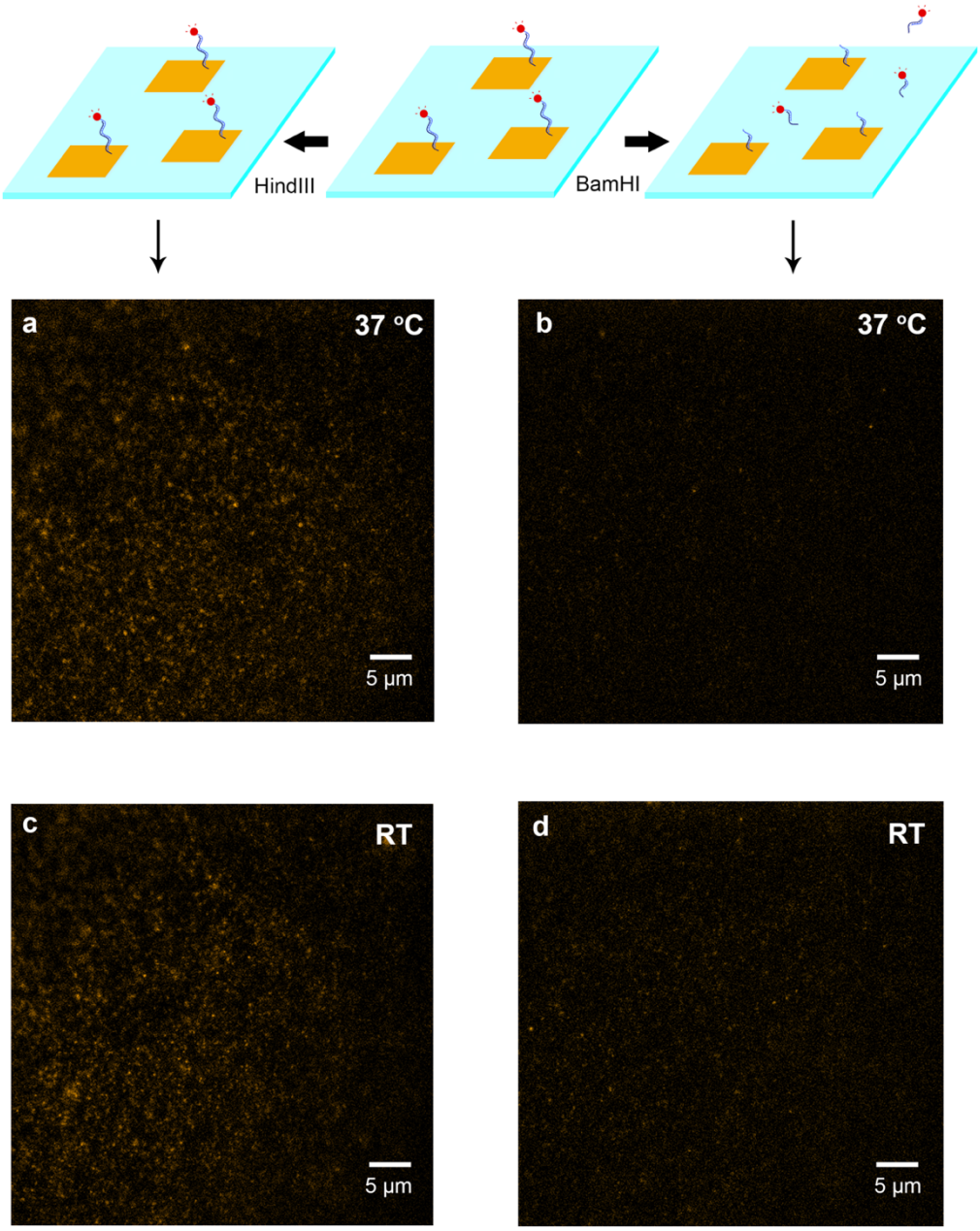

Figure 3.24 TIRF images of restriction enzyme cleavage on surface. **a)** TIRF image of HindIII control sample at 37 °C. **b)** BamHI cleavage at 37 °C. A large scale of Cy3

signal reduction were observed. **c)** HindIII control sample at room temperature. **d)** BamHI cleavage at room temperature. A smaller scale of cleavage was observed.

3.2.4 Amino Anchors Modifications

DNA origami can be modified with amino groups that can be employed as anchors for surface immobilisation. The amino group can be introduced to carry out EDC/NHS conjugation linage. As a result, amino groups modified DNA origami can be covalently linked to the carboxylic functionalised substrate surface. Amino group modified staple strands were ordered and replaced with ordinary staple strands in the origami synthesis. Employing this approach, DNA origami can be formed with amino anchors (see section 2.3.3.3). The amino anchors can covalently bond to the carboxylic group on the silane treated glass or silica surfaces, via EDC/NHS coupling (see section 3.1.3.4 and 4.1.2) (Figure 3.25).

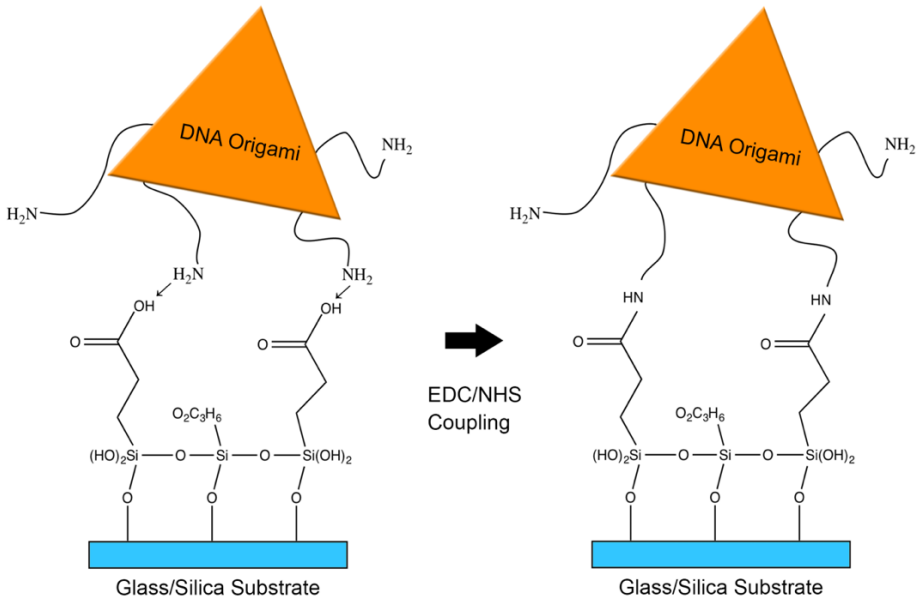

Figure 3.25 Schematic of covalently immobilisation of DNA origami.

To validate the successful assembly and functionalisation (with amino anchors), the DNA origami were covalently immobilised on surface, and a control experiment of noncovalent immobilisation strategy (magnesium bridged physisorption): both kind of samples were incubated with PBS buffer overnight. The removal of origami structures on noncovalently immobilised substrates was compared to the preservation of origami on covalently immobilised substrates (Figure 3.26). This indicates the stable bonding of the origami to the surface via the covalent approach based on amino anchors modifications.

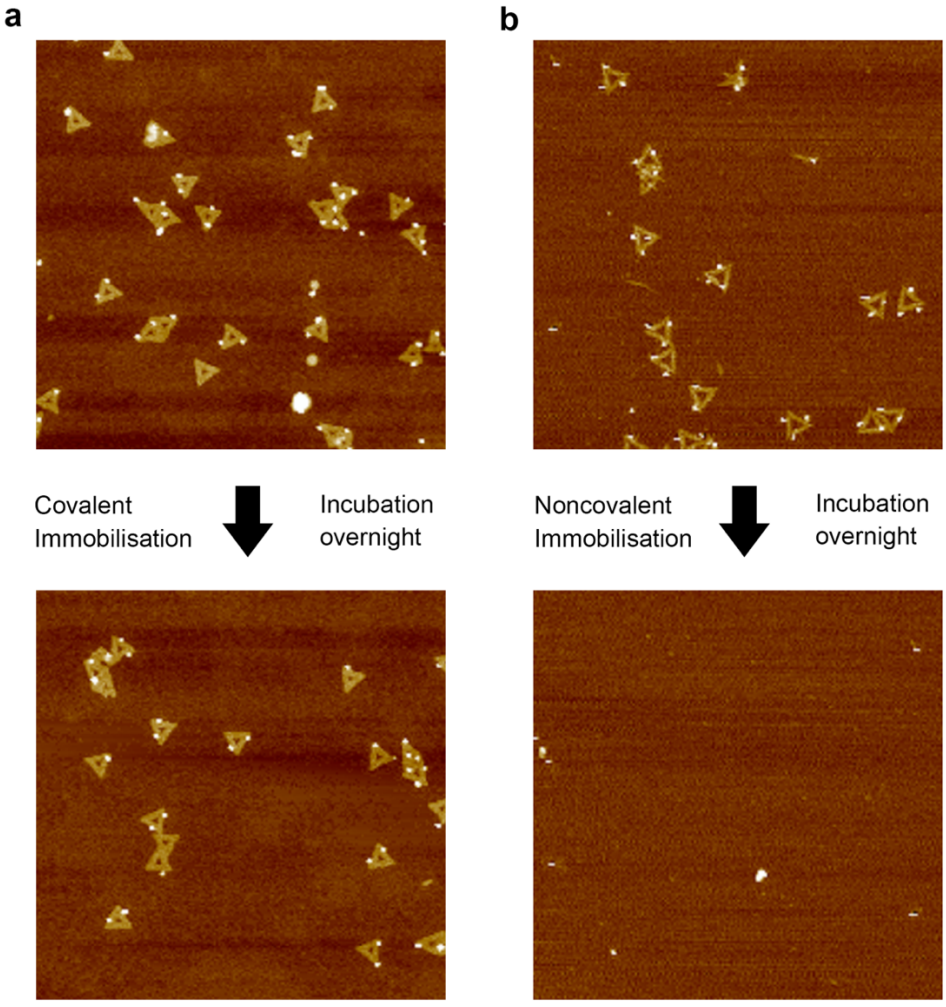

Figure 3.26 Comparison of covalent and noncovalent immobilisations. **a)** Incubation in PBS overnight for covalent immobilisation substrate. The origami structures remain

on the surface after incubation. **b)** Incubation for noncovalent immobilisation substrate. DNA origami was removed from surface after incubation.

The amino anchors modification allows DNA nanostructures to be covalently immobilised to the substrate surface and be stable in various of conditions. This can be used for controlling the patterning of DNA origami and several DNA nanostructures for investigations on substrate surface. More applications will be discussed in Chapter 4 and 5.

3.3 Summary

In summary, I have discussed an efficient way to design modified staple strands for the functionalisation of DNA origami and presented various strategies for the assembly on functional DNA origami nanostructures.

DNA origami as a basic platform was successfully synthesis via a thermal self-assembly approach. Different types of QD modification, including single QD and multiple QDs, were achieved via biotinylated staple strands or complementary sticky ends processes. In particular, utilising the coding nature of DNA structures played a key role in modifying the same DNA origami with different types of QDs. Multiple different QDs modified DNA origami showed the precise spacing of QDs fluorescent signal and localisation as a gene ruler via a super-resolution imaging based spectral separation approach.

Additionally, fluorescent labelling molecules were successfully assembled on DNA origami. Multiple fluorophores modified DNA origami was employed in a

dynamic controlling process utilising restriction enzymic digestion. The enzyme cleavage results indicated that DNA origami can be employed in enzyme recognition events with single-molecule control.

Various additional modifications, including peptides and amino functional groups, were also successfully assembled on DNA origami structures. These approaches were carried out using several conjugation techniques involving streptavidin-biotin recognition, maleimide-thiol linkage and EDC/NHS coupling.

Overall, the multiple modification ability of DNA origami was explored in presence of various types of modifying molecules. Some of the applications exploiting the functionalised DNA origami were investigated (spectral separation as gene ruler, and restriction enzyme dynamic control). The controlled surface immobilisation of the functionalised DNA origami will be part of the applications discussed in the following chapters (Chapter 4 and 5).

Chapter 4

Surface Patterning of DNA Origami

This chapter presents a newly developed strategy of DNA-mediated single-molecule controlled immobilisation on Focused Ion Beam (FIB) patterned surfaces. The strategy includes the nanofabrication of patterns on substrate and the precise assembly of DNA nanostructures according to the patterns.

4.1 Introduction

As discussed in chapter 1 and 3, DNA nanostructures have great potential in creating useful surface devices via constructing composite nanoscale geometries and coupling arbitrary functional molecules on them. Based on the various nanostructures and vast functional modifications on them, DNA or CNT based electronic devices [106, 107], optical structures [108, 109], biosensing assays [110], and custom single-molecule technologies for answering biological questions [111] can be formed. A key requirement for all the aforementioned applications, and for the future miniaturization of integrated

devices, is the controlled organization of nanostructures from solution to surfaces. In this regard, the precise patterning of colloidal semiconductor nanocrystals into hierarchical structures has attracted substantial research interest in recent years. Various strategies have been presented for the geometrically controlled assembly of DNA origami on different substrates.

Photolithography techniques are conventionally used in fabricating patterned surfaces. E-beam lithographically patterned substrates have also been used, followed by silane based or thiol-gold interaction immobilisation approaches [112, 113, 114] for the fabrication of specific (bio)molecules and nanostructures (see also section 1.3). E-beam lithography can achieve nanometre resolution by overcoming the diffraction limit of light [37]. These approaches request several steps of processes including photoresist coating, e-beam shadowing and development, and lift-off resist, to fabricate a patterned substrate.

Nanoimprint lithography techniques have been developed to achieve high-throughput patterning with high resolution [115]. These strategy transfers a topographic mold into a thermoplastic polymer film to generate desired patterns on a substrate. Selective placement of DNA origami on surface was accomplished using nanoimprint based process with a passivating layer of hexamethyldisilazane (HMDS) [116]. Moreover, scanning beam lithography techniques attracted researchers' attention in recent years because of their maskless and step-less properties with high resolution [117].

Focused ion beam can pattern features on substrate surface with resolution down to about 20 nm and with the smallest lateral dimensions down to 5 nm [118]. These properties are ideal for patterning DNA nanostructures for various investigations. In this project, we present a facile strategy to fabricate nanoapertures for the assembly of

DNA origami using a FIB nanopatterning approach and a selective surface chemical functionalisation strategy. Highly uniform nanoarrays can be formed with a one-step lithographic process. Compared to other lithographic approaches, this is a more straightforward method (fewer fabrication steps) for surface nanofabrication. Additionally, the reusable capacity of the developed platform is explored via a simple cleaning process. Based on the programmable control of FIB, this strategy can be designed to exhibit different geometrical arrangements on a sample surface.

4.1.1 FIB nanofabrication

FIB utilises Gallium ion beam to mill the substrate surface for fabricating desired topographic patterns. The Ga^+ ion beam has a large energy density that allows mill various of martials including metals and polymers.

Under the control by a user interface software, the ion beam moves to a precise pixel-by-pixel to mill substrate surface [119] (Figure 4.1); notably there are several parameters involved in control of the beam movement. The milling spot size (beam diameter) is linked to the beam current that is applied: increasing of beam current will expand the beam diameter. Typically, the Ga^+ in beam have a limit spot size of about 8 nm when a 1 pA current is applied (Quanta FEG FIB system user manual). The time that the ion beam stays at a particular pixel position is defined as dwell time. The milling depth can be affected by the length of the dwell time: when the beam stays longer in a target position, the substrate surface will be milled deeper. The overlap indicates the area overlapped when the beam moves from one pixel to the next. This is normally shown as percentage of total beam area, while the distance between the frontier of two

neighbouring pixels along the milling direction is defined as the pixel spacing. Pixel spacing corresponds to the overlap that specifies the moving rate of the ion beam and can be applied to speed up or slow down the milling.

These parameters need to be adjusted appropriately to mill desired size and shape of the patterned features on the sample surface. For example, 1 µs dwell time and 50% overlap are normally used for Si substrates. Reducing this to 0.5 µs dwell time and 0% overlap can allow for a quick but rough milling.

As mentioned earlier, the ion beam can be controlled with a software interface, to scan across the sample surface in a raster or serpentine movement. The beam movement is carried out line by line. In a raster scan, the ion beam is always in the same direction throughout every line. However, the beam moves in a reversed direction after each line in a serpentine movement. There are no conspicuous impacts on milling by changing different types of beam movement [119].

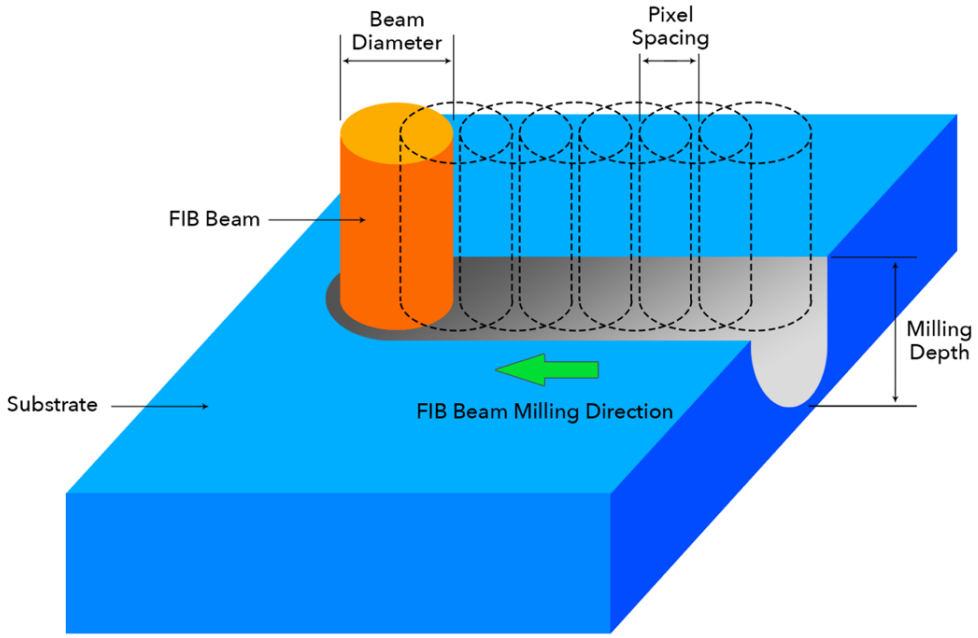

Figure 4.1 Schematic of FIB milling [119].

4.1.2 Silane and covalent surface immobilisation

FIB can allow fabrication of a patterned substrate. In addition, strategies are needed to immobilise target molecules or nanostructures on the substrate surface according to the patterns. Silane based approaches are a strong method to place nanoparticles in a controlled fashion on silicon and silicon dioxide surfaces.

Silanes are monomeric silicon chemicals. They have a hydrolytically sensitive centre which can react with inorganic substrates such as silicon dioxide to generate covalent bonds [120]. The silanes molecules can also have different substituents to modify the chemical and physical nature of the substrate surface.

A typical structure of a silane molecule is shown in Figure 4.2. Normally, a silane molecule contain hydrolysable alkoxy groups as a head and an organic substitution tail [121]. The hydrolysable head is the reaction centre to attach to the substrate and the substitution tail contribute the functional modifications [122]. Based on the different types of substitutions, there are different varieties of silanes including hydrophilic silanes containing ionic, polar or hydroxylic groups, and hydrophobic silanes containing such as methyl, linear or branched alkyl, or fluorinated alkyl groups [123].

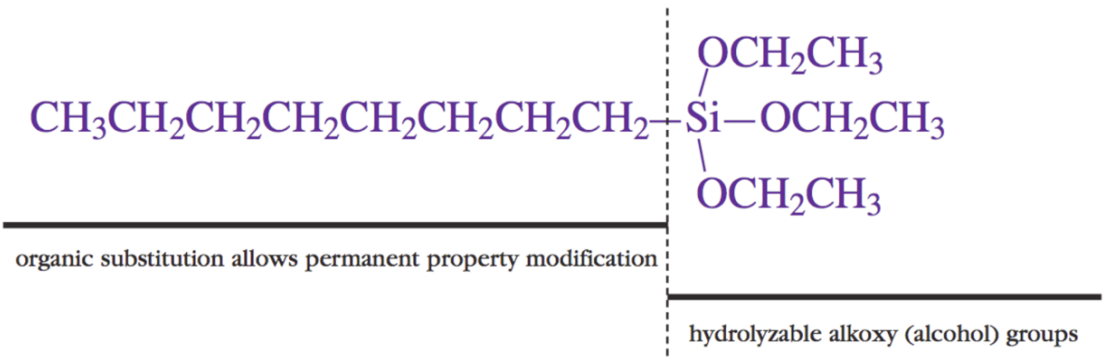

Figure 4.2 Structure of a typical silane molecule [120].

Silanes play an important role in the surface treatment based on their ability to covalently bond to the substrate surface. The trialkoxy hydrolysable head of silane molecules can be hydrolysed to attach to the OH groups of the substrate. The details of the reactions of silanisation are shown in Figure 4.3. At first, the trialkoxy head are hydrolysed and then condensed to form oligomers. Then hydrogen bonds bind these oligomers to OH groups on the substrate surface. At last, concomitant with a loss of water by drying or curing, covalent bond is formed to link silane molecules to the substrate surface [124]. Although described sequentially, these reactions can occur simultaneously after the initial hydrolysis step. Normally, there is only one silane bond linkage per silane molecule; the other two alkoxy groups in the trialkoxy head are free or condensed with other silane molecules.

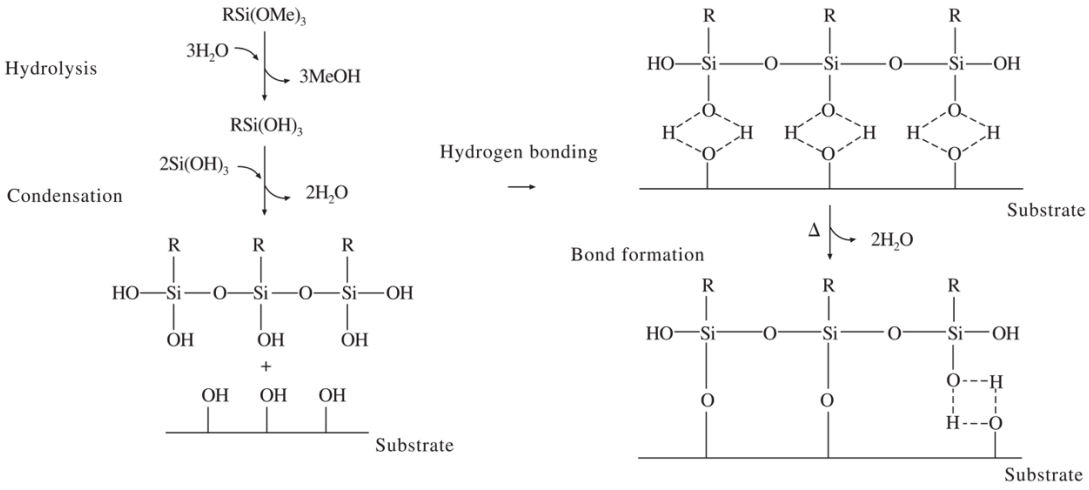

Figure 4.3 Reactions of silanisation on substrate [124].

The substitution tail of the silane molecule is the key of surface treatment. There are different types of substitution for various of modifications. For example, (3-(2,3-epoxypropoxy)propyl)trimethoxysilane were applied on surface to assemble ZnO QDs

for ultra-stable luminescence [125], while an amino silane functionalised porous silicon for the selective assembly of neuronal cells was reported by Sweetman et al [126]. In this project, carboxylic tail silane was chosen to modify the surface in order link to the DNA nanostructures containing amino groups (via a EDC/NHS conjugation strategy: the conjugation approach was discussed in Chapter 3, section 3.1.3.4).

4.2 Results and Discussion

4.2.1 Au Islands

A FIB-based lithographic approach was carried out first to form patterned Au islands on surfaces (Figure 4.4 a), that were intended then to work as anchoring areas for the subsequent immobilisation of (thiol-funcitonalised) DNA nanostructures. The strategy employed Poly(methyl methacrylate) (PMMA) as a resist in the lithographic step. HMDS (hexamethyldisilazane) coating enables better adhesion of the hydrophobic resist PMMA and reduces the non-specific binding for the non-patterned area. HMDS was deposited by spin coating; a spin coating speed of 2000 RPM for 40 seconds was used to deposit HMDS on glass or silicon dioxide substrate surfaces. PMMA was then spin coated on HMDS coated substrates. The thickness of the PMMA layer corresponds to the spin coating speed and time used in the process. The thickness and the corresponding concentration, speed, and time are shown in the table 4.1 (the thickness was measured by AFM, allowing for the calibration of the parameters to be employed in the spinning cast deposition method).

Table 4.1 PMMA spin coating parameters

Concentration	Speed (RPM)	Time (s)	Thickness (nm)
1%	2000	40	52
1%	4000	40	34
2%	2000	40	80
2%	4000	40	50
4%	2000	40	210
4%	4000	40	116

Based on the thickness, a 2% in anisole PMMA solution was used in a spin coating procedure at 4000 RPM for 40 seconds. A thickness of 50 nm was needed for quick FIB milling. A thin conductive layer of gold (Au) was evaporated on top of the PMMA. The FIB was employed to scan the substrate surface following a designed pattern of dots arrays. Re-evaporation was carried out after forming the nanoapertures. Chromium (Cr) was evaporated as an adhesion layer to stabilise the adhesion of Au [127]. After a lift-off process in N-Methyl-2-pyrrolidone (NMP), the resist (PMMA) was removed from the substrate; this process also removed the metal layer present on top of the PMMA. As a result, the Au evaporated on the bottom of the nanoapertures formed Au islands on the surface. AFM scanning of the substrate shows the Au islands to be round shape with a diameter of about 210 nm and a height of 30nm (Figure 4.4 b).

The spacing of each island is around 2 μm corresponding to the pattern drawn by FIB milling. However, the height of the Au islands was revealed to be higher than expect. The Cr and Au was evaporated at about 8 nm but the outcome thickness of the Au islands was found to be of 30 nm. This was believed to be the result of an implantation effect of Ga^+ in the PMMA [128, 129]. The Ga^+ is was very likely implanted in the PMMA structure by the ion beam of the FIB. This might change the properties

of PMMA and result in residual PMMA after lift-off: the higher height represented the residual PMMA with a metal layer on top of it.

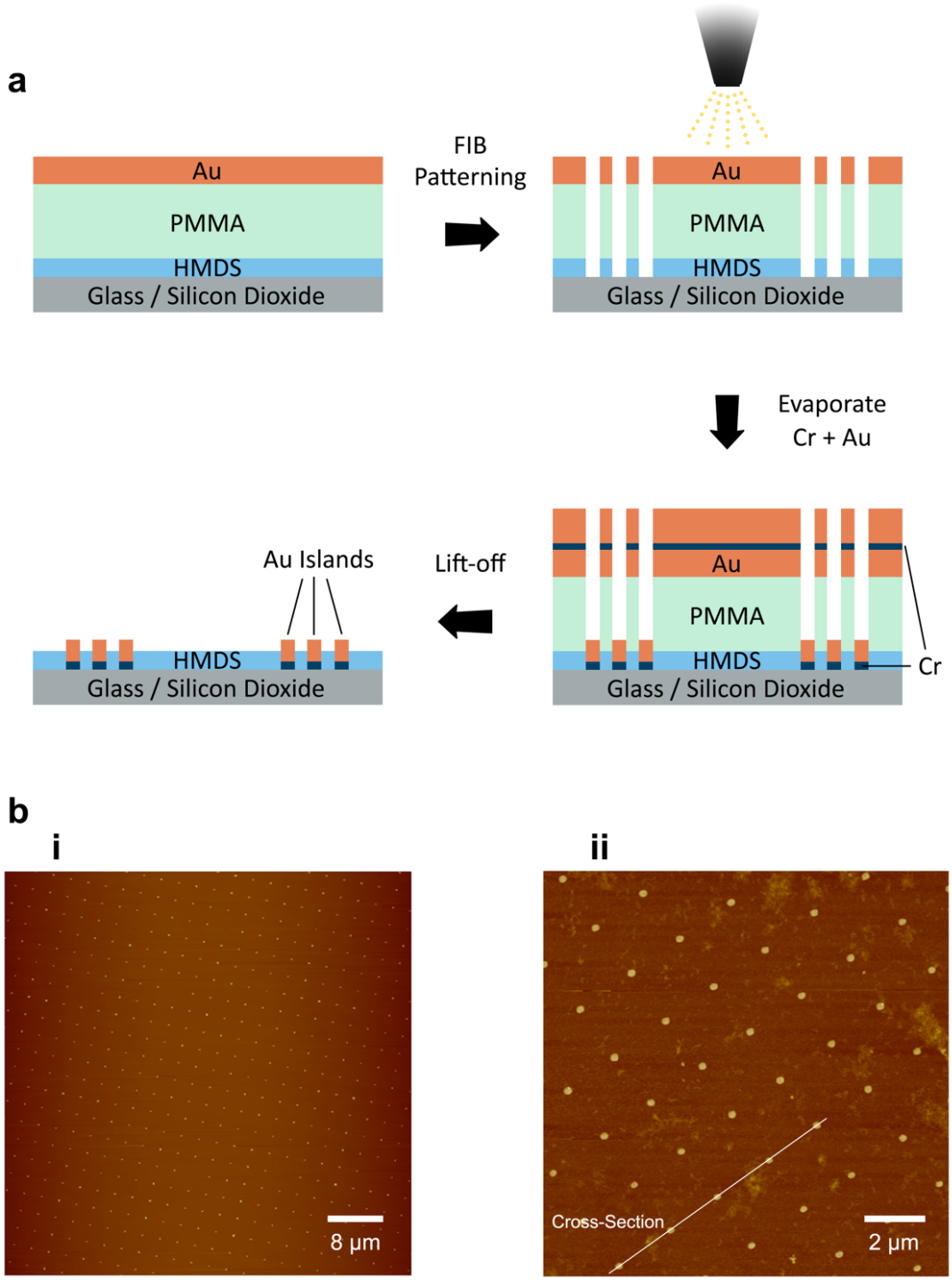

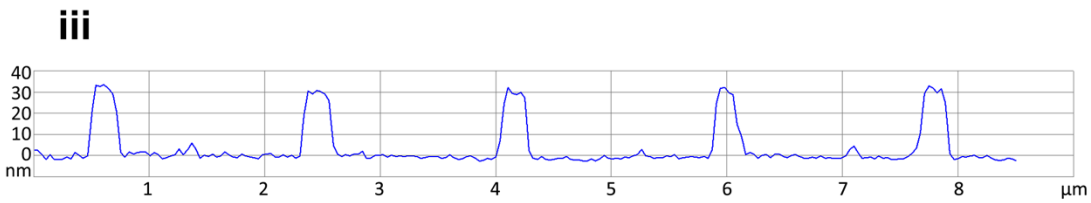

Figure 4.4 Schematic and AFM images of pattern of Au islands. **a)** Schematic of forming Au islands on glass/silicon dioxide surfaces using FIB milling. **b)** AFM images of Au islands: **i)** Large scale image of Au islands; **ii)** Zoom in image of Au islands, showing a distance around 2 µm of each roundish shape Au island with a diameter of about 210 nm; **iii)** Cross-section of Au islands shown in the inset of ii. The height of Au islands is represented as around 30 nm.

Form the section analysis of Au islands in Figure 4.4 b-iii, the height was measured as around 30 nm. However, the second time of Au evaporation was believed to deposited around 10 nm metal. In order to investigate this difference further, a lithographic approach was carried out without the metal re-evaporation step (Figure 4.5 a). After spin coating of HMDS/PMMA and Au evaporation, the substrate was scanned under FIB following pattern design. Then the scanned substrate was incubated in in NMP to remove the PMMA (lift-off), that this time does not have the Au conductive layer on top of it. A pattern of PMMA islands was then found on the substrate surface, as confirmed by AFM. The island found after patterning indicate the differences of the theoretical calculation of the height of island (thought to be 10 nm) but turned out to be 30 nm under AFM. These PMMA islands were found to be of ca. 15 nm in height (Figure 4.5 b), and are believed to be formed by the Ga^{+}, via a potential chemical change

of the exposed PMMA resist layer that was then not soluble in the lift-off solvents. The remain 15 nm of PMMA island and re-evaporated metal layer together formed the 30-nm height island showed in the Figure 4.4 b. Therefore, employing this facile procedure it is possible to use PMMA as a negative resist for FIB-induced direct nanoscale patterning of a surface.

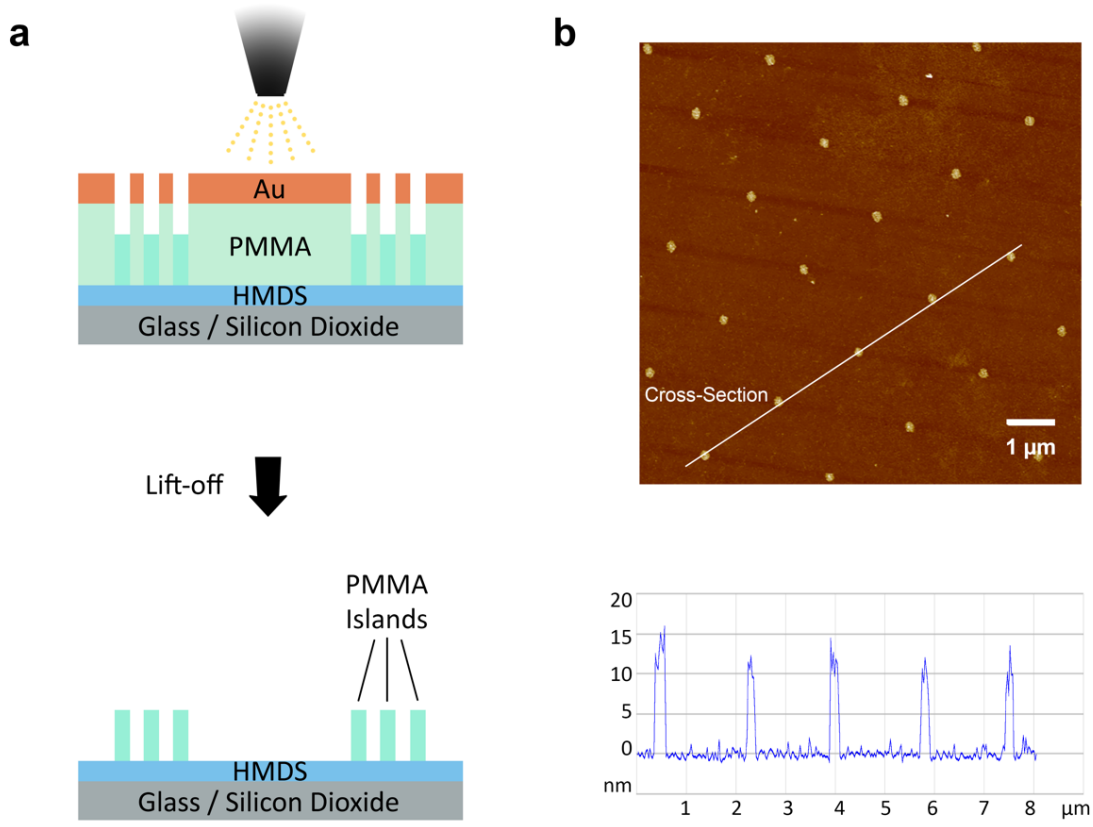

Figure 4.5 Schematic and AFM image of pattern of PMMA islands. **a)** Schematic of forming PMMA islands. **b)** AFM image of PMMA islands. Cross-section analysis shows the height of around 15 nm for PMMA islands.

Additional work is needed to control the PMMA thickness of the islands generated in this way (by changing the corresponding ion beam settings). However, it is clear from these preliminary results that it is possible to perform patterns on substrate surface using FIB techniques with sub-200 nm horizontal resolution and sub-10nm in vertical resolution. Because of the focus of this work/thesis, we decided not to investigate this further at the present time, and instead developed a complementary approach as discussed in the following section.

4.2.2 FIB Patterned Nanoapertures

In order to fabricate the nanopatterns needed for our project, we moved away from the patterning approach described in the previous section and developed a reversed strategy to fabricate our nanopatterns. Instead of forming Au islands, nanoapertures were fabricated on metal coated substrates. Figure 4.6 shows the schematic of this strategy and the AFM validation of the fabricated substrate.

The substrates themselves consist of a gold (Au) metal layer on glass or SiO_2 (with Cr adhesion layer under Au). Nanoapertures were formed via Focused Ion Beam nanofabrication. The exposed substrate surface (the underlying SiO_2) is designed as the DNA nanostructures binding area, while the remaining metal area would protect the substrate from nonspecific binding of DNA origami. The spacing of the nanoapertures can be controlled via FIB programing and varies for investigation goals. The size, shape, and arrangement of the apertures are also controllable to meet different requirements for further research.

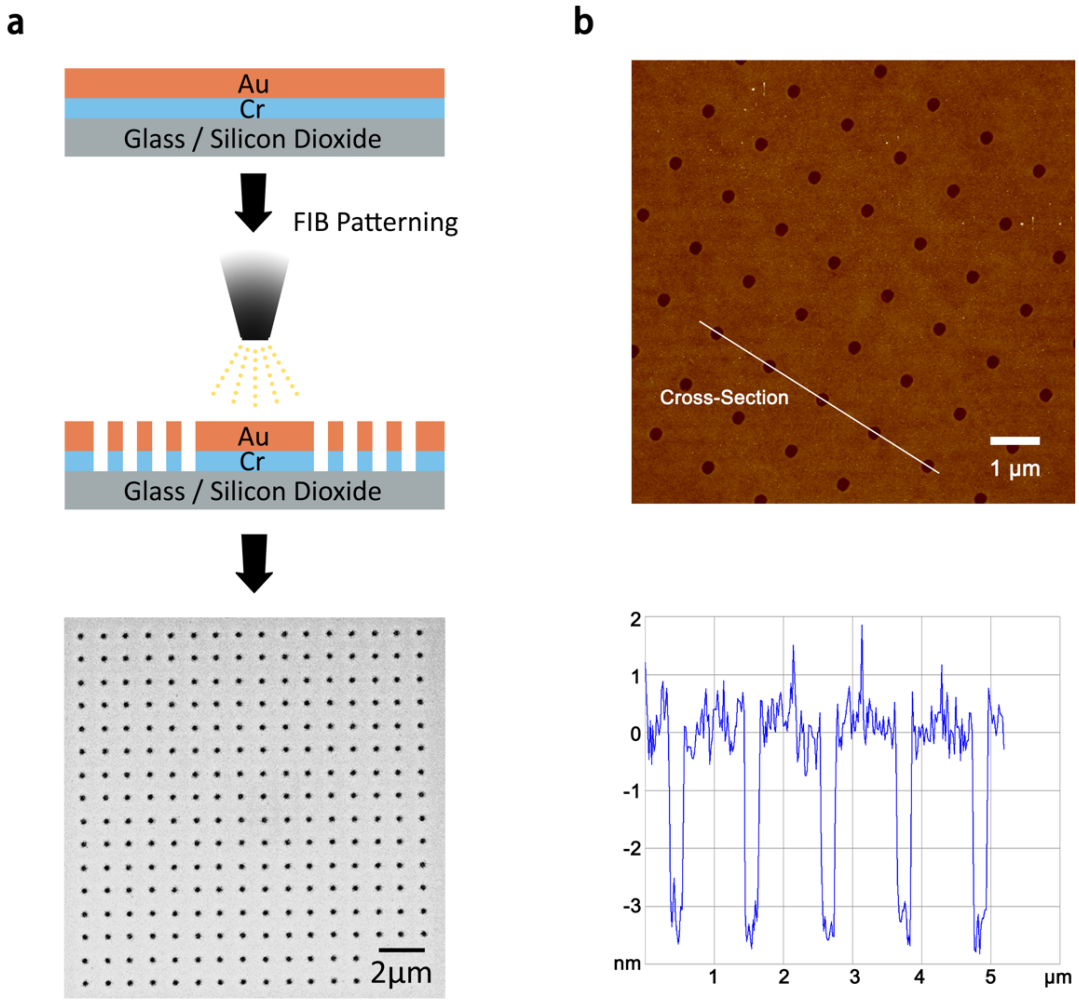

Figure 4.6 Schematic and SEM/FIB images of FIB nanofabricated surface. **a)** Schematic of fabricating nanoapertures via FIB. SEM image shows patterned nanoapertures on surface. **b)** AFM image of nanoapertures arrays. Cross-section shows that the depth of apertures is around 3 nm.

This strategy allowed the facile fabrication of a patterned substrate which is also reusable. We used FIB to fabricate nano-apertures arrays on the metal coated substrates with just one lithographic step. Different parameters have been varied in order to obtain the specific designed pattern (Figure 4.7). The nanopatterns with different sizes,

spacing and arrangements can be designed to meet different requirements for nanostructures immobilisation.

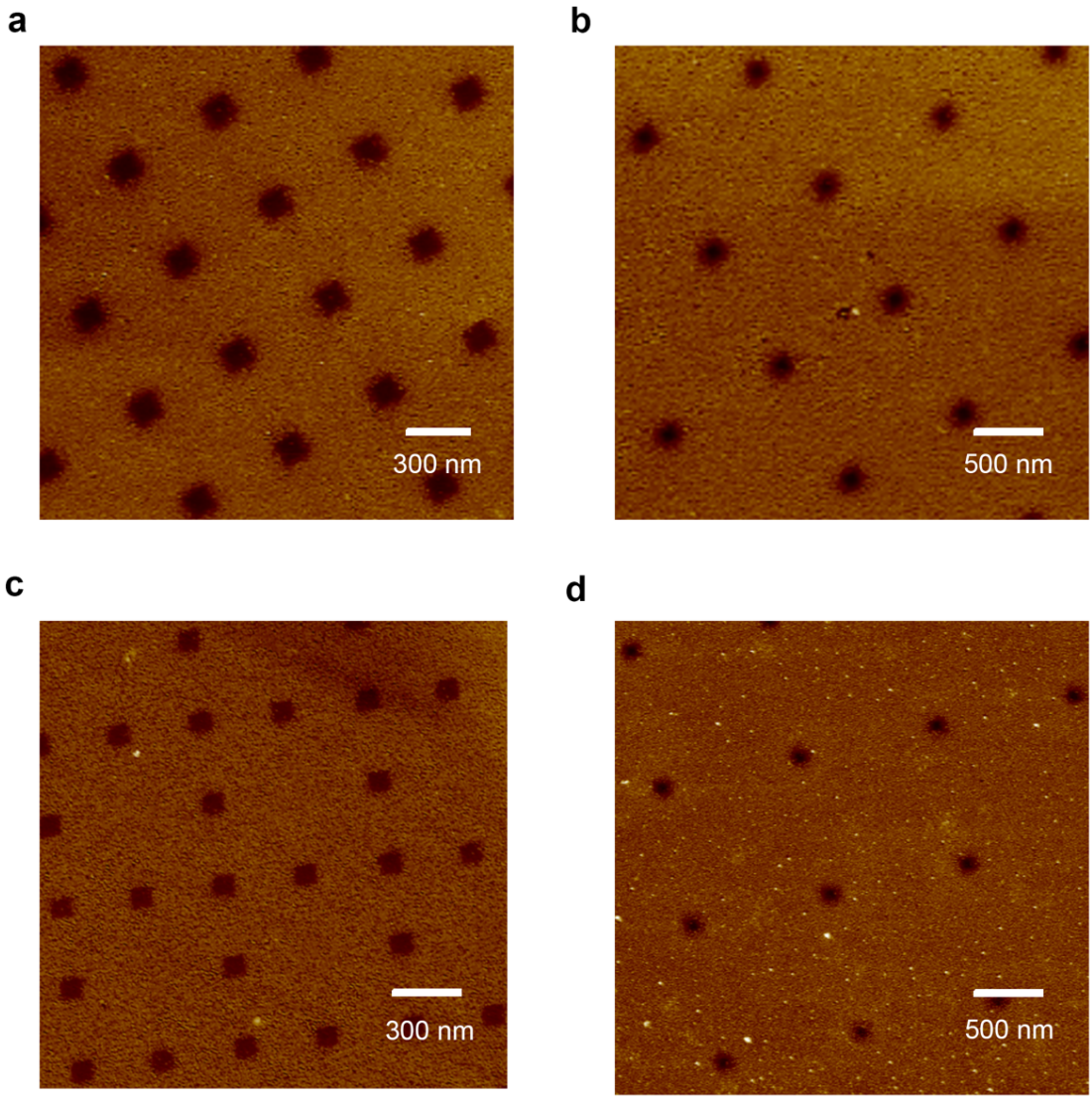

Figure 4.7 Nanopatterned substrates with various of parameters. **a)** Nanoapertures as 200 × 200 nm squares with a spacing approximately 300 nm. **b)** Nanoapertures as 200 nm diameter round shapes with a spacing approximately 1 μm. **c)** Frame type of

arrangement of nanoapertures. **d)** Nanoapertures as 100 nm diameter round shapes with a spacing approximately 1 μm.

4.2.3 DNA Immobilisation in Patterned Arrays

For our studies, we employed plain rectangular DNA origami structures with 120 nm in length and 60 nm in width to be assembled in the patterned nanoapertures (Figure 4.8 a). The rectangular DNA was modified with four amino anchors on the four corners for covalent binding to the carboxylic silane treated surface (Synthesis of DNA origami structure with amino modification was discussed in Chapter 2, section 2.3.3.3). The covalent bonding was carried out via EDC/NHS reaction between the amino groups on DNA origami and carboxylic groups on the silanes (see Chapter 3, section 3.1.3.4) (Figure 4.8 a and b). The amino anchors and their functions were validated via incubation removal approaches (see Chapter 3, section 3.2.5 for details). The covalent bonding of DNA nanostructures to the surface was revealed to be stable in long term buffer incubation.

AFM images show the successful individual immobilisation of rectangular DNA origami in the patterned nanoapertures (Figure 4.8c). This was a preliminary approach to test the controlled immobilisation of origami nanostructures on surfaces. The rectangular shaped structures immobilised in the nanoapertures were not clear enough via AFM, probably due to the similar height exhibited by the surrounding metal. Therefore, an improved strategy based on QD(s) modified triangular DNA origami was developed, and will be discussed in the next section.

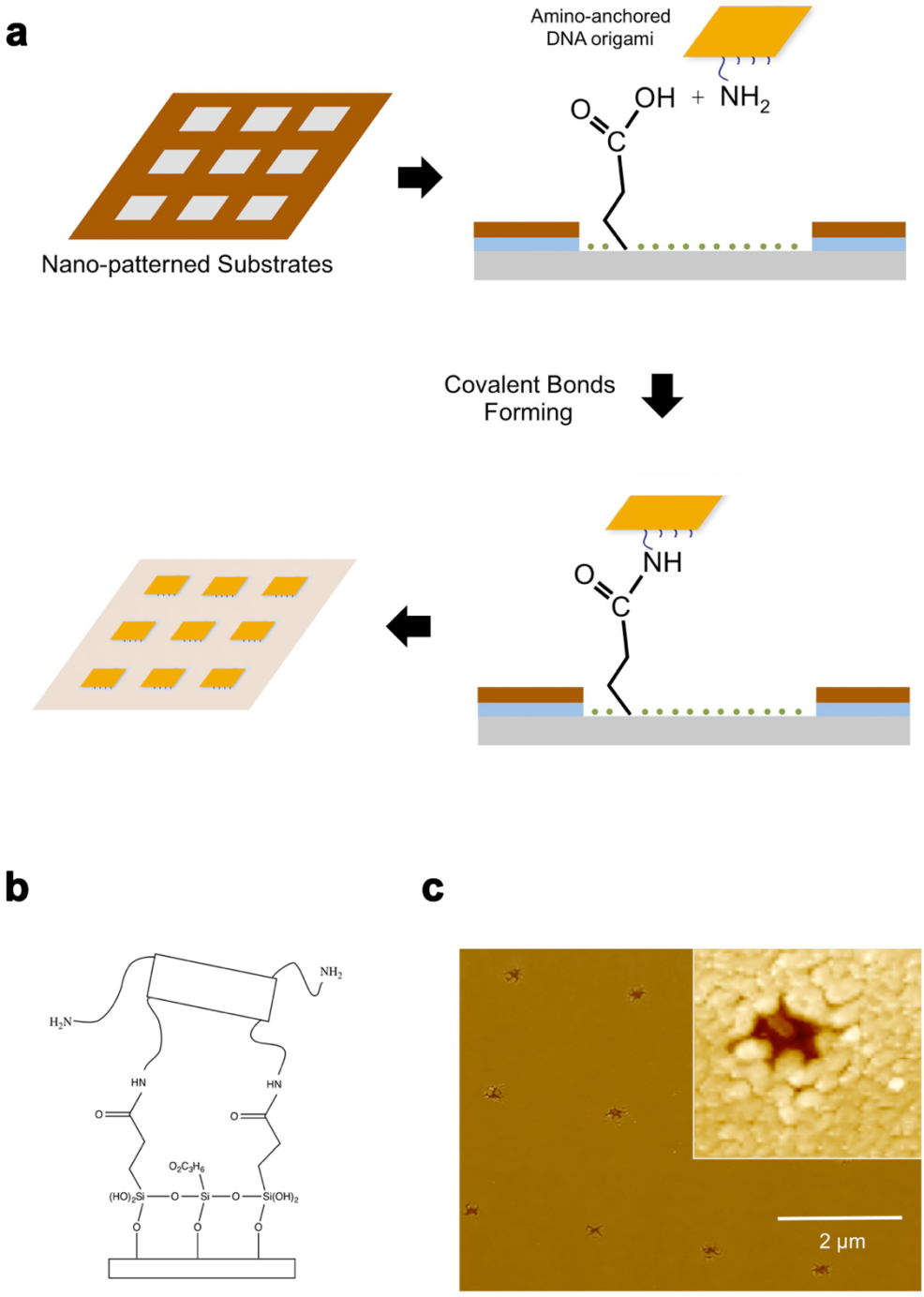

Figure 4.8 Controlled organization of rectangular DNA origami on nano-patterned surfaces. **a)** Schematic representation of DNA origami immobilization on the exposed patterned glass/silicon dioxide surfaces (nanoapertures). Covalent bond (amide bond) is formed between amino-anchored DNA origami and glass/silicon dioxide surface. **b)**

Schematic of covalent bond for the immobilisation of origami on silanised surface. Each origami is modified with four amino anchors on the four corners in order to strength the immobilization (only show two on scheme) [130, 131]. **c)** AFM image for validation of the DNA origami immobilisation in the nanoapertures.

Because triangular DNA origami gave us higher yield in functionalisation (and are known to be more rigid structures) compared to rectangular origami, we employed triangular DNA nanostructures in the studies presented here. Triangular DNA origami structures of 120nm by side were designed and assembled as molecular breadboards for the assembly of individual CdSe/ZnS core/shell QDs (Figure 4.9). Binding sites for (streptavidin-coated) nanocrystals were incorporated along the axis of the DNA nanostructure using biotin-labelled staple strands. This allowed us to design individual DNA origami scaffolds for the tethering of either one, two, or three QDs per DNA nanostructure, with a 60nm interdot spacing. Figure 4.9 b shows AFM images of the triangular DNA origami employed, and the successful organization of individual QDs on the DNA scaffold. The yield of QD attachment on our triangular DNA origami was found to be of 86% for three QDs, 89% for two QDs, and 91% for one QD per origami (also see Chapter 3, section 3.2.2.2). We designed our triangular DNA nanostructures to exhibit 15 amino-terminated DNA strands protruding out of plane of the origami, in addition to the QD-anchoring staple strands (Figure 4.9 a). These amino anchors will provide binding sites to attach to the carboxylic silane treated surface. The large numbers of amino anchors increase the strength of immobilisation.

In order to generate predefined locations for the immobilization of the aforementioned QD-labelled DNA nanostructures from solution to surfaces, we

patterned nanoaperture arrays on silicon wafers and transparent insulating glass coverslips. A one-step Focused Ion Beam (FIB) lithography process was employed to selectively fabricate arrays of nanoapertures on metal coated (1.5 nm Cr, 3 nm Au) substrates as discussed in last section 4.2.2. The employed strategy allows for the facile pattering on transparent surfaces and is of general applicability for the concomitant fabrication of cavities in different materials. Moreover, the fabrication can be easily tailored towards inter-aperture spacing of a few µm to prevent any crosstalk between optical signals from neighbouring QDs once immobilized on the patterned surface.

The exposed SiO_2 surface in the fabricated nanoapertures can be chemically modified to covalently tether amino-functionalized moieties, including DNA origami. Briefly, the triangular DNA origami solution was cast on the patterned substrate in the presence of Mg^{2+} (to induce initial physisorption) and carboxyethylsilane. The latter forms carboxylic terminating monolayers on the SiO_2 surface exposed in the patterned nanoapertures. Standard amide coupling and activating agents were then used to activate the carboxylic groups. Therefore, upon silanisation (with carboxyl groups) of the SiO_2 surface exposed in the patterned nanoapertures, we covalently tethered our QD-labelled DNA Origami.

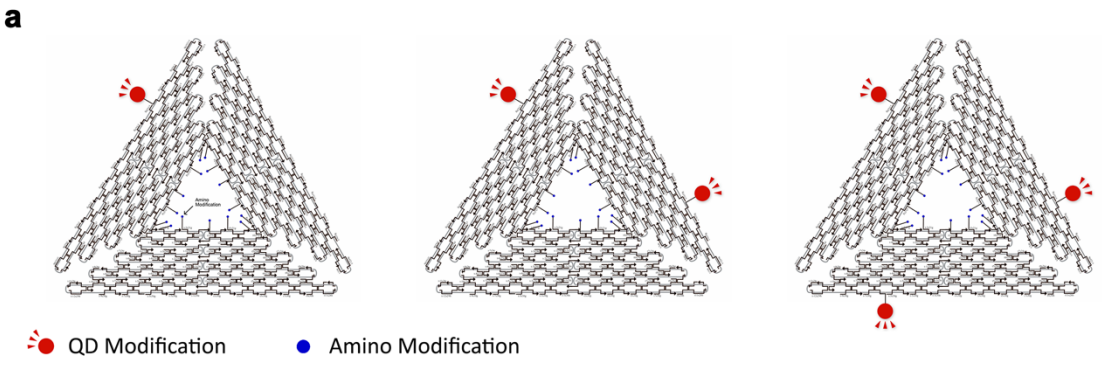

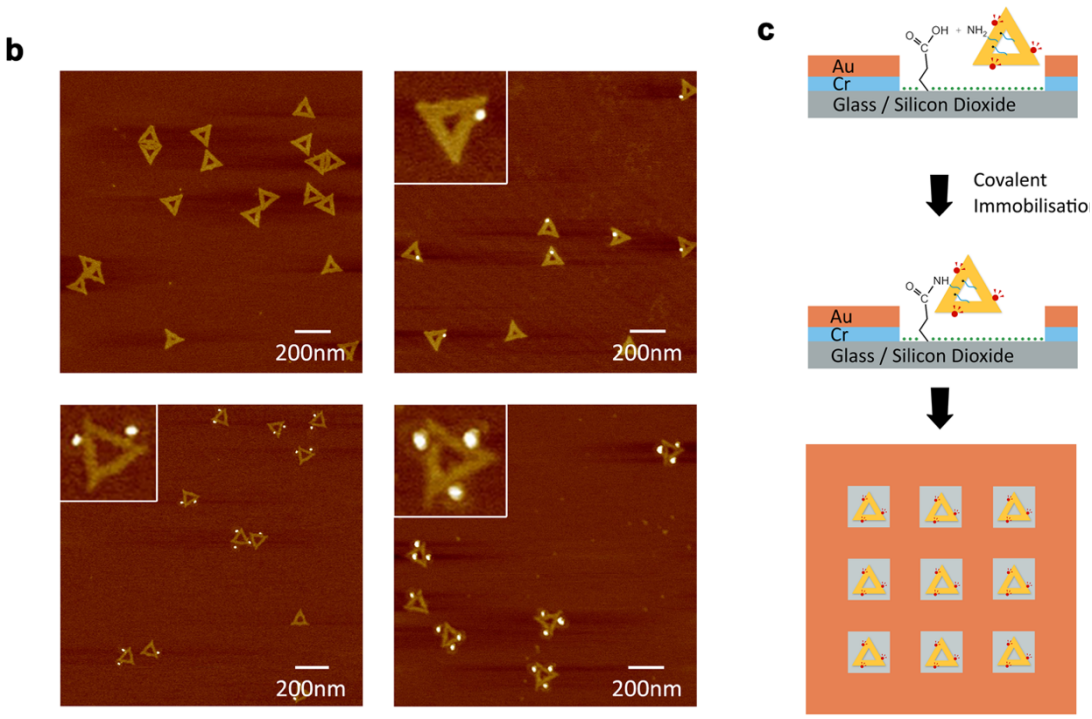

Figure 4.9 Schematic and AFM images of QD(s) modified triangular DNA origami. **a)** Schematic of DNA origami with 1, 2, and 3 QDs modifications. All the origami structures were designed to be assembled with 15 amino modifications on the inner edges. **b)** AFM images of pristine origami, and modified origami functionalized with one, two, and three QDs. **c)** Schematic of controlled immobilisation of triangular DNA origami.

Figure 4.10 shows AFM images demonstrating the selective placement of three (Figure 4.10 a), two (Figure 4.10 b) and one (Figure 4.10 c) QD(s) per nanoaperture, via the covalent immobilisation of arrays of QD-labelled triangular DNA origami nanostructures on SiO_2 (also see Figure 4.11 for the zoom out AFM images of controlled immobilisation of DNA origami shown within triangular wireframes). We have employed nanoapertures of different sizes (easily tailored via FIB patterning), ranging

from 120nm (the size of the DNA triangles) to 250nm. Notably, even in the larger 250 nm cavities we obtained close to complete immobilisation of a single triangular DNA origami per aperture (90%), rather than multiple (3%), or none (7%). Counted the yield of QD(s) modification, the overall yield of single-dot assembly was found to be of 82% over arrays of 64 μm^2 and 80% for double-dots and 77% for triple-dots. This high yield of one-to-one immobilisation of DNA origami per nanoaperture is most likely due to steric hindrance effects and electrostatic repulsion among the DNA triangles upon their physisorption in the apertures (via a Mg^{2+} bridge) prior to covalent attachment (see also the Methods section and the SI). As a proof of principle, we present here the results obtained with the large apertures because of the higher clarity of the AFM images. The obtained QD assembly is highly selective as the employed QD-labelled DNA origami do not bind to the metal surface surrounding the apertures. (Non-specific adsorption can be easily minimized by simply rinsing the substrates with buffer solution and DI water after the covalent immobilisation). Evidence of this is shown in Figure 4.10 d, where individual apertures fabricated to exhibit a 1 μm spacing are clearly resolvable via conventional epifluorescence microscopy imaging. This further demonstrates the applicability of the presented strategy to insulating transparent glass coverslips. Cross-section analysis is also carried out to reveal the right height of QD (7nm) in the nanoapertures (Figure 4.10 e and f).

Notably, the platform presented here is reusable by simple Ultraviolet/Ozone treatment of the substrate, followed by a mild ultrasonic cleaning in water, and final rinsing. This facile cleaning procedure, allows for the complete removal of DNA nanostructures in the nanoapertures, without damaging the surrounding metal nor the underlying SiO_2 surface. The yield of subsequent QD-labelled DNA origami

immobilisation on recycled substrates is not meaningfully affected by this cleaning process, remaining of ca 80% in single-dot patterning (Figure 4.11).

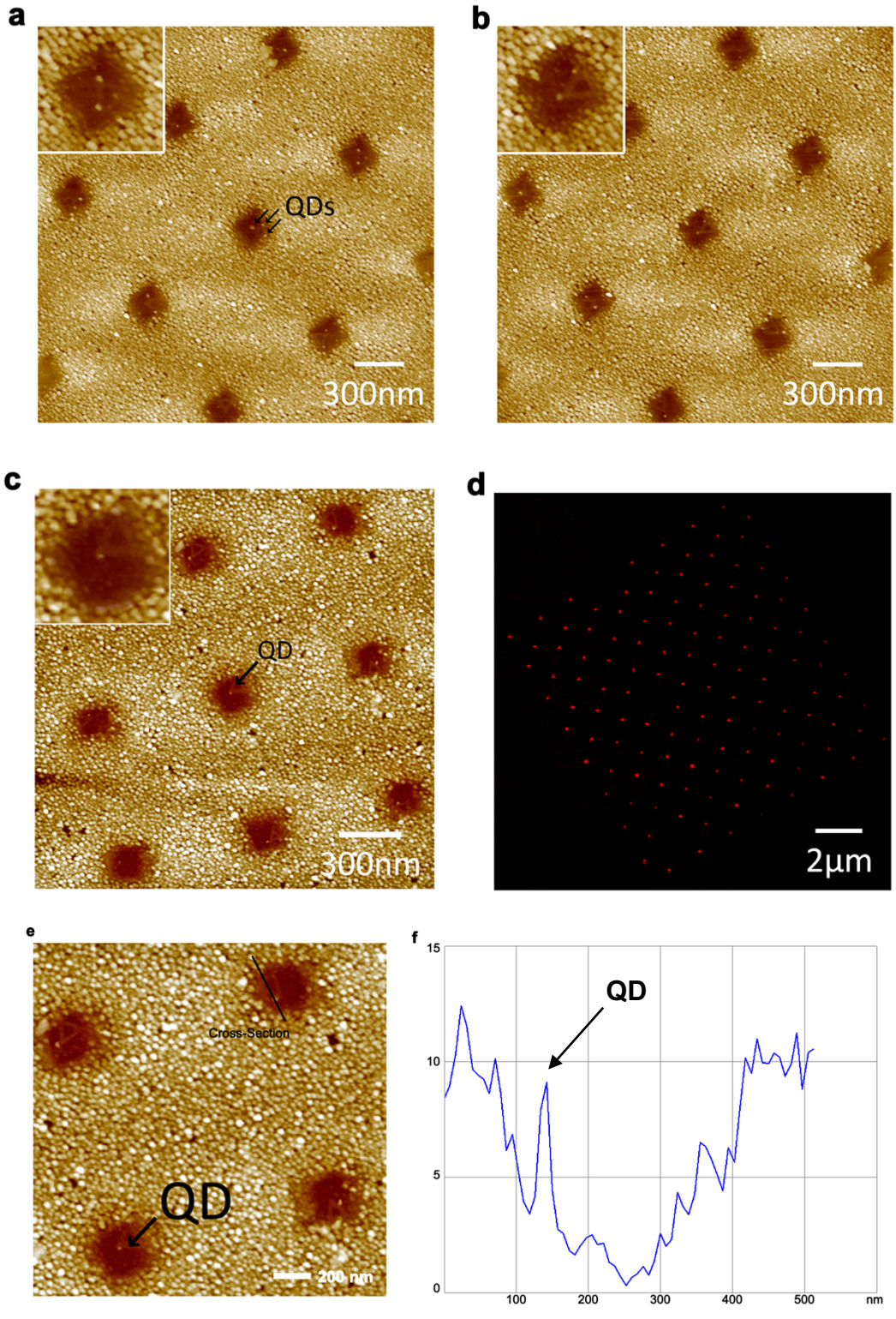

Figure 4.10 Images of the assembly of QDs in nanoarrays via the covalent immobilisation of QD-labelled triangular DNA origami in pre-patterned nanoapertures. **a)** AFM image for the case of 3 QDs per origami, and hence per aperture; **b)** AFM image for the case of 2 QDs; **c)** AFM image for the case of 1 QD. **d)** Epifluorescence microscopy image of a glass substrate patterned with 3 QDs per 1μm spaced nanoaperture: each nanoaperture is optically resolvable. **e)** Cross-section analysis of DNA origami in the nanoapertures. **f)** Cross-section curve indicate the right height of QD (7 nm) and DNA origami.

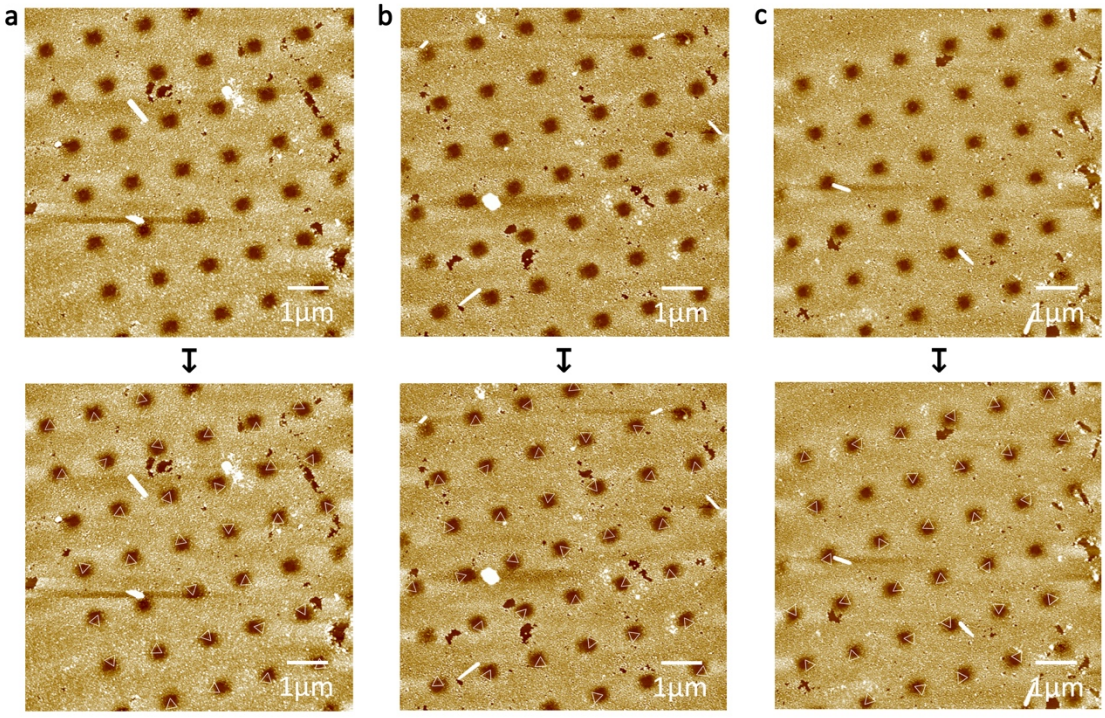

Figure 4.11 Reuse of the patterned substrate. **a)** Re-immobilisation of three QDs modified DNA origami on the patterned substrate that cleaned from last usage. The

triangular outlines in white colour show the location of each DNA origami. The same reuse approaches were applied on two QDs **b)** and one QD **c)** modified origami.

Furthermore, if needed, only the DNA in the nanoapertures can be removed, leaving the QDs in the array. This can be achieved by exposing the substrate only to Ultraviolet/Ozone treatment without any subsequent sonication and/or rinsing step. The plasma removed the DNA nanostructures and keep the QDs in the remaining position. Figure 4.12 shows that after such treatment most of the QDs remain in the nanoapertures, while the DNA nanostructures are successfully removed. In this case, the overall final yield of single-QD patterning is slightly reduced to ~65%.

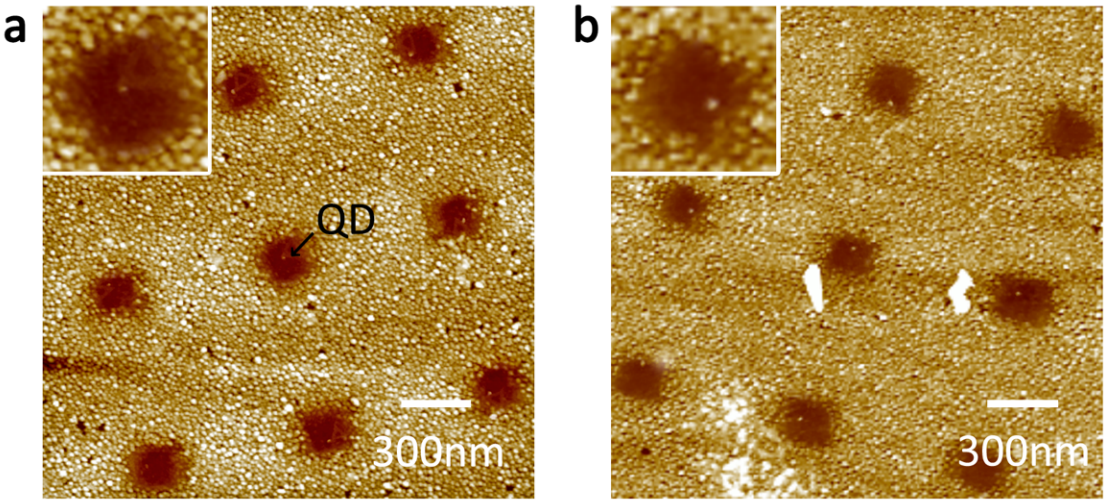

Figure 4.12 AFM images of single-QD patterning and UV/Ozone treatment. **a)** Single-QD patterning via the covalent immobilisation of triangular DNA origami labelled with one QD: 82% yield; **b)** AFM image of the same sample after UV/Ozone treatment showing the successful removal of the DNA origami but the remain of QD nanoparticles in the apertures.

4.3 Summary

In summary, we have developed a reusable platform of general applicability for the assembly of individual nanoscale moieties with single-molecule control, in array configurations. As a proof of concept, we presented the patterning of individual CdSe/ZnS colloidal QDs on silicon and transparent insulating glass coverslips. Single-dot patterning was achieved via the use of DNA nanostructures as a scaffolding material, and their immobilisation in fabricated metal-based nanoaperture arrays. We demonstrated high level of control in the assembly of individual QDs (either one, two, or three) in nanoarray configurations, with a 60 nm interdot spacing within each cluster, and with a yield of up to 82% in single-dot patterning. The results presented here are specifically of interest for the development of single-QD based optoelectronic devices with applications in light harvesting, quantum information technology, data storage, and nanoscale optical circuitry. Additionally, this highly stable and reusable platform can be designed to exhibit different geometrical arrangements, and be employed for parallel single-molecule investigations of various nature, depending on the nanostructures employed. A cell adhesion study based on this nanopatterned substrate will be discussed in Chapter 5.

Chapter 5

Patterned DNA Origami for Cancer Cell Adhesion: Multi-valent Investigations with Single-Molecule Control

The patterned DNA origami substrate, presented in the previous chapter, is a powerful platform for various of applications, due to its ability to control the organization of surface of individual moleucles/nanomoieties (e.g. QDs) with nanoscale spatial resolution (in principle down to 6nm [28]). In particular, based on the variability of modification on DNA origami, cell behaviour and signal pathways can be potentially studied at the single molecule level. Via a collaboration with the Barts Cancer Research Institute, a preliminary investigation of cancer cell adhesion as a function of the nanoscale spacing of integrin binding ligands will be presented in this chapter. The cooperation of integrins with epidermal growth factor (EGF) was investigated, based on the multiple modification capability of DNA origami and the controlled immobilisation of this nanostructure.

5.1 Introduction

The microenvironment is important in progressing cell behaviour and dictates cell fate. The extracellular matrix (ECM) and in particular the roles of growth factor, hormones, signalling molecules and protein complex have been extensively investigated in recent years with interesting and fascinating results [132]. The structures and functions of cells rely on the adhesion to the ECM in a large part to control the tissue architecture and cell motility [133]. The ECM helps the construction of tissue scaffolds and gathers the connection to other cells. The cell behaviour is controlled and affected by the physical properties of the ECM including its biological/chemical geometry and surface topography [134]. The ECM is formed of an interlocking network of glycosaminoglycans (GAGs) and fibrous proteins. The structural proteins (collagen, elastin) and adhesive proteins (fibronectin, laminin) are two main kind of fibrous proteins [135] which are important in maintaining cell structures and interconnecting cells to the ECM.

5.1.1 Focal Adhesions and Integrins

Focal adhesion (FA) is an adhesive behaviour of the cell with the ECM via the interaction between transmembrane proteins (integrins) and their extracellular ligands, as well as the connection of intracellular multiprotein with the actin cytoskeleton. Focal adhesion and its complexes are key in cell behaviour research. Through focal adhesion, cells communicate with the ECM via forming several macromolecular structures and generating various nano-molecules for attachment and signal transduction [136]. The

communication with the ECM and other cells enables the regulation of cell proliferation, survival, migration, and invasion [137]. The large molecular assemblies' of focal adhesion contain massive structures and molecules such as numerous factors and protein complexes [138]; they are responsible for various functional activities for cell behaviour regulation.

The integrin family is an important part of focal adhesion complex structures [139]. These transmembrane cell adhesion molecules are normally constructed with two non-covalently associated subunits, α and β, to form heterodimers structures. These two subunits are both type I single-pass transmembrane proteins [140] (Figure 5.1). The binding of integrins to their extracellular domains is the primary approach which responsible for cell adhesion to the ECM. It has been shown that integrins ligands are important for embryonic development [141], tissue maintenance [142], tumorigenesis [143] and haemostasis [144]. The information of the adhesive situation, cell position, cell migration, and signalling environment are communicated by integrins between the ECM and cells.

Based on different permutational combinations of α and β subunits, researchers have revealed 24 types of integrins in mammalian cells [145]. In humans, these combinations are known to be formed from 8 different α and 8 different β subunits that generate heterodimers. Different functions and ligand specificities are regulated by different types of heterodimers complexes [146]. Expression of the different heterodimers is extremely variable; for example β1 integrins are common in many human cells, but β6 is only combined with αυ found in epithelial cells [147]. The integrin αυβ6 can be found spatially in the processes of tissue remodelling including cancer: this makes the integrin αυβ6 and its binding molecules as crucial targets for cancer research.

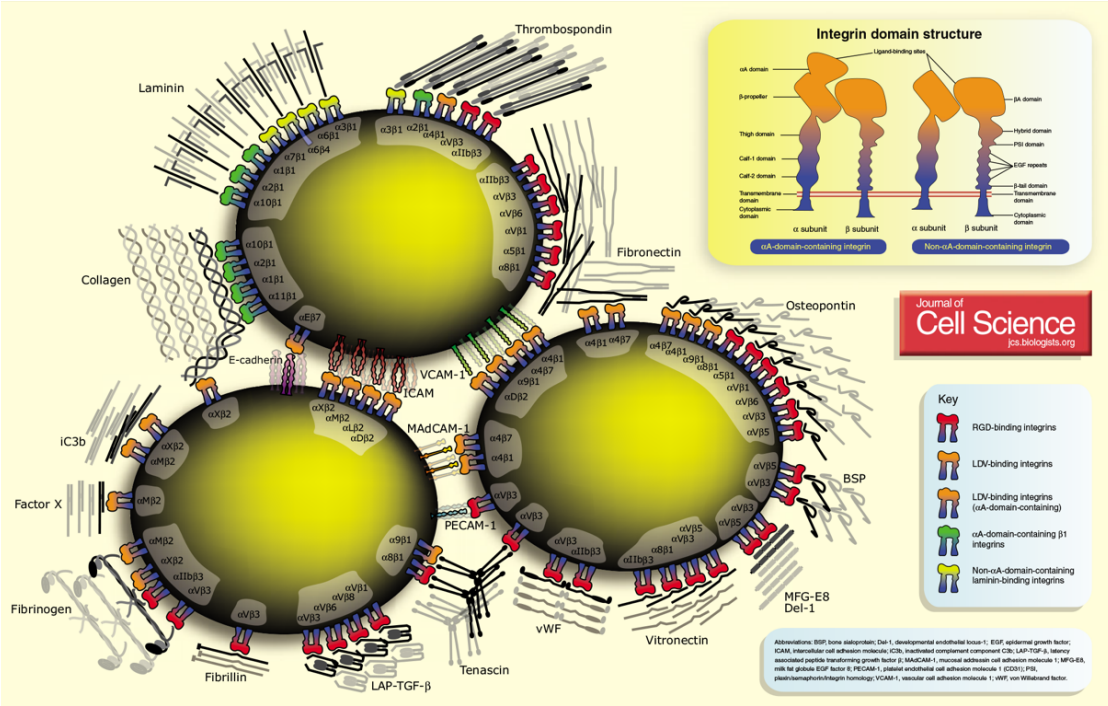

Figure 5.1 Integrin ligands family [139].

Integrins are known to bind to the ECM through not only large proteins but also small peptides. The tripeptide, arginine-glycine-aspartic acid (RGD) sequence containing peptides, is a crucial molecule which directs the cell adhesion via constructing the fibronectin as a minimal component [148]. RGD can selectively bind to different types of integrins and many adhesive proteins contain this sequence [149]. These RGD-containing adhesion-promoting proteins and peptides are important in cell adhesion investigations. Notably, it has been demonstrated that nanoscale clustering of RGD domains enhances cell attachment to substrates and reinforcement of focal adhesions [43]. Moreover, cell spreading efficiency are also controlled by different geometric arrangements of liganded sites with a dramatically increase when at least four ligands are spaced within 60 nm or less [44].

Therefore, it is crucial to study cell focal adhesions with single-molecule resolution, and this can be achieved by controlling the spatial arrangement of ECM-mimicking and cell-binding peptides, with true nanoscale control. The approaches used so far have demonstrated this but are limited by the ability to control the spatial arrangement on surfaces of only one type of ligand at the time (see again section 1.3 and figure 1.7). Utilising the multivalence capability of DNA origami, and a patterning strategy (e.g. the one presented in this thesis: see chapter 4), different types of ligands can be controlled within one arrangement, in order to carry out investigations on cooperative effects in the establishment of cell focal adhesions.

5.1.2 Peptide A20FMDV2

Among the peptides affecting cancer cell behaviour, A20FMDV2 (with a sequence of NAVPNLRGDLQVLAQKVART), a linear conformation of RGD peptide, was found to bind more selectively to αυβ6 integrin [150], an integrin family that is over-expressed in specific types of cancers, such as colon and oral cancer [151, 152]. A20FMDV2 is derived from the VP1 coat protein of foot-and-mouth-disease virus [151] as shown by our collaborator, Professor John Marshall at the Barts Cancer Research Institute. This is a two disulphide-cyclised variant leaded peptide which has a general structure containing an Arg-Gly-Asp sequence at the tip of a hairpin turn followed immediately by a C-terminal helix (Figure 5.2). In this peptide structure, the two Leu residues at Asp^{+1} and Asp^{+4} position face outside of the helix, which allows an extra hydrophobic interaction with αυβ6 integrin. The hydrophobic interaction added with RGD interaction make A20FMDV2 a strong binding peptide to the αυβ6 integrin.

The linear structure of A20FMDV2 peptide is stable in many conditions including wide arrange of pH and temperature. The peptide remains functional even when heated up to 97 ^{o}C (from the data that was acquired by our collaborators at John Marshall's group). This makes it possible to apply A20FMDV2 in many approaches including thermal synthesis with DNA nanostructures.

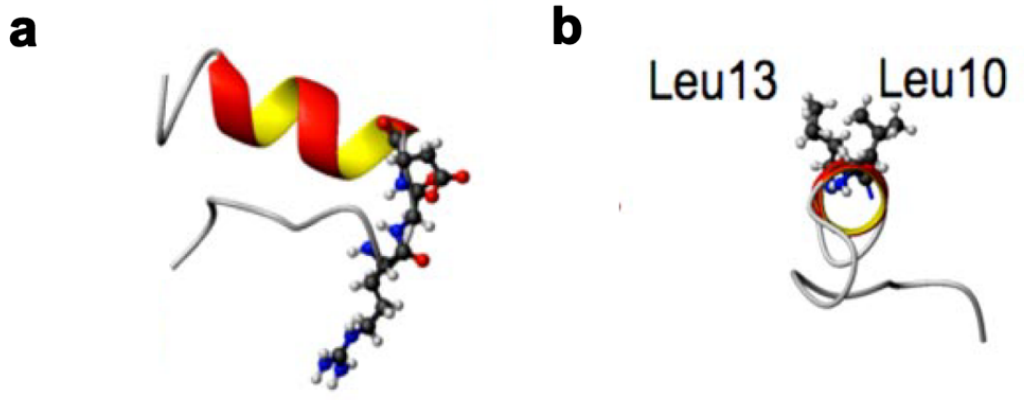

Figure 5.2 Schematic of peptide A20FMDV2 [151]. **a)** Ribbon diagrams for the side view of the A20FMDV2 structure with the RGD residues in ball-and-stick mode. **b)** The end-on view of and A20FMDV2 structure. The Asp^{+1} and Asp^{+4} residues are shown in ball-and-stick mode.

For these reasons, we have engineered DNA origami with A20FMDV2 peptides in order to study cancer cell adhesion with single-molecule control and nanoscale spatial resolution: we will discuss this in this chapter.

5.1.3 Epidermal Growth Factor (EGF)

Another type of family of cell adhesion molecules that can influence normal cancer cell differentiation is represented by growth factors. The growth factor is a

varied group of polypeptides that regulate cell proliferation [153]. The synthesis and functionality of different growth factors is restricted to defined tissues. Epidermal growth factor (EGF) is essential in modifying epidermal proliferation. Schreiber et al. reported EGF as a potent inducer for angiogenesis *in vivo* as well as a binding ligand to endothelial cells *in vitro* [154]. EGF was also reported to attractants for a heart vascular endothelial cell line [155]. Several studies had shown the EGF and its receptor, EGFR are important in the cancer therapy investigations [156]. For example, Activated EGF receptor (EGFR) signalling was shown to be fundamental in glioblastoma progression. EGF treatment induced in cancer cell was reveal to up-regulate the cell adhesion molecule-1 (VCAM-1) expression and resulted in promotion of tumour cell interaction with ECM as well as tumour cell invasion [157]. As a result, EGF was chosen here as a cooperative ligand to A20FMDV2, in order to engineer DNA origami to investigate cancer cell adhesions with single-molecule control.

5.2 Results and Discussion

In order to investigate the molecular mechanism of integrin dependent biological responses and their cooperation with EGF that modulate cell behaviour in specific cancer cells (colon, oral), we engineered DNA origami nanostructures with A20FMDV2 peptides and/or EGF. These were immobilised on patterned substrates, employing the strategy we developed and presented in chapter 4, in order to mimic the ECM experienced by cutaneous melanoma cells, and study cell adhesion with single-molecule control and nanoscale spatial resolution.

This approach is unique due to the ability to not only control the spacing between cell-adhesion ligands with true nanoscale control (down to 6nm, intrinsic to DNA origami structures: see again section 3.2.1) but also to immobilise multiple and different molecules (peptides A20FMDV2 / EGF) on the same DNA nanostructure. We have indeed demonstrated this multi-valent ability via the assembly of different QDs (see Chapter 3, section 3.2.2.3); we will now take advantage of this property for cancer cell adhesion investigations.

Notably, to the best of our knowledge this DNA-origami based strategy is the only approach that can overcome the limitations of the nanopatterning and assembly strategies employed so far in the investigation of cell-adhesion with single integrin control/resolution (see again our sections 1.3 and 5.1.1). Indeed, while the copolymer strategy developed by Spatz allows to control the nanoscale spacing of cell-adhesion peptides [43], and the approach presented by Schvartzman et al. showed how integrin clustering is key to these studies [44], neither of the two strategies can investigate the role of multiple ligands (and their cooperation) on the same substrate. This is due to the intrinsic limitation of these otherwise powerful strategies: the same metal has to be used in the assembly of the anchoring nanodots, hence it is not possible to tether two different peptides on two different anchoring dots, with nanoscale spatial control. Interestingly, polymer brushes can be modified with different peptides, but there are limitations in controlling local densities on the substrate surface with this approach, unless a post-processing strategy is developed via a subsequent nano-patterning (but this has yet to be demonstrated, and would anyway require multiple time-consuming and expensive lithographic steps).

In the following sections, we will discuss how by combing DNA nanotechnology tools (functionalised DNA origami: Chapter 3) with our nanopatterning strategy (Chapter 4), we can fabricate biochips for the investigation of cancer cell adhesion complexes with single-molecule control and nanoscale resolution.

5.2.1 Engineering of DNA Origami

DNA origami was modified with A20FMDV2 peptide and/or EGF. For the A20FMDV2 peptide modification, a sticky end complementary binding strategy was used to control the density of peptides on the origami (see Chapter 2, section 2.3.3.4) (Figure 5.3). The A20FMDV2 peptide was first conjugated with ssDNA which was designed to be complementary to the sticky ends present on the DNA origami by design. The conjugation was carried out via maleimide-thiol conjugation which binds the thiol group (on the cysteine modification of A20FMDV2) with deprotected maleimide (on ssDNA). The conjugation products were validated and purified via size exclusive HPLC (Figure 5.3 c). The shift of the DNA absorbance peak indicates the change of molecule weights after conjugation. The larger molecules were believed to be the peptide-ssDNA conjugation and collected via combining the effluent among the peak time area. The yield of conjugation was calculated as 63% from the peak area. The conjugations then were concentrated via freeze dry and resuspension. The density of the peptides per DNA origami was controlled by sticky ends modification. The numbers of complementary sticky ends on the origami corresponded to the intended numbers of peptides per origami. A temperature controlled process was employed to hybridise the peptide-ssDNA with sticky ends on origami via heating up to 47 ^{o}C and slowly cooling

down to room temperature. The 6 peptides modified DNA origami nanostructure was achieved at first and analysed by polyacrylamide gel electrophoresis (PAGE, 15%, 1× TBE). Comparison of modified and unmodified DNA origami, peptides functionalised origami showed a lag of migration in gel which indicated a larger molecule. The comparison is carried out between origami with 6 peptide-ssDNA and origami with 6 ssDNA. The only differences in molecule weight and size are due to the presence of the peptides. As a result, we can state to have achieved the peptide-modified DNA origami nanostructures. This structure represents a cluster of 6 A20FMDV2 peptides with 60 nm spacing.

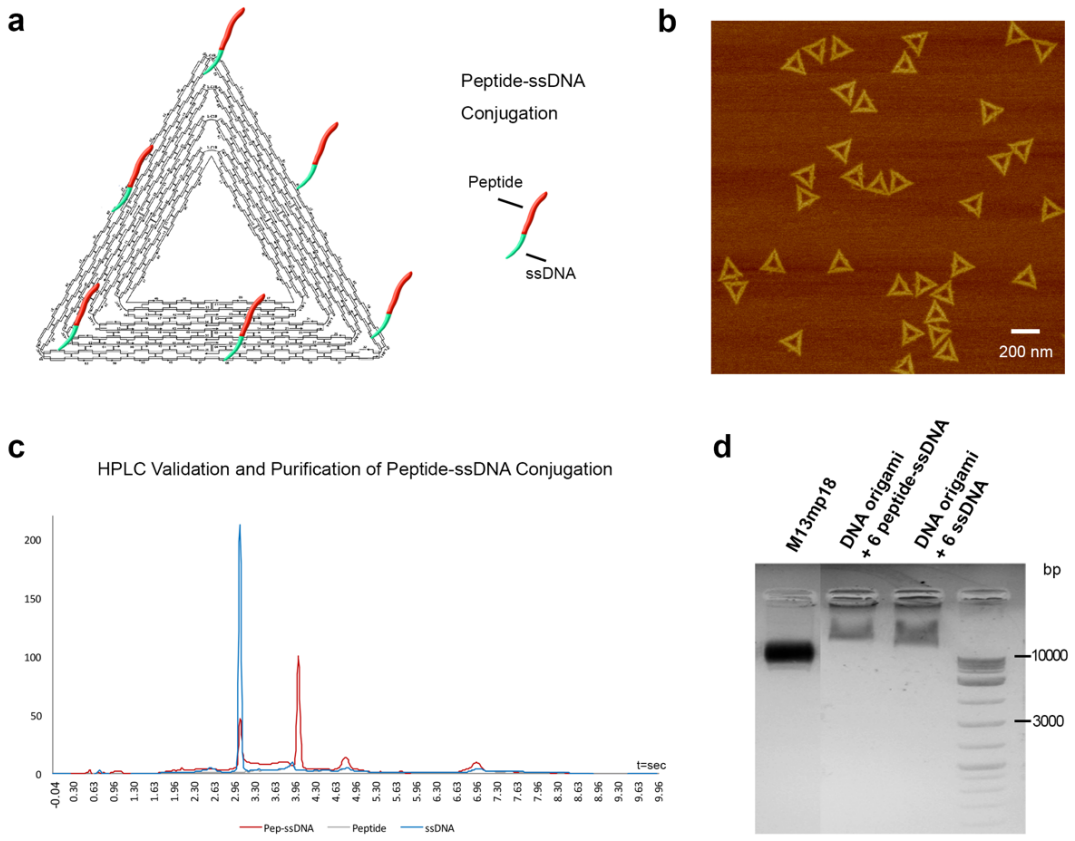

Figure 5.3 Schematic and validation of A20FMDV2 modified DNA origami. **a)** Schematic of modifying 6 A20FMDV2 on triangular DNA origami. Peptide-ssDNA

conjugation structure were shown. **b)** AFM image of modified DNA origami. The origami structures were validated but the peptide molecules are too small to be revealed under AFM. **c)** HPLC validation of A20FMDV2-ssDNA conjugation. The red line contained two peaks which are ssDNA peak (same time as only ssDNA sample (blue line)) and peptide-ssDNA peak (with larger molecule weight that lag the effluent). Only peptide sample didn't show any peak because of no absorbance under 260 wavelengths. **d)** PAGE validation of A20FMDV2-ssDNA conjugation.

For the EGF modification approach, streptavidin conjugated EGF was used to target the biotin modified sticky ends on the DNA origami. A simple process of incubation at 37 ^{o}C and then cooling down to room temperature was carried out to assemble EGF on to DNA origami (Figure 5.4). Both the A20FMDV2 peptide and EGF modified DNA origami system can be achieved via the assembly of the EGF-streptavidin conjugate on successfully constructed A20FMDV2 modified DNA origami (with biotinylated sticky ends on three edges, which differ from the A20FMDV2 modified positions, see Figure 5.4 a). The assembled nanostructures were validated under AFM (Figure 5.4 b). The EGF was visible under AFM and are shown as bright dots that modified the edges of triangular DNA origami, as expected by the employed design. The EGF dots were revealed to be around 5 nm in height which were close to the validation results of EGF by themselves under AFM via cross-section (Figure 5.4 b-i, b-iii). Notably, the yield of EGF modification was found to be up to 87%. The AFM images indicate the successful assembly of EGF modified origami structures. Because of the EGF modification carried out on A20FMDV2 conjugated origami (successfully

synthesised, see Figure 5.3), the desired nanostructures were achieved and we could then proceed to the cell adhesion study.

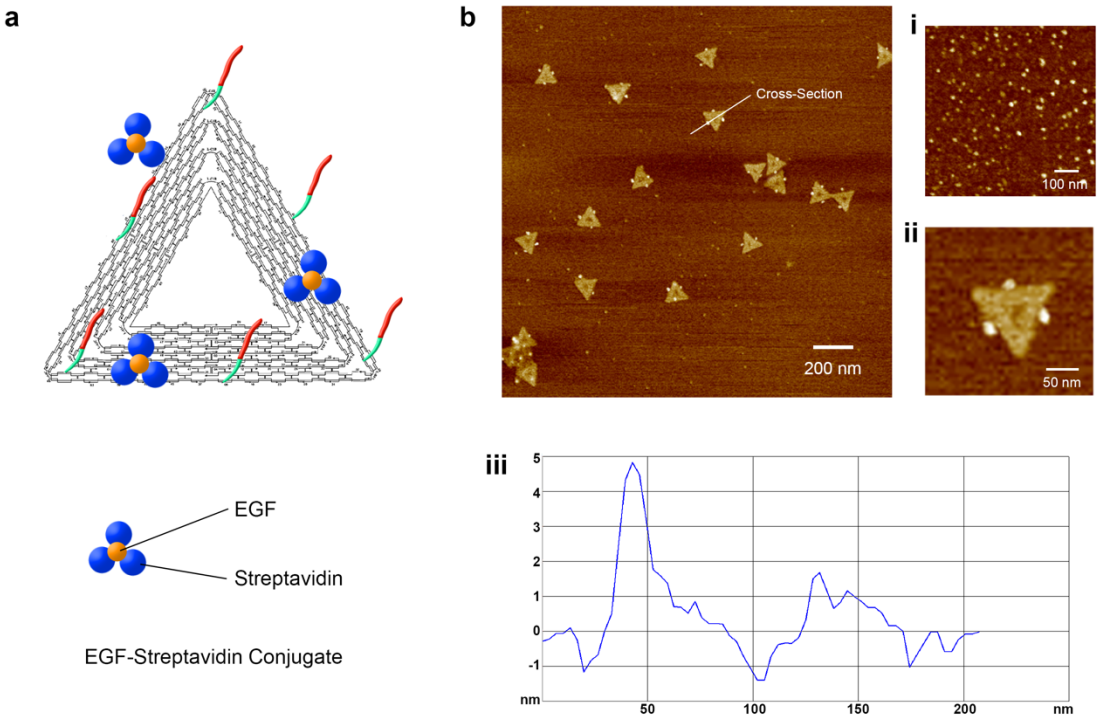

Figure 5.4 Schematic and validation of EGF modified DNA origami. **a)** Schematic of modifying EGF on A20FMDV2 modified triangular DNA origami. **b)** AFM images of EGF modified DNA origami. **i)** The EGF by itself scanned under AFM is shown. **ii)** The zoom-in AFM image of EGF modified origami. **iii)** Cross-section shown in the inset of b). The EGF was revealed to be around 5 nm in height.

5.2.2 Cell Adhesion Study on Patterned DNA Origami

Combining the FIB patterning strategy (discussed in Chapter 4), with the DNA origami assembly and functionalisation discussed above, different types of peptide-modified DNA origami were immobilised on surface with different nanoscale

arrangements of the functional peptides, i.e. of A20FMDV2 and EGF. Cell adhesion studies were applied on these patterned functionalised origami substrates: Figure 5.5 shows a schematic of the typical experimental set-up.

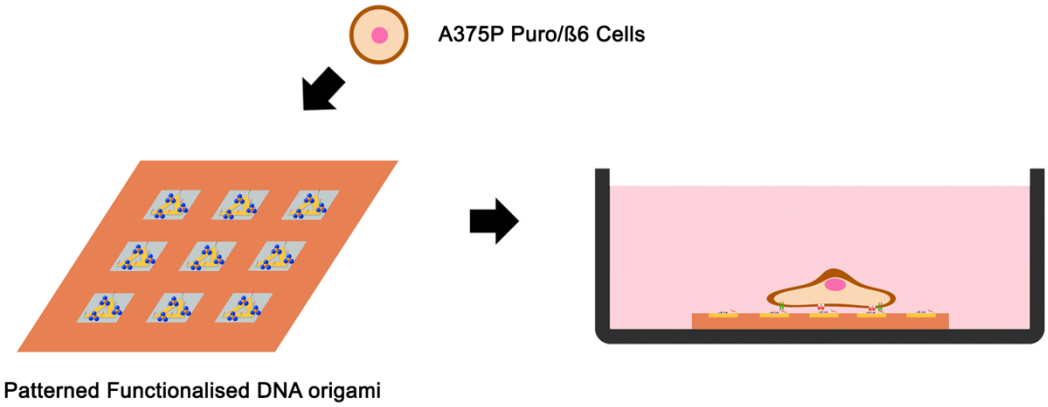

Figure 5.5 Schematic of cell adhesions studies on patterned functionalised DNA origami.

Cell adhesion studies were first carried out on substrates exhibiting different pattern spacing. Patterned nanoarrays with 1 μm and 300 nm spacing between the different DNA origami were employed for the controlled immobilisation of 6 A20FMDV2 peptides modified triangular DNA origami.

Human cutaneous melanoma cell lines A375P containing human integrin β6 cDNA gene retroviral infection type, A375P β6 cell line and puromycin-resistance gene only type, and A375P Puro cell line (not express β6 integrin), were cast and incubated on the substrates (using the same numbers of cells in each case). The binding to A375P β6 cells compared to the binding to A375P Puro cells can be taken as an indication of binding to αvβ6. A375P Puro is negative for αvβ6, in contrast to A375P β6. Therefore, differential binding to A375P β6 was used as a model for binding to αvβ6.

Figure 5.6 a and 5.7 a show DIC (differential interference contrast microscopy) images of A375P cells (both Puro and β6 cells) on substrates nanopatterned with triangular DNA origami containing 6 peptides each, where the spacing between the DNA origami was 1μm (Figure 5.6) and 300 nm (Figure 5.7). All patterned substrates were blocked with 1% BSA prior cell plating in order to reduce the nonspecific adhesion and only expose the patterned ligands. Plain patterned substrates without any DNA immobilised on the surface were employed as blank control samples, while non-modified origami immobilised on the substrates were used as another set of control samples (i.e. with origami that did not exhibit any peptides). Moreover, both types of cells were also plated on unmodified glass coverslips, employed as positive control samples (i.e. exhibiting saturating biding sites). The same numbers of cells were plated on each substrate and incubated for 1.5 hours. Careful PBS washing was carried out after cell incubation, and the substrates were then imaged under DIC microscopy. The number of adherent cells per field of view (FOV) was counted: the FOV covered a 4×10^4 μm^2 square area (four 100 μm ×100 μm patterned squares, visible in DIC images). FOVs from three independent experiments were quantified and used to calculate the percent of adherent cells compared to the positive controls (Figure 5.6 b and Figure 5.7 b).

The substrates engineered with the DNA origami containing the A20FMDV2 peptides induced a higher degree of A375P β6 cell adhesion (up to 40% on 1 μm spacing substrates, and up to 63% on 300 nm spacing substrates) compared to those on blank patterned and plain origami functionalised slides (both close to 1%). Notably, on the peptide modified substrates, the Puro cells exhibited a lower adhesion degree compared to β6 cells for both patterns (1 μm and 300 nm). This is likely due to the

integrin αvβ6 infection for β6 cells but not for Puro. Plain DNA origami nanostructures were revealed to have no binding effects to both types of cells (both close to 1%). The result indicates that cell adhesions here only relied on the A20FMDV2 peptides.

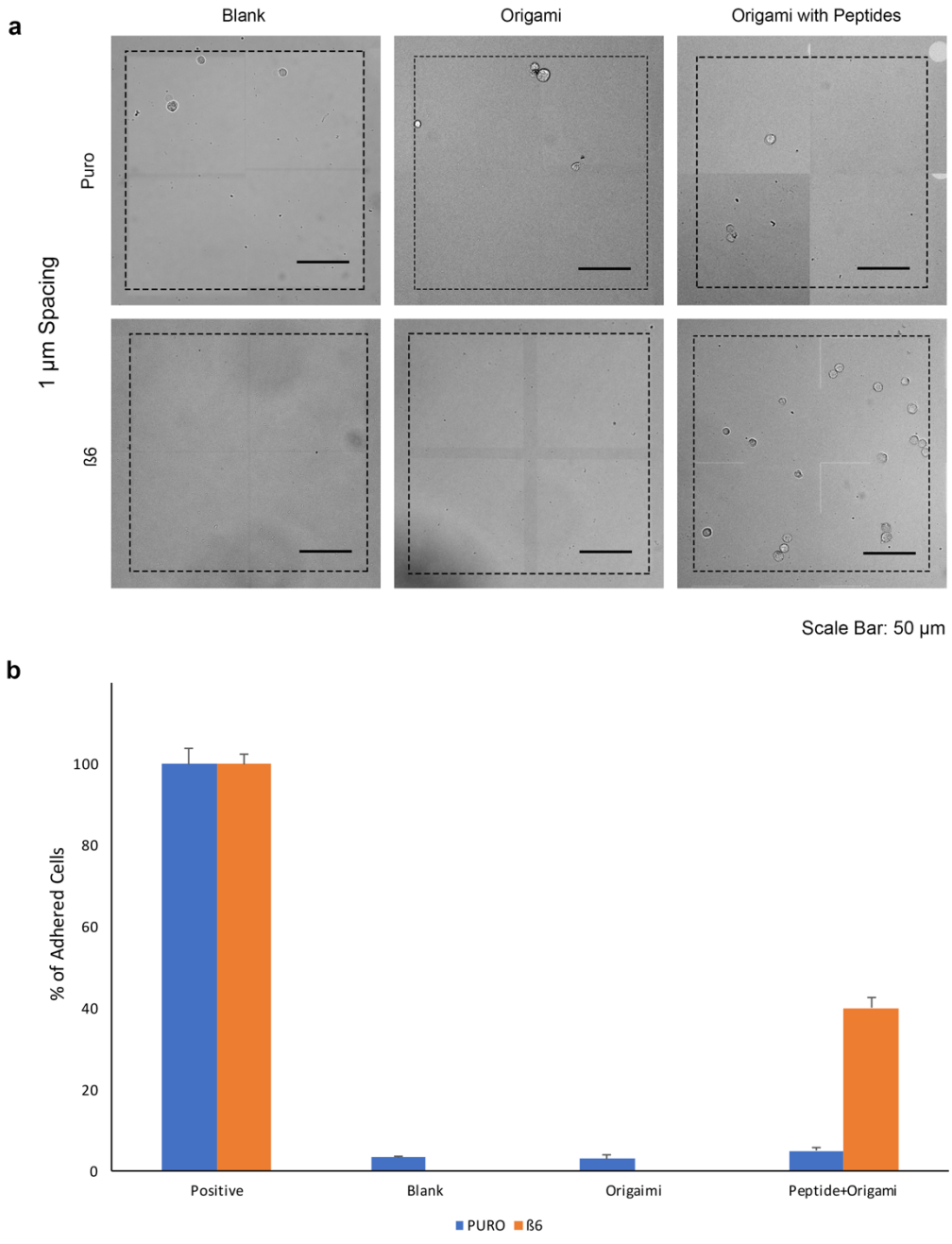

Figure 5.6 A375P Puro and β6 cell adhesions study on patterned DNA origami substrates with 1 µm spacing. **a)** DIC images of cell adhesions on different substrates.

b) Quantitative analysis of cell adhesions on each substrate. Percent of the numbers of adherent cells compared to positive control and standard errors are shown. A promotion of β6 cells spreading was shown on the peptides modified origami substrate (40%).

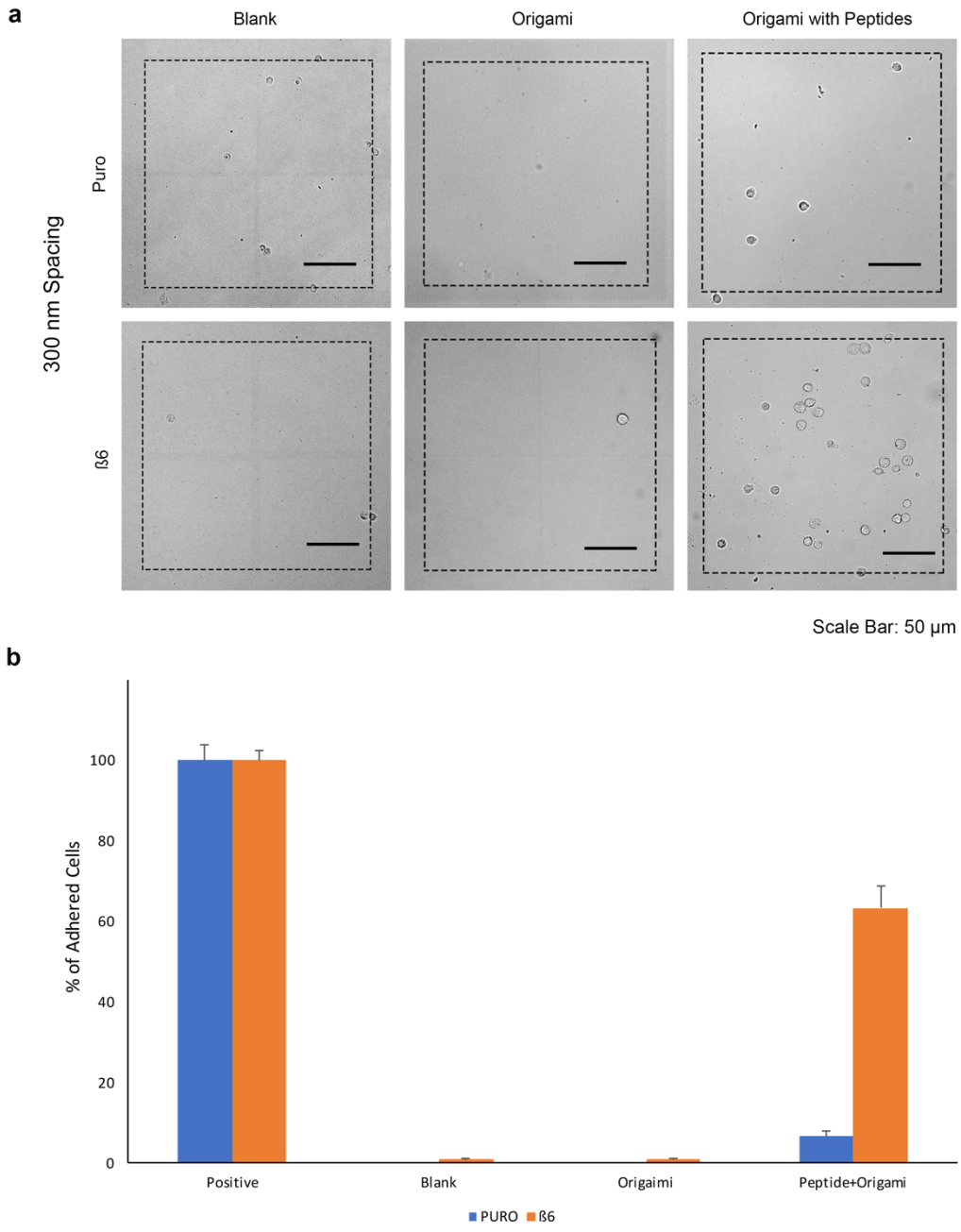

Figure 5.7 A375P Puro and β6 cell adhesions study on patterned DNA origami substrates with 300 nm spacing. **a)** DIC images of cell adhesions on different substrates.

b) Quantitative analysis of cell adhesions on each substrate. Percent of adherent cells compared to positive control and standard errors are shown. A promotion of β6 cells spreading was shown on the peptides modified origami substrate (63%).

The higher increase of cell adhesion on 300 nm spacing substrate than 1 μm spacing substrate revealed cell adhesion was improved when the integrin ligands on surface are spaced 300 nm apart, with each cluster containing 6 ligands spaced 60-nm apart (see again the schematic of peptides modification on origami, Figure 5.3 a). This is in line with a more reasonable density of 87 ligands per μm^2 (300 nm spacing) compared to 9 ligands/μm^2 (1 μm spacing). For this reason, the subsequent experiments were carried out on 300nm spacing substrates.

In this regard, the cell adhesion study was moved further employing substrates modified with both A20FMDV2 peptides and EGF (see again the schematic of peptides and EGF modification, Figure 5.4 a): 300 nm spacing patterns were chosen in this experiment. Substrates modified with only A20FMDV2 peptides, and subtracted modified to only exhibit EGF were also applied as control samples, in order to reveal the independent binding properties of these two ligands and to compare this with the sample of contain both ligands, in order to highlight the cooperative nature of the two ligands. Because we employed a EGF-streptavidin-biotin conjugation approach to modify the DNA origami with EGF, streptavidin-only modified substrates were also used as controls to investigate the actual binding properties of EGF. Moreover, plain patterned substrates without any DNA immobilised and plain glass coverslips were employed as usual as blank controls and positive controls. A375P Puro and β6 cells were plated on all these substrates, and cell adhesions were investigated (the same

approach as the previous A20FMDV2 peptides study was employed) via DIC imaging (Figure 5.8 a). A quantitative analysis was performed and the percent of adhering cells was calculated for each experiment (Figure 5.7 b).

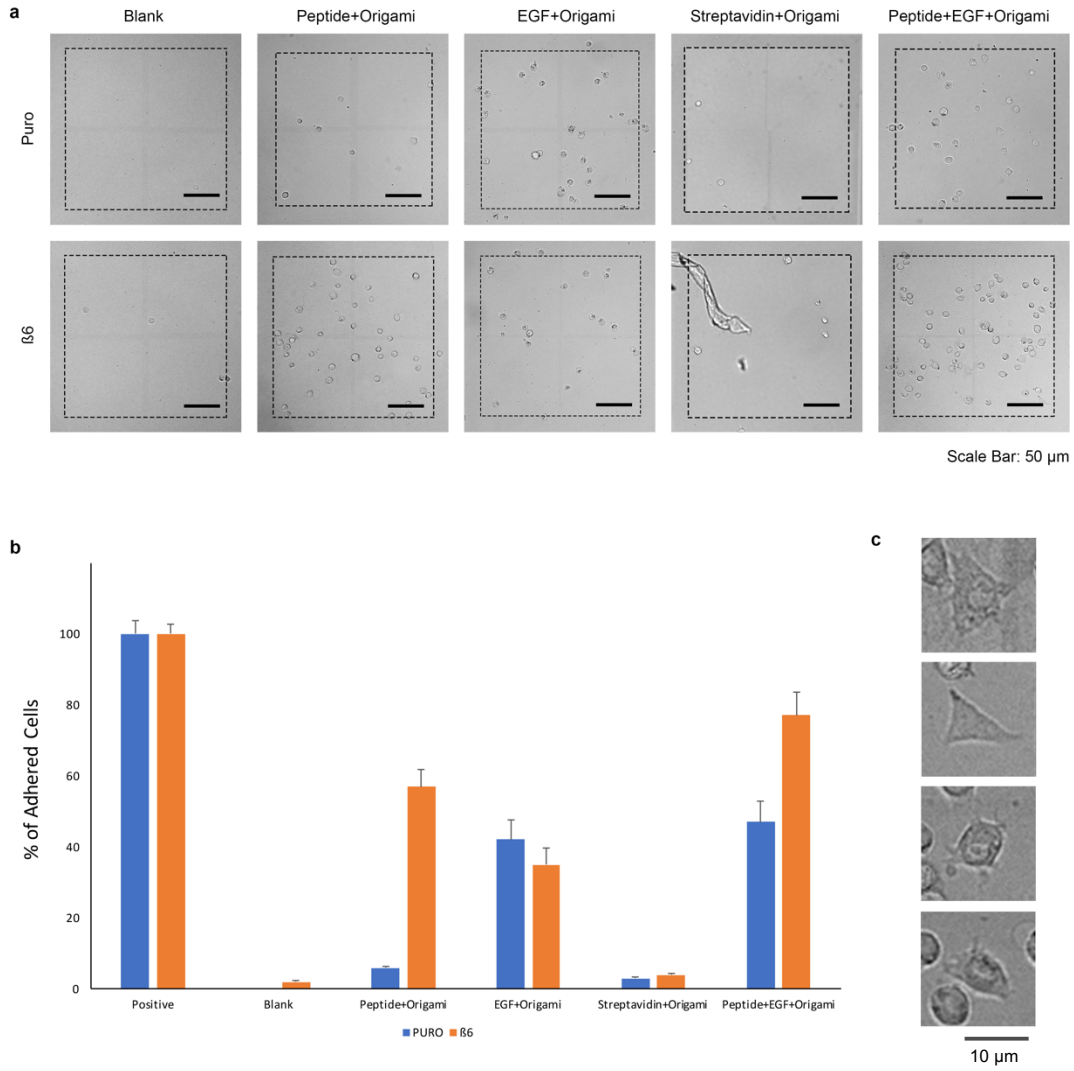

Figure 5.8 A375P Puro and β6 cell adhesions study on both A20FMDV2 peptide and EGF modified substrate. **a)** DIC images of cells adhesions on different substrates. **b)** Quantitative analysis of cell adhesions on each substrate. Percent of adherent cells compared to positive control and standard errors are shown. A significant promotion of β6 cells spreading was shown on both ligands modified substrates (77%) compared to

other substrates. Puro cells also showed promotion of cell adhesion on both ligands modified substrates (47%) Peptide modified substrate showed that 57% of β6 cells adhered and 6% of Puro cells which is similar to the experiment showed in figure 5.6 and 5.7. EGF modified substrates showed a promotion of cell adhesion for both Puro and β6 cells (42% for Puro and 35% for β6). The substrates presenting DNA origami functionalised with streptavidin only, showed negative binding for cells **c)** Zoom-in DIC images of β6 cell adhesions on both A20FMDV2 peptide and EGF modified origami substrate. Higher level of spreading is represented.

On substrates modified with both ligands (with a density of 87 peptides/μm^2 and 44 EGF/ μm^2), the β6 cells showed a significant higher degree of focal adhesions (77%) than the other substrates. This is likely due to the positive cooperation of the two ligands: as a comparison, it should be noted that we observed 57% of cell adhesions on A20FMDV2 peptide-only substrate and 35% on EGF-only substrate. Puro cells showed less adhesions (47%) because puro cells didn't exhibit adhesion onto A20FMDV2 peptides (a negative influence on the adhesion on A20FMDV2 peptides-only substrate, 6%), but showed binding to EGF modified substrates (a positive adhesion on EGF-only substrate, 42%). Additionally, Streptavidin modified substrates showed extremely low cell adhesions (3% for Puro cells and 4% for β6 cells) which indicated the bindings were based on EGF instead of streptavidin. Finally, for β6 cells, higher spreading cell behaviour could be observed on substrates modified with both ligands (Figure 5.8 c). Nevertheless, for Puro cells this higher degree of spreading in the presence of both ligands, when compared to the spreading substrates with only one ligand, was still below 50%, unlike the more than 75% of spreading for β6 cells.

From this cell adhesion study, it can be concluded that A20FMDV2 peptides and EGF both showed a positive effect on the establishment of focal adhesion for β6 cell. However, A20FMDV2 shows selective binding to β6 but not to Puro cells, while EGF was positive to both Puro and β6 cells. The cooperative effect of these two ligands, in highlighted by the promotion of cell adhesion for both cell types. Notably, it is important to remark that a boost was observed especially for β6: 77% for β6 compared to 47% for Puro. This strongly suggest that both types of ligands need to be present for the establishment of a significant yield of focal adhesion for A375P cell lines. This is in line with the role of EGF in binding to the EGF receptors (EGFR) on the surface membrane of human cutaneous carcinoma cell lines [160, 161] and its role in regulating cell growth [162] Ours is the first study demonstrating, with single-molecule control and nanoscale resolution, the need and cooperativity of A20FMDV2 peptides and EGF in cell adhesion (see gain Figure 5.8 c). This has important implications in the understanding and potential regulation of cancer cells behaviour.

5.3 Summary

A375P cell adhesion behaviours were investigated employing substrates modified with different combinations of ligands, with single-molecule control and nanoscale spatial separation. The substrates were patterned using the DNA origami platform presented in chapter 4, this time modified to exhibit cell-adhesion ligands spaced 60nm apart. A20FMDV2 peptides and EGF were the two ligands investigated here, because of their known roles in binding to the ligands receptors on the surface membrane of human cutaneous carcinoma cell lines (αvβ6 integrin for A20FMDV2

peptide and EGFR for EGF). The DNA origami nanostructures were modified with a combination of these two ligands and immobilised on substrates with specific patterns for cell adhesion studies.

The A20FMDV2 peptides were revealed to be positive for A375P β6 cell adhesions, while negative for Puro cells. EGF showed promotion of adhesions and spreading for both cells types. The cooperation of these two ligands significantly promoted cells adhesion and cell growth for Human cutaneous melanoma cell lines β6 cells compared to when only one type of ligand was present. This demonstrates, with single-molecule control, the promotion of cell adhesions and growth in the presence of both types of ligands, and hence their cooperative behaviour: to the best of our knowledge this is the first study demonstrating this with such nanoscale resolution and single-molecule control. The cooperation of αυβ6 integrin specific binding peptide (A20FMDV2) and EGF was investigated with the spatial control of the ligands at the same time via the patterned DNA origami cargo strategy. The combined presence of integrin binding peptide and EGF demonstrated an increase of cell adhesion. The cooperation of the integrin and EGFR was demonstrated as cross talk of signalling between each other. Integrin was revealed to partially evolve in activation of EGFR [158, 159].

Further investigations currently ongoing in the Palma Laboratory are focusing on the role of cytoskeleton and protein complex. This will be discussed in the next Conclusion chapter (section 6.2 Outlook).

Chapter 6

Conclusion

6.1 Conclusion

In this project, we have explored the functionalisation of self-assembled DNA nanostructures, DNA origami, their organization of nanopatterned surfaces, and their use for single-molecule investigations. In particular, semiconductor quantum dots (QDs), fluorescence molecules, linear small peptides and structural proteins were tethered with single-molecule accuracy on DNA origami (with nanoscale spatial control). In addition, the combinations of different types of nanomoieties on DNA origami was achieved. Different types of QDs and fluorophores modified DNA origami were successfully constructed. The QD, fluorophores, peptides and proteins can be tethered on DNA origami with amino anchors modification at the same time. Several chemical and biological conjugation techniques, including streptavidin-biotin interaction, amidation reaction, maleimide-thiol reaction and EDC/NHS coupling, were explored to construct such nanostructures. All the functionalised DNA origami

nanostructures were imaged via AFM in order to validate the aforementioned modifications.

Additionally, we have achieved the selective immobilisation of DNA origami on surfaces for single-molecule investigations. Their organization in array configuration on nanopatterned surfaces allowed us to fabricate and test different platforms for single-molecule studies.

We developed a Focused Ion Beam (FIB) nanofabrication strategy to pattern the substrate surfaces for the desired studies. The general applicability for the assembly of functionalised DNA nanostructures in highly uniform nanoarrays, with single-molecule control, was developed via a one-step lithography and a simple surface covalent binding reaction. FIB allowed us to create nanoapertures arrays in a convenient and low cost way. Functionalised DNA origami were successfully immobilised to the surface according to the patterned nanoapertures via covalent bonding. Single molecule arrangement was achieved using this strategy that can be further explored for different patterning arrangements. Notably, the platform developed is reusable with simple cleaning procedures. Investigations have been carried out with a combination of different techniques including fluorescence microscopy, SEM, FIB and AFM.

Furthermore, we have studied the application of the aforementioned functionalised DNA origami and its patterned immobilisation platforms. We developed DNA origami to form a platform for monitoring cleavage events by restriction enzymes. This dynamic control strategy allowed us to manipulate the modifications on DNA origami. The nanoscale spacing of modifications had been studied via spectral separation (collaboration with Dr Sapelkin research group) for the precise control of

the functionalisation; this can be further applied as a gene ruler for several biological investigations.

Lastly, we have investigated cancer cell adhesions based on the use of the patterned functionalised DNA nanostructures as a nanoscale biochip. The surface arrangements of cell adhesion ligands including RGD peptide A20FMDV2 and EGF (epidermal growth factor) were manipulated via their assembly on DNA origami and the organization of these on patterned surfaces. In this regard, patterned peptide modified DNA origami nanoarrays were employed to mimic the extracellular matrix and investigate integrin and EGFR binding behaviour for A375P cancer cells. The cooperation of A20FMDV2 peptide and EGF for the promotion in cell adhesions has been demonstrated with single-molecule control and nanoscale spatial resolution. By and large, combining the programming ability of DNA as a scaffolding material with a one-step lithographic process, we have developed a platform of general applicability for the fabrication of nanoscale chips that can be employed in a variety of single-molecule investigations.

6.2 Outlook

In this thesis, we have explored the multi-functionalisation capability of DNA origami. The high complexity of functionalisation is key for the exploration of different applications of DNA origami.

In this regard, the dynamic control capability on origami can be further exploited for DNA-protein interaction studies (e.g. restriction enzyme cleavage). A real-time study can reveal the details of enzymic digestion with single-molecule

resolution. DNA-antibodies nanostructures can be applied as a multi-valent cell targeting molecule in gene transfer and cell imaging studies.

We indeed envision several future applications for the developed platform as a biochip. The cell adhesion study presented here can be moved further to reveal the details of binding sites and binding complex by immunostaining the receptors on the cell surface and ligands on the patterned surface. This can allow the investigations of ligands binding through a direct imaging approach. The dynamic mechanism of binding could be revealed via combining FRET biosensors in/on the cells and ligands on the DNA origami. The signalling pathways and their activation levels after binding can be monitored via analysing activation levels and partitioning of these signalling molecules by acceptor photobleaching FRET in fixed cells stained with endosomal markers. In a similar way, the role of cytoskeleton and protein complex in the cell adhesion can be mapped based on this platform.

Additionally, different and additional types of ligands on the same origami will provide a more complex system to further study the cooperation of cell-binding ligands with single-molecule resolution. Designing different geometrical arrangements of nanopatterned surfaces can allow the investigation of the effects of ligands' orientation and organisation on cell adhesion. This can go beyond cancer cells, to include other cell lines and systems for multi-valent ligand-receptor single-molecule studies. In this regard, interesting opportunities can be found in the investigation of the effects on integrin signaling, for example by applying the platform developed here on cardiomyocytes. Current efforts in the Palma laboratory are indeed focused in this direction.

In addition to biological investigations, the platform developed here holds great promise for the assembly and organization of nanomoieties of interest in materials science. By assembling different inorganic (e.g. QDs) or organic (e.g. carbon nanotubes) nanostructures in nanoarray, and potentially device, configurations, the strategies presented in this thesis hold great promise for the solution-processable fabrication of single-molecule devices for optoelectronic applications. By and large, the ability to control the assembly of individual molecules and nanostructures from solution to surfaces in pre-defined orientations is key to the advancement of the broad field of nanotechnology, in all its applications.

Appendix

i. Original Staple Strands Sequences of Rectangular DNA origami

R1	TATAAGTATAGCCCGGAATAGGTGTATCACCG
R2	TGAGGCAGCCGCCGCCAGCATTGAATCTCCAA
R3	GACTTGAGTAAAGGTGAATTATCACTAAAACA
R4	GCAATAGCATAAGAGCAAGAAACATGGTTTAA
R5	AGGTTTTGTTAGCGAACCTCCCGAAATCGTCA
R6	TAAAGTACTTTCGAGCCAGTAATAAGTTTCAT
R7	TAACCTCCCATAGGTCTGAGAGACTAATGTGT
R8	CTTTTACACAGATGAATATACAGTGCCATCAA
R9	AGATTAGATCTTTAGGTGCACTAAGCAAGGCG
R10	GCCAACAGACCAGTAATAAAAGGGCGCCAGGG
R11	CACCAGAGGTCAGACGATTGGCCTCCGTCGAGAGGGTTGA
R12	ACAAACGACCTCAGAGCCGCCACCGCCAGCAA
R13	TTATTCATCCATTTGGGAATTAGAAGAACCAC
R14	AATCACCAAGGGAAGGTAAATATTTTTTTAAG
R15	GCCCAATATATCTTACCGAAGCCCGACGGAAA
R16	AAAAGTAAGATAACCCACAAGAATTTAGTTGC
R17	GAGGCGTTAAGCCTTAAATCAAGATGAGTTAA
R18	TATTTTGCGCTTATCCGGTATTCTAATTCTGT
R19	AGAGGCATCGACAAAAGGTAAAGTAAGAACGC
R20	CCAGACGAACAACGCCAACATGTATATAACTA
R21	ATCAAAATGGCTTAGGTTGGGTTAATTTAGGC
R22	TATGTAAACTGAGAAGAGTCAATACGGATTCG
R23	TTTAACGTTCGGGAGAAACAATAAGTGAATTT
R24	CCTGATTGAAAGAAATTGCGTAGAACATTTGA
R25	CTAAAATAGCCGTCAATAGATAATTTTTCAGG
R26	GGATTTAGTAGAAAGGAATTGAGGACCTGAAA
R27	GTCACACGAGATAGAACCCTTCTGAAGGTTAT
R28	GCGTAAGATTATTTACATTGGCAGTTAAAGGG
R29	CTAAACAGGAGGCCGAATTCACCA
R30	TGCTCAGTACCAGGCGGATAAGTGTGATATTC
R31	GCCACCACATGGATCTTCATTAAACGGGGTTT
R32	GGAAAGCGACCCTCAGAACCGCCATAGCAAGG
R33	ATTGAGGGGTAGCACCATTACCATCCCTCAGA
R34	CCGGAAACAGACAAAAGGGCGACAAGTTACCT
R35	ATCAGAGAGCAGATAGCCGAACAATTCAACCG

R36	GAAGGAAAGTCAGAGGGTAATTGAATCCTGAA
R37	TATAGAAGACCCACGTACAATTTTGCGCTAAT
R38	TCTTACCAGCGCCCAATAGCAAGCGTTCAGCT
R39	CATATTTACGACAATAAACAACATAAATCAGA
R40	AATGCAGACAGTAGGGCTTAATTGATCGCAAG
R41	TTAAGACGTGCTGATGCAAATCCAAGAATCGC
R42	ACAAAGAATTGAAAACATAGCGATACAAAATC
R43	ACAGAAATCTTTGAATACCAAGTTAGCTTAGA
R44	GCGCAGAGATATCAAAATTATTAGAAACAATT
R45	ATCAACACAAGTATTAGACTTTACCACGTAAA
R46	CGACAACTAATCAATATCTGGTCAATATTTTT
R47	GAAATGGAATACGTGGCACAGACAGTTGGCAA
R48	GAATGGCTCTACATTTTGACGCTCGAATCTTG
R49	ATTTTAGACAGGAACGGTACGCCAAATCGTCT
R50	CCTCAAGAGAAGGATTAGGATTAGGCCAGAAT
R51	GAGCCGCCCAGTCTCTGAATTTACCTGAGACT
R52	TAAGCGTCCCACCACCGGAACCGCTCGATAGC
R53	AGCGCCAAGTCACCAATGAAACCACTCCCTCA
R54	AGCACCGTAATAGAAAATTCATATATAACGGA
R55	TGAACAAACCGAGGAAACGCAATAGGTTTACC
R56	ATACCCAAGACGGGAGAATTAACTTTCCAGAG
R57	TCATTACCACGCTAACGAGCGTCTGAACACCC
R58	CCTAATTTCCGTTTTTATTTTCATACAATAGA
R59	ACGCTCAAACGCGCCTGTTTATCACGTAGGAA
R60	TAAGTCCTCAAATTCTTACCAGTACAAATATA
R61	TAGAATCCCGCGAGAAAACTTTTTTAAAGCCA
R62	TTTTAGTTCGTCGCTATTAATTAAAATTACCT
R63	AACCAACCGCGAATTATTCATTTCTTTTCCCT
R64	GAGCAAAAACTTCTGAATTATGGACCCGAACG
R65	AAACCCTCCGTATTAAATCCTTTGAGGAATTG
R66	TTATTAATTCACCAAGCTGAACCTCGAACTGA
R67	GGAAATACATTAGTCTTTAATGCGCAAATATC
R68	TAGCCCTACATTGCAACAGGAAAAGCCACCGA
R69	AGAAGTGTTTTTATAATCAGTGAGACGCTCAT
R70	CTGAAACATGAAAGTATTAAGAGGCGTTCCAG
R71	AACCAGAGATACATGGCTTTTGATCTATTATT
R72	AGTGTACTTCTTTTCATAATCAAAATCAAGTT
R73	TCACAATCAATCAGTAGCGACAGAATCACCGG
R74	TGCCTTTAACACCACGGAATAAGTAAGACTCC
R75	GCGCATTAAAGAACTGGCATGATTTTATTTTG
R76	TTATTACGAGAGAATAACATAAAAACAGCCAT
R77	CAAGCAAGGCCAGTTACAAAATAAACAGGGAA
R78	ATTATTTAACCAAGTACCGCACTCATCCCATC

R79	GCGTTATAGAACAAGAAAAATAATATCGAGAA
R80	CTAATTTAGAAAAAGCCTGTTTAGCTAAATTT
R81	CTGTAAATAATTTCATCTTCTGACTATCATAT
R82	AATGGTTTATATGTGAGTGAATAAACATCAAG
R83	TGGATTATGAAGATGATGAAACAACCTTGCTT
R84	AAAACAAATTCATCAATATAATCCACATTATC
R85	CTAAAGCATTTAAAAGTTTGAGTATGATTGTT
R86	ATTTTGCGGAGAGCCAGCAGCAAAAATACCGA
R87	CCGCCAGCAAACATCGCCATTAAATGAAAAAT
R88	ACGAACCACTGGTAATATCCAGAAAATTAACC
R89	GTAAAAGAGTCTGTCCATCACGCACAATATTA
R90	AATGCCCCCTGCCTATTTCGGAACGATACAGG
R91	GTTTGCCAGGTAATAAGTTTTAACAAACAGTT
R92	ACGCAAAGGCGTCAGACTGTAGCGTTATTAGC
R93	CTTTACAGCAGTATGTTAGCAAACTAAAAGAA
R94	GGTATTAATCCCAATCCAAATAAGATAGCAGC
R95	AATTACTACGAGCATGTAGAAACCCAAGAACG
R96	AAATCAATGAAATACCGACCGTGTGGAATCAT
R97	GATGGCAAATTAATTACATTTAACCAGTACAT
R98	GCCACGCTGAACAAAGAAACCACCTATCAGTA
R99	CGGCCTTGCCAGCAGAAGATAAAAGCAACAGT
R100	GTTGTAGCAATACTTCTTTGATTACAAACTAT
R101	CAGTGCCCGTATGGGGTCAGTGCC
R102	GTCATAGCCCCCCGTTTTCATCGG
R103	GGTGGCAACATAGTAGAAAATACA
R104	TCAAAAATGAAAAAACGATTTTTT
R105	TCCTTATCATTCAATCAATAATCG
R106	AGAATAAACACCGATAAATAAGGC
R107	TTTTAATGGAAAAATTTCATTTGA
R108	CATATTCCTGATAGAAGGAGCGGA
R109	TTAACACCGCCTCAGAGGTGAGGC
R110	AGTAGAAGAACTGTAATAACATCA
R111	AAAAAAGGTTTTTTCACGTTGAAACAGGAGGT
R112	CTCATCTTGAGGCGAAAGAATACACCGTCACC
R113	TTTCAACTTAAATTGGGCTTGAGAATGAAATA
R114	TAAATATTGCGTCCAATACTGCGGCTTGCGGG
R115	TCCATGTAAAGTACGGTGTCTGGAAGAGAATA
R116	AGGTAAAGAAATGCAATGCCTGAGTACCTTTT
R117	AAATAATTTTTAACCAATAGGAACAACAGTAC
R118	ATTAAGTTGAAAGGGGGATGTGCTCAACTAAT
R119	TGGTTTTTCGGTTTGCGTATTGGGACATTCTG
R120	TACTCAGGAGGTTTATGAATTGCG
R121	AATAATAACTCCAAAAGGAGCCTTCCAACCTA

R122	TCGGTTTAAAAGGAACAACTAAAGTACCGCCA
R123	AAACGAAATGACCCCCAGCGATTAACACCAGA
R124	GCGAAACATGCCACTACGAAGGCATAATTGTA
R125	ACGAGTAGTTAATCATTGTGAATTATGTTTAG
R126	CGATTTTAGCTTGCCCTGACGAGATACCAAGC
R127	ACTGGATACATTGAATCCCCCTCATTTAAATA
R128	AAACAGTTAGGGGGTAATAGTAAAACCTTATG
R129	TGCAACTAACAGTTGATTCCCAATAACCCTCA
R130	CGAGTAGACTGTAGCTCAACATGTAATGCTTT
R131	TATATTTTATTCAAAAGGGTGAGATTAAATCA
R132	AGACAGTCGGATAAAAATTTTTAGTCTGCGAA
R133	GCTCATTTCGCGTCTGGCCTTCCTTATTACGC
R134	CTTTCATCTCGCGTTAAATTTTTGAAGGCCGG
R135	CAGCTGGCGGGTAACGCCAGGGTTAACGCGCG
R136	CACGACGTGTGCGGGCCTCTTCGCGTAGCCAG
R137	GGGAGAGGCTTTTCACCAGTGAGAGAGGTGCCGTAAAGCA
R138	AGCTGATTCATTAATGAATCGGCCTTCCCAGT
R139	CTAAATCGGAACCCTAGGAATCAGAGCGGGAG
R140	CCCTCAGAACCGCCACCCTCAGAAAGCGGAGT
R141	GAGAATAGTCAGCTTGCTTTCGAGCGGGTAAA
R142	CTTAAACAAACTTTCAACAGTTTCCCGCCACC
R143	ATACGTAAAAGTACAACGGAGATTTCATTCAG
R144	CGCCTGATGGAAGTTTCCATTAAAGTGAATTT
R145	TGAATAAGAGAACTGGCTCATTATAAAGAAGT
R146	GGACGTTGAACGTAACAAAGCTGCTGTATCAT
R147	TTTGCCAGCAGAAAACGAGAACGAATTGCTGA
R148	CAAAAATCGCGAGAGGCTTTTGCAACCAGTCA
R149	ATCTGGTGTTTAGTTTGACCATTACTTTATTT
R150	TCGCAAATGATGGCTTAGAGCTTACCATAAAT
R151	CAACGCAAAAATCACCATCAATATAATATTTT
R152	ACCGTTCTCTTTTGCGGGAGAAGCGATACATT
R153	GTTAAAATAACATTAAATGTGAGCTTGGGAAG
R154	ACCCGTGGTTAAATTGTAAACGTTGATATTCA
R155	GGCGATCGTGTAAAACGACGGCCACCTGTCGT
R156	CTTGCATGTCAGGCTGCGCAACTGGAGTAACA
R157	GCCAGCTGGCCCTTCACCGCCTGGGAACCATC
R158	GAGTTGCACTTTCCAGTCGGGAAAGTGCCAAG
R159	ACCCAAATCAAGTTTTTTGGGGTCCGGGCAAT
R160	CTCAGAGCCACCACCCTCATTTTCTGGGATTT
R161	TGCTAAACGCTTGATACCGATAGTAAAGACTT
R162	CAATGACAAAATGAATTTTCTGTAAGGGATAG
R163	TTTCATGAAAATTGTGTCGAAATCATTCATTA
R164	GCTCCATGAGAGGCTTTGAGGACTTGCGCCGA

R165	CCCAAATCGGAAGAAAAATCTACGGATAAAAA
R166	ACGAACTATCGACAAGAACCGGATCGCGACCT
R167	CCAAAATAAGGTCTTTACCCTGACAGAGGTCA
R168	TCAGAAGCTCGTTTACCAGACGACTTAATAAA
R169	TTTTTGCGGGTCAATAACCTGTTTTTATGACC
R170	TTTCATTTATTGCTCCTTTTGATATATTATAG
R171	CTGTAATAAGCTGATAAATTAATGTTGTATAA
R172	GGTAGCTAGGTTGTACCAAAAACAAGCTATAT
R173	GCAAATATGATTCTCCGTGGGAACAAGCGCCA
R174	GATTGACCCCCAAAAACAGGAAGACCGGAGAG
R175	TTCGCCATCCTGCAGGTCGACTCTTTGCGCTC
R176	CCCGGGTATGCCGGAAACCAGGCAAAACGGCG
R177	ACTGCCCGGCAAGCGGTCCACGCTAAACCGTC
R178	CCAGCAGGACTCACATTAATTGCGAGAGGATC
R179	TATCAGGGCGATGGCCCACTACGTCCCTGAGA
R180	CAAGCCCAATAGGAACCCATGTACCTTTCCAG
R181	ACGTTAGTACAACCATCGCCCACGGGGTAGCA
R182	ATATATTCTCTAAAGTTTTGTCGTCGTAACAC
R183	ACGGCTACTTACTTAGCCGGAACGTCATCAAG
R184	ACGGTCAAGACAGCATCGGAACGACATAACCG
R185	AGTAATCTACGGAACAACATTATTAACACTAT
R186	AAAGATTCATAGGCTGGCTGACCTAGGCGCAG
R187	CATAACCCAAAGCGGATTGCATCATTAGAGAG
R188	AAGAGGAAGAGGCATAGTAAGAGCACAGGTAG
R189	TACCTTTAGGGGCGCGAGCTGAAAAGCATAAA
R190	TCAATTCTCTCCAACAGGTCAGGAAAAAGATT
R191	GCTAAATCTTTTTGAGAGATCTACTGATAATC
R192	TCAGGTCAAGCAATAAAGCCTCAGAGGTGGCA
R193	AGAAAAGCGTAATGGGATAGGTTACCGGCACC
R194	TAGATGGGTCATATGTACCCCGGTAAAGGCTA
R195	GCTTCTGGCCGAGCTCGAATTCGTCCTAATGA
R196	TCATAGCTCACTCCAGCCAGCTTTCGTTGGTG
R197	GTGAGCTACGAAAATCCTGTTTGAAAAGAACG
R198	CCGAAATCTGTAAAGCCTGGGGTGAATCATGG
R199	TGGACTCCAACGTCAAAGGGCGAAGGTTTGCC
R200	TGAGTTTCGTCACCAGTACAAACTATAGTTAG
R201	CGTAACGAGGTCGCTGAGGCTTGCACCCTCAG
R202	CAGCGAAATCATAAGGGAACCGAATGTACAGA
R203	CCAGGCGCATCAGTTGAGATTTAGCGCCAAAA
R204	GGAATTACGCCCGAAAGACTTCAACCAGACCG
R205	GAAGCAAAACTAATAGTAGTAGCAAGAATTAG
R206	CAAAATTATTGCCTGAGAGTCTGGAAAACTAG
R207	CATGTCAACGCATCGTAACCGTGCGGCCTCAG

R208	GAAGATCGGTTTCCTGTGTGAAATAGCCGGAA
R209	GCATAAAGGGCAAAATCCCTTATAGTTGTTCC
R210	AGTTTGGAACAAGAGTCCACTATTTGGTGGTT
R211	CAGACAGCCCTCACAACGCCTGTA
R212	TGCGGGATCGTCAGGGAGTTAAAG
R213	ACAGATGAACGGCTGACCAACTTT
R214	GCAGATACATAAGAATACCACATT
R215	CTTCAAAGCGAAATATCGCGTTTT
R216	CAGGCAAGGCAATTAACATCCAAT
R217	AACGGTAATCGTAGCAAACAAGAG
R218	GACGACCGTATCATCTGCCAGTTT
R219	ACACAACATACGTGTTATCCGCTC
R220	ATAGGGTTGAGTAATCAAAAGAAT

ii. Original Sequences of Triangular DNA origami

A01	CGGGGTTTCCTCAAGAGAAGGATTTTGAATTA
A02	AGCGTCATGTCTCTGAATTTACCGACTACCTT
A03	TTCATAATCCCCTTATTAGCGTTTTTCTTACC
A04	ATGGTTTATGTCACAATCAATAGATATTAAAC
A05	TTTGATGATTAAGAGGCTGAGACTTGCTCAGTACCAGGCG
A06	CCGGAACCCAGAATGGAAAGCGCAACATGGCT
A07	AAAGACAACATTTTCGGTCATAGCCAAAATCA
A08	GACGGGAGAATTAACTCGGAATAAGTTTATTTCCAGCGCC
A09	GATAAGTGCCGTCGAGCTGAAACATGAAAGTATACAGGAG
A10	TGTACTGGAAATCCTCATTAAAGCAGAGCCAC
A11	CACCGGAAAGCGCGTTTTCATCGGAAGGGCGA
A12	CATTCAACAAACGCAAAGACACCAGAACACCCTGAACAAA
A13	TTTAACGGTTCGGAACCTATTATTAGGGTTGATATAAGTA
A14	CTCAGAGCATATTCACAAACAAATTAATAAGT
A15	GGAGGGAATTTAGCGTCAGACTGTCCGCCTCC
A16	GTCAGAGGGTAATTGATGGCAACATATAAAAGCGATTGAG
A17	TAGCCCGGAATAGGTGAATGCCCCCTGCCTATGGTCAGTG
A18	CCTTGAGTCAGACGATTGGCCTTGCGCCACCC
A19	TCAGAACCCAGAATCAAGTTTGCCGGTAAATA
A20	TTGACGGAAATACATACATAAAGGGCGCTAATATCAGAGA
A21	CAGAGCCAGGAGGTTGAGGCAGGTAACAGTGCCCG
A22	ATTAAAGGCCGTAATCAGTAGCGAGCCACCCT
A23	GATAACCCACAAGAATGTTAGCAAACGTAGAAAATTATTC
A24	GCCGCCAGCATTGACACCACCCTC

A25	AGAGCCGCACCATCGATAGCAGCATGAATTAT
A26	CACCGTCACCTTATTACGCAGTATTGAGTTAAGCCCAATA
A27	AGCCATTTAAACGTCACCAATGAACACCAGAACCA
A28	ATAAGAGCAAGAAACATGGCATGATTAAGACTCCGACTTG
A29	CCATTAGCAAGGCCGGGGGAATTA
A30	GAGCCAGCGAATACCCAAAAGAACATGAAATAGCAATAGC
A31	TATCTTACCGAAGCCCAAACGCAATAATAACGAAAATCACCAG
A32	CAGAAGGAAACCGAGGTTTTTAAGAAAAGTAAGCAGATAGCCG
A33	CCTTTTTTCATTTAACAATTTCATAGGATTAG
A34	TTTAACCTATCATAGGTCTGAGAGTTCCAGTA
A35	AGTATAAAATATGCGTTATACAAAGCCATCTT
A36	CAAGTACCTCATTCCAAGAACGGGAAATTCAT
A37	AGAGAATAACATAAAAACAGGGAAGCGCATTA
A38	AAAACAAAATTAATTAAATGGAAACAGTACATTAGTGAAT
A39	TTATCAAACCGGCTTAGGTTGGGTAAGCCTGT
A40	TTAGTATCGCCAACGCTCAACAGTCGGCTGTC
A41	TTTCCTTAGCACTCATCGAGAACAATAGCAGCCTTTACAG
A42	AGAGTCAAAAATCAATATATGTGATGAAACAAACATCAAG
A43	ACTAGAAATATATAACTATATGTACGCTGAGA
A44	TCAATAATAGGGCTTAATTGAGAATCATAATT
A45	AACGTCAAAAATGAAAAGCAAGCCGTTTTTATGAAACCAA
A46	GAGCAAAAGAAGATGAGTGAATAACCTTGCTTATAGCTTA
A47	GATTAAGAAATGCTGATGCAAATCAGAATAAA
A48	CACCGGAATCGCCATATTTAACAAAATTTACG
A49	AGCATGTATTTCATCGTAGGAATCAAACGATTTTTTGTTT
A50	ACATAGCGCTGTAAATCGTCGCTATTCATTTCAATTACCT
A51	GTTAAATACAATCGCAAGACAAAGCCTTGAAA
A52	CCCATCCTCGCCAACATGTAATTTAATAAGGC
A53	TCCCAATCCAAATAAGATTACCGCGCCCAATAAATAATAT
A54	TCCCTTAGAATAACGCGAGAAAACTTTTACCGACC
A55	GTGTGATAAGGCAGAGGCATTTTCAGTCCTGA
A56	ACAAGAAAGCAAGCAAATCAGATAACAGCCATATTATTTA
A57	GTTTGAAATTCAAATATATTTTAG
A58	AATAGATAGAGCCAGTAATAAGAGATTTAATG
A59	GCCAGTTACAAAATAATAGAAGGCTTATCCGGTTATCAAC
A60	TTCTGACCTAAAATATAAAGTACCGACTGCAGAAC
A61	GCGCCTGTTATTCTAAGAACGCGATTCCAGAGCCTAATTT
A62	TCAGCTAAAAAAGGTAAAGTAATT
A63	ACGCTAACGAGCGTCTGGCGTTTTAGCGAACCCAACATGT
A64	ACGACAATAAATCCCGACTTGCGGGAGATCCTGAATCTTACCA

A65	TGCTATTTTGCACCCAGCTACAATTTTGTTTTGAAGCCTTAAA
B01	TCATATGTGTAATCGTAAAACTAGTCATTTTC
B02	GTGAGAAAATGTGTAGGTAAAGATACAACTTT
B03	GGCATCAAATTTGGGGCGCGAGCTAGTTAAAG
B04	TTCGAGCTAAGACTTCAAATATCGGGAACGAG
B05	ACAGTCAAAGAGAATCGATGAACGACCCCGGTTGATAATC
B06	ATAGTAGTATGCAATGCCTGAGTAGGCCGGAG
B07	AACCAGACGTTTAGCTATATTTTCTTCTACTA
B08	GAATACCACATTCAACTTAAGAGGAAGCCCGATCAAAGCG
B09	AGAAAAGCCCCAAAAAGAGTCTGGAGCAAACAATCACCAT
B10	CAATATGACCCTCATATATTTTAAAGCATTAA
B11	CATCCAATAAATGGTCAATAACCTCGGAAGCA
B12	AACTCCAAGATTGCATCAAAAAGATAATGCAGATACATAA
B13	CGTTCTAGTCAGGTCATTGCCTGACAGGAAGATTGTATAA
B14	CAGGCAAGATAAAAATTTTTAGAATATTCAAC
B15	GATTAGAGATTAGATACATTTCGCAAATCATA
B16	CGCCAAAAGGAATTACAGTCAGAAGCAAAGCGCAGGTCAG
B17	GCAAATATTTAAATTGAGATCTACAAAGGCTACTGATAAA
B18	TTAATGCCTTATTTCAACGCAAGGGCAAAGAA
B19	TTAGCAAATAGATTTAGTTTGACCAGTACCTT
B20	TAATTGCTTTACCCTGACTATTATGAGGCATAGTAAGAGC
B21	ATAAAGCCTTTGCGGGAGAAGCCTGGAGAGGGTAG
B22	TAAGAGGTCAATTCTGCGAACGAGATTAAGCA
B23	AACACTATCATAACCCATCAAAAATCAGGTCTCCTTTTGA
B24	ATGACCCTGTAATACTTCAGAGCA
B25	TAAAGCTATATAACAGTTGATTCCCATTTTTG
B26	CGGATGGCACGAGAATGACCATAATCGTTTACCAGACGAC
B27	TAATTGCTTGGAAGTTTCATTCCAAATCGGTTGTA
B28	GATAAAAACCAAAATATTAAACAGTTCAGAAATTAGAGCT
B29	ACTAAAGTACGGTGTCGAATATAA
B30	TGCTGTAGATCCCCCTCAAATGCTGCGAGAGGCTTTTGCA
B31	AAAGAAGTTTTGCCAGCATAAATATTCATTGACTCAACATGTT
B32	AATACTGCGGAATCGTAGGGGGTAATAGTAAAATGTTTAGACT
B33	AGGGATAGCTCAGAGCCACCACCCCATGTCAA
B34	CAACAGTTTATGGGATTTTGCTAATCAAAAGG
B35	GCCGCTTTGCTGAGGCTTGCAGGGGAAAAGGT
B36	GCGCAGACTCCATGTTACTTAGCCCGTTTTAA
B37	ACAGGTAGAAAGATTCATCAGTTGAGATTTAG
B38	CCTCAGAACCGCCACCCAAGCCCAATAGGAACGTAAATGA
B39	ATTTTCTGTCAGCGGAGTGAGAATACCGATAT

B40	ATTCGGTCTGCGGGATCGTCACCCGAAATCCG
B41	CGACCTGCGGTCAATCATAAGGGAACGGAACAACATTATT
B42	AGACGTTACCATGTACCGTAACACCCCTCAGAACCGCCAC
B43	CACGCATAAGAAAGGAACAACTAAGTCTTTCC
B44	ATTGTGTCTCAGCAGCGAAAGACACCATCGCC
B45	TTAATAAAACGAACTAACCGAACTGACCAACTCCTGATAA
B46	AGGTTTAGTACCGCCATGAGTTTCGTCACCAGGATCTAAA
B47	GTTTTGTCAGGAATTGCGAATAATCCGACAAT
B48	GACAACAAGCATCGGAACGAGGGTGAGATTTG
B49	TATCATCGTTGAAAGAGGACAGATGGAAGAAAAATCTACG
B50	AGCGTAACTACAAACTACAACGCCTATCACCGTACTCAGG
B51	TAGTTGCGAATTTTTTCACGTTGATCATAGTT
B52	GTACAACGAGCAACGGCTACAGAGGATACCGA
B53	ACCAGTCAGGACGTTGGAACGGTGTACAGACCGAAACAAA
B54	ACAGACAGCCCAAATCTCCAAAAAAAAATTTCTTA
B55	AACAGCTTGCTTTGAGGACTAAAGCGATTATA
B56	CCAAGCGCAGGCGCATAGGCTGGCAGAACTGGCTCATTAT
B57	CGAGGTGAGGCTCCAAAAGGAGCC
B58	ACCCCCAGACTTTTTCATGAGGAACTTGCTTT
B59	ACCTTATGCGATTTTATGACCTTCATCAAGAGCATCTTTG
B60	CGGTTTATCAGGTTTCCATTAAACGGGAATACACT
B61	AAAACACTTAATCTTGACAAGAACTTAATCATTGTGAATT
B62	GGCAAAAGTAAAATACGTAATGCC
B63	TGGTTTAATTTCAACTCGGATATTCATTACCCACGAAAGA
B64	ACCAACCTAAAAAATCAACGTAACAAATAAATTGGGCTTGAGA
B65	CCTGACGAGAAACACCAGAACGAGTAGGCTGCTCATTCAGTGA
C01	TCGGGAGATATACAGTAACAGTACAAATAATT
C02	CCTGATTAAAGGAGCGGAATTATCTCGGCCTC
C03	GCAAATCACCTCAATCAATATCTGCAGGTCGA
C04	CGACCAGTACATTGGCAGATTCACCTGATTGC
C05	TGGCAATTTTTAACGTCAGATGAAAACAATAACGGATTCG
C06	AAGGAATTACAAAGAAACCACCAGTCAGATGA
C07	GGACATTCACCTCAAATATCAAACACAGTTGA
C08	TTGACGAGCACGTATACTGAAATGGATTATTTAATAAAAG
C09	CCTGATTGCTTTGAATTGCGTAGATTTTCAGGCATCAATA
C10	TAATCCTGATTATCATTTTGCGGAGAGGAAGG
C11	TTATCTAAAGCATCACCTTGCTGATGGCCAAC
C12	AGAGATAGTTTGACGCTCAATCGTACGTGCTTTCCTCGTT
C13	GATTATACACAGAAATAAAGAAATACCAAGTTACAAAATC
C14	TAGGAGCATAAAAGTTTGAGTAACATTGTTTG

C15	TGACCTGACAAATGAAAAATCTAAAATATCTT
C16	AGAATCAGAGCGGGAGATGGAAATACCTACATAACCCTTC
C17	GCGCAGAGGCGAATTAATTATTTGCACGTAAATTCTGAAT
C18	AATGGAAGCGAACGTTATTAATTTCTAACAAC
C19	TAATAGATCGCTGAGAGCCAGCAGAAGCGTAA
C20	GAATACGTAACAGGAAAAACGCTCCTAAACAGGAGGCCGA
C21	TCAATAGATATTAAATCCTTTGCCGGTTAGAACCT
C22	CAATATTTGCCTGCAACAGTGCCATAGAGCCG
C23	TTAAAGGGATTTTAGATACCGCCAGCCATTGCGGCACAGA
C24	ACAATTCGACAACTCGTAATACAT
C25	TTGAGGATGGTCAGTATTAACACCTTGAATGG
C26	CTATTAGTATATCCAGAACAATATCAGGAACGGTACGCCA
C27	CGCGAACTAAAACAGAGGTGAGGCTTAGAAGTATT
C28	GAATCCTGAGAAGTGTATCGGCCTTGCTGGTACTTTAATG
C29	ACCACCAGCAGAAGATGATAGCCC
C30	TAAAACATTAGAAGAACTCAAACTTTTTATAATCAGTGAG
C31	GCCACCGAGTAAAAGAACATCACTTGCCTGAGCGCCATTAAAA
C32	TCTTTGATTAGTAATAGTCTGTCCATCACGCAAATTAACCGTT
C33	CGCGTCTGATAGGAACGCCATCAACTTTTACA
C34	AGGAAGATGGGGACGACGACAGTAATCATATT
C35	CTCTAGAGCAAGCTTGCATGCCTGGTCAGTTG
C36	CCTTCACCGTGAGACGGGCAACAGCAGTCACA
C37	CGAGAAAGGAAGGGAAGCGTACTATGGTTGCT
C38	GCTCATTTTTTAACCAGCCTTCCTGTAGCCAGGCATCTGC
C39	CAGTTTGACGCACTCCAGCCAGCTAAACGACG
C40	GCCAGTGCGATCCCCGGGTACCGAGTTTTTCT
C41	TTTCACCAGCCTGGCCCTGAGAGAAAGCCGGCGAACGTGG
C42	GTAACCGTCTTTCATCAACATTAAAATTTTTGTTAAATCA
C43	ACGTTGTATTCCGGCACCGCTTCTGGCGCATC
C44	CCAGGGTGGCTCGAATTCGTAATCCAGTCACG
C45	TAGAGCTTGACGGGGAGTTGCAGCAAGCGGTCATTGGGCG
C46	GTTAAAATTCGCATTAATGTGAGCGAGTAACACACGTTGG
C47	TGTAGATGGGTGCCGGAAACCAGGAACGCCAG
C48	GGTTTTCCATGGTCATAGCTGTTTGAGAGGCG
C49	GTTTGCGTCACGCTGGTTTGCCCCAAGGGAGCCCCCGATT
C50	GGATAGGTACCCGTCGGATTCTCCTAAACGTTAATATTTT
C51	AGTTGGGTCAAAGCGCCATTCGCCCCGTAATG
C52	CGCGCGGGCCTGTGTGAAATTGTTGGCGATTA
C53	CTAAATCGGAACCCTAAGCAGGCGAAAATCCTTCGGCCAA
C54	CGGCGGATTGAATTCAGGCTGCGCAACGGGGGATG

C55	TGCTGCAAATCCGCTCACAATTCCCAGCTGCA
C56	TTAATGAAGTTTGATGGTGGTTCCGAGGTGCCGTAAAGCA
C57	TGGCGAAATGTTGGGAAGGGCGAT
C58	TGTCGTGCACACAACATACGAGCCACGCCAGC
C59	CAAGTTTTTTGGGGTCGAAATCGGCAAAATCCGGGAAACC
C60	TCTTCGCTATTGGAAGCATAAAGTGTATGCCCGCT
C61	TTCCAGTCCTTATAAATCAAAAGAGAACCATCACCCAAAT
C62	GCGCTCACAAGCCTGGGGTGCCTA
C63	CGATGGCCCACTACGTATAGCCCGAGATAGGGATTGCGTT
C64	AACTCACATTATTGAGTGTTGTTCCAGAAACCGTCTATCAGGG
C65	ACGTGGACTCCAACGTCAAAGGGCGAATTTGGAACAAGAGTCC
Link-A1C	TTAATTAATTTTTTACCATATCAAA
Link-A2C	TTAATTTCATCTTAGACTTTACAA
Link-A3C	CTGTCCAGACGTATACCGAACGA
Link-A4C	TCAAGATTAGTGTAGCAATACT
Link-B1A	TGTAGCATTCCTTTTATAAACAGTT
Link-B2A	TTTAATTGTATTTCCACCAGAGCC
Link-B3A	ACTACGAAGGCTTAGCACCATTA
Link-B4A	ATAAGGCTTGCAACAAAGTTAC
Link-C1B	GTGGGAACAAATTTCTATTTTTGAG
Link-C2B	CGGTGCGGGCCTTCCAAAAACATT
Link-C3B	ATGAGTGAGCTTTTAAATATGCA
Link-C4B	ACTATTAAAGAGGATAGCGTCC
Loop	GCGCTTAATGCGCCGCTACAGGGC

iii. Sequences for QD Modification

a. Sequences for Single QD Modification

R75-Biotin	GCGCATTAAAGAACTGGCATGATTTTATTTTGAGTTGTGGATCCTACT-Biotin
A19-Biotin	TCAGAACCCAGAATCAAGTTTGCCGGTAAATAAGTTGTGGATCCTACT-Biotin

b. Sequences for Multi-QDs (same) Modification

A56-Biotin	ACAAGAAAGCAAGCAAATCAGATAACAGCCATATTATTTAAGTTGTGGATCCTACT-Biotin
B56-Biotin	CCAAGCGCAGGCGCATAGGCTGGCAGAACTGGCTCATTATAGTTGTGGATCCTACT-Biotin

C56-Biotin	TTAATGAAGTTTGATGGTGGTTCCGAGGTGCCGTAAAGCAAGTTGTGGATCCTACT-Biotin

c. Sequences for Multi-QDs (different) Modification

A56-Sticky End	ACAAGAAAGCAAGCAAATCAGATAACAGCCATATTATTTATGTGGTGGTG
B56-Sticky End	CCAAGCGCAGGCGCATAGGCTGGCAGAACTGGCTCATTATGCATGGGCGG
C56-Sticky End	TTAATGAAGTTTGATGGTGGTTCCGAGGTGCCGTAAAGCAAGCTTTGAGG
A56_Complementary-Biotin	Biotin-AAAAACACCACCACA
B56_Complementary-Biotin	Biotin-AAAAACCGCCCATGC
C56_Complementary-Biotin	Biotin-AAAAACCTCAAAGCT

iv. Sequences for Fluorescent Modification

R57-Sticky End	TTAGCCAAGCTTTAGGTCATTACCACGCTAACGAGCGTCTGAACACCC
R184-Sticky End	AGTTGTGGATCCTACTACGGTCAAGACAGCATCGGAACGACATAACCG
R57_Complementary-Red	CCTAAAGCTTGGCTAA-Rhodamine Red™
R184_Complementary-Green	AGTAGGATCCACAACT-Alexa Fluor® 488

v. Sequences for Peptides

A32_Complementary_peptide	CAGAAGGAAACCGAGGTTTTTAAGAAAAGTAAGCAGATAGCCGAGTTGTGGATCCTACT
B32_Complementary_peptide	AATACTGCGGAATCGTAGGGGGTAATAGTAAAATGTTTAGACTAGTTGTGGATCCTACT
C32_Complementary_peptide	TCTTTGATTAGTAATAGTCTGTCCATCACGCAAATTAACCGTTAGTTGTGGATCCTACT
A37_Complementary_peptide	AGAGAATAACATAAAAACAGGGAAGCGCATTAAGTTGTGGATCCTACT
B37_Complementary_peptide	ACAGGTAGAAAGATTCATCAGTTGAGATTTAGAGTTGTGGATCCTACT
C37_Complementary_peptide	CGAGAAAGGAAGGGAAGCGTACTATGGTTGCTAGTTGTGGATCCTACT
Maleimide-Peptide	Maleimide-AGTAGGATCCACAACT

vi. Sequences for EGF

A56-Biotin	ACAAGAAAGCAAGCAAATCAGATAACAGCCATATTATTTAGTTATGTAACT CTGATA-Biotin
B56-Biotin	CCAAGCGCAGGCGCATAGGCTGGCAGAACTGGCTCATTATGTTATGTAAC TCTGATA-Biotin
C56-Biotin	TTAATGAAGTTTGATGGTGGTTCCGAGGTGCCGTAAAGCAGTTATGTAACT CTGATA-Biotin

vii. Sequences for Amino Anchors

A5-Amino	TTTGATGATTAAGAGGCTGAGACTTGCTCAGTACCAGGCGCCGATTCAG-Amino
B5-Amino	ACAGTCAAAGAGAATCGATGAACGACCCCGGTTGATAATCCCGATTCAG-Amino
C5-Amino	TGGCAATTTTTAACGTCAGATGAAAACAATAACGGATTCGCCGATTCAG-Amino
A13-Amino	TTTAACGGTTCGGAACCTATTATTAGGGTTGATATAAGTACCGATTCAG-Amino
B13-Amino	CGTTCTAGTCAGGTCATTGCCTGACAGGAAGATTGTATAACCGATTCAG-Amino
C13-Amino	GATTATACACAGAAATAAAGAAATACCAAGTTACAAAATCCCGATTCAG-Amino
A33-Amino	CGCGTCTGATAGGAACGCCATCAACTTTTACACCGATTCAG-Amino
B33-Amino	AGGGATAGCTCAGAGCCACCACCCCATGTCAACCGATTCAG-Amino
C33-Amino	GATTATACACAGAAATAAAGAAATACCAAGTTCCGATTCAG-Amino
A42-Amino	AGAGTCAAAAATCAATATATGTGATGAAACAAACATCAAGCCGATTCAG-Amino
B42-Amino	AGACGTTACCATGTACCGTAACACCCCTCAGAACCGCCACCCGATTCAG-Amino
C42-Amino	GTAACCGTCTTTCATCAACATTAAAATTTTTGTTAAATCACCGATTCAG-Amino
A50-Amino	ACATAGCGCTGTAAATCGTCGCTATTCATTTCAATTACCTCCGATTCAG-Amino
B50-Amino	AGCGTAACTACAAACTACAACGCCTATCACCGTACTCAGGCCGATTCAG-Amino
C50-Amino	GGATAGGTACCCGTCGGATTCTCCTAAACGTTAATATTTTCCGATTCAG-Amino

Reference

1. Ishijima, A. & Yanagida, T. Single molecule nanobioscience. *Trends Biochem. Sci.* **26,** 438–44 (2001).

2. Ho, W. Single-molecule chemistry. *J. Chem. Phys.* **117,** 11033–11061 (2002).

3. Knight, A. E. *Single molecule biology*. (Academic Press, 2009).

4. Cornish, P. V & Ha, T. A Survey of Single-Molecule Techniques in Chemical Biology. *ACS Chem. Biol.* **2,** 53–61 (2007).

5. Zlatanova, J. & van Holde, K. Single-Molecule Biology: What Is It and How Does It Work? *Mol. Cell* **24,** 317–329 (2006).

6. Pinheiro, A. V., Han, D., Shih, W. M. & Yan, H. Challenges and opportunities for structural DNA nanotechnology. *Nat. Nanotechnol.* **6,** 763–772 (2011).

7. Watson, J. D. & Crick, F. H. C. Molecular structure of nucleic acids. *Nature* **171,** 737–738 (1953).

8. Pray, L. Discovery of DNA Structure and Function: Watson and Crick. *Nature Education* 1(1):100 (2008). Available at: https://www.nature.com/scitable/topicpage/discovery-of-dna-structure-and-function-watson-397.

9. Mandelkern, M., Elias, J. G., Eden, D. & Crothers, D. M. The dimensions of DNA in solution. *J. Mol. Biol.* **152,** 153–161 (1981).

10. Seeman, N. C. Nanomaterials based on DNA. *Annu. Rev. Biochem.* **79,** 65–87 (2010).

11. Holliday, R. A mechanism for gene conversion in fungi. *Genet. Res.* **5,** 282 (1964).

12. Seeman, N. C. Nucleic acid junctions and lattices. *J. Theor. Biol.* **99,** 237–247 (1982).

13. Seeman, N. C. DNA Nicks and Nodes and Nanotechnology. *Nano Lett.* **1,** 22–26 (2001).

14. Winfree, E., Liu, F., Wenzler, L. a & Seeman, N. C. Design and self-assembly of two-dimensional DNA crystals. *Nature* **394,** 539–44 (1998).

15. Mao, C., Sun, W., Shen, Z. & Seeman, N. C. A nanomechanical device based on the B-Z transition of DNA. *Nature* **397,** 144–6 (1999).

16. Yan, H., Zhang, X., Shen, Z. & Seeman, N. C. A robust DNA mechanical device controlled by hybridization topology. *Nature* **415,** 62–65 (2002).

17. Sherman, W. B. & Seeman, N. C. A Precisely Controlled DNA Biped Walking Device. *Nano Lett.* **4,** 1203–1207 (2004).

18. Niemeyer, C. M. Semisynthetic DNA-protein conjugates for biosensing and nanofabrication. *Angew. Chem. Int. Ed. Engl.* **49,** 1200–16 (2010).

19. Yan, H., Park, S. H., Finkelstein, G., Reif, J. H. & LaBean, T. H. DNA-templated self-assembly of protein arrays and highly conductive nanowires. *Science* **301,** 1882–4 (2003).

20. Wang, R., Nuckolls, C. & Wind, S. J. Assembly of heterogeneous functional nanomaterials on DNA origami scaffolds. *Angew. Chem. Int. Ed. Engl.* **51,** 11325–7 (2012).

21. Zanchet, D., Micheel, C. M., Parak, W. J., Gerion, D. & Alivisatos, A. P. Electrophoretic Isolation of Discrete Au Nanocrystal/DNA Conjugates. *Nano Lett.* **1,** 32–35 (2001).

22. Fu, A. *et al.* Discrete Nanostructures of Quantum Dots/Au with DNA. *J. Am. Chem. Soc.* **126,** 10832–10833 (2004).

23. Yu, W. W., Chang, E., Drezek, R. & Colvin, V. L. Water-soluble quantum dots for biomedical applications. *Biochem. Biophys. Res. Commun.* **348,** 781–786 (2006).

24. Park, S. H. *et al.* Finite-Size, Fully Addressable DNA Tile Lattices Formed by Hierarchical Assembly Procedures. *Angew. Chemie* **118,** 749–753 (2006).

25. Saccà, B. & Niemeyer, C. M. DNA origami: the art of folding DNA. *Angew. Chem. Int. Ed. Engl.* **51,** 58–66 (2012).

26. Yan, H., LaBean, T. H., Feng, L. & Reif, J. H. Directed nucleation assembly of DNA tile complexes for barcode-patterned lattices. *Proc. Natl. Acad. Sci. U. S. A.* **100,** 8103–8 (2003).

27. Shih, W. M., Quispe, J. D. & Joyce, G. F. A 1.7-kilobase single-stranded DNA that folds into a nanoscale octahedron. *Nature* **427,** 618–21 (2004).

28. Rothemund, P. W. K. Folding DNA to create nanoscale shapes and patterns. *Nature* **440,** 297–302 (2006).

29. Douglas, S. M. *et al.* Rapid prototyping of 3D DNA-origami shapes with caDNAno. *Nucleic Acids Res.* **37,** 5001–6 (2009).

30. Zhang, Z., Song, J., Besenbacher, F., Dong, M. & Gothelf, K. V. Self-assembly of DNA origami and single-stranded tile structures at room temperature. *Angew. Chem. Int. Ed. Engl.* **52,** 9219–23 (2013).

31. Douglas, S. M. *et al.* Self-assembly of DNA into nanoscale three-dimensional

shapes. *Nature* **459,** 414–418 (2009).

32. Dietz, H., Douglas, S. M. & Shih, W. M. Folding DNA into twisted and curved nanoscale shapes. *Science (80-.).* **325,** 725–30 (2009).

33. Kuzuya, A. & Komiyama, M. Design and construction of a box-shaped 3D-DNA origami. *Chem. Commun.* **45,** 4182 (2009).

34. Han, D. *et al.* DNA Origami with Complex Curvatures in Three-Dimensional Space. *Science (80-.).* **332,** 342–346 (2011).

35. Gates, B. D. *et al.* New Approaches to Nanofabrication: Molding, Printing, and Other Techniques. *Chem. Rev.* **105,** 1171–1196 (2005).

36. Chen, Y. & Pépin, A. Nanofabrication: Conventional and nonconventional methods. *Electrophoresis* **22,** 187–207 (2001).

37. Biswas, A. *et al.* Advances in top–down and bottom–up surface nanofabrication: Techniques, applications & future prospects. *Adv. Colloid Interface Sci.* **170,** 2–27 (2012).

38. Aizenberg, J. Crystallization in patterns: A bio-inspired approach. *Adv. Mater.* **16,** 1295–1302 (2004).

39. Gautrot, J. E., Huck, W. T. S., Welch, M. & Ramstedt, M. Protein-resistant NTA-functionalized polymer brushes for selective and stable immobilization of histidine-tagged proteins. *ACS Appl. Mater. Interfaces* **2,** 193–202 (2010).

40. Torres, A. J., Wu, M., Holowka, D. & Baird, B. Nanobiotechnology and cell biology: micro- and nanofabricated surfaces to investigate receptor-mediated signaling. *Annu. Rev. Biophys.* **37,** 265–88 (2008).

41. Schlapak, R. *et al.* Painting with Biomolecules at the Nanoscale: Biofunctionalization with Tunable Surface Densities. *Nano Lett.* **12,** 1983–1989 (2012).

42. Qian, T. & Wang, Y. Micro/nano-fabrication technologies for cell biology. *Med. Biol. Eng. Comput.* **48,** 1023–1032 (2010).

43. Huang, J. *et al.* Impact of order and disorder in RGD nanopatterns on cell adhesion. *Nano Lett.* **9,** 1111–1116 (2009).

44. Schvartzman, M. *et al.* Nanolithographic control of the spatial organization of cellular adhesion receptors at the single-molecule level. *Nano Lett.* **11,** 1306–12 (2011).

45. Cai, H. *et al.* Molecular Occupancy of Nanodot Arrays. *ACS Nano* **10,** 4173–4183 (2016).

46. Wang, R., Palma, M., Penzo, E. & Wind, S. J. Lithographically directed assembly of one-dimensional DNA nanostructures via bivalent binding interactions. *Nano Res.* **6,** 409–417 (2013).

47. Penzo, E. *et al.* Directed Assembly of End-Functionalized Single Wall Carbon Nanotube Segments. *Nano Lett.* **15,** 6547–6552 (2015).

48. Massia, S. P. & Hubbell, J. A. an Rgd Spacing of 440Nm Is Sufficient for Integrin Alpha-V-Beta-3-Mediated Fibroblast Spreading and 140Nm for Focal Contact and Stress Fiber Formation. *J. Cell Biol.* **114,** 1089–1100 (1991).

49. Binnig, G., Quate, C. F. & Gerber, C. Atomic Force Microscope. *Phys. Rev. Lett.* **56,** 930–933 (1986).

50. Radmacher, M., Tillmann, R. W., Fritz, M. & Gaub, H. E. From molecules to cells: imaging soft samples with the atomic force microscope. *Science (80-.).* **257,** 1900–1906 (1992).

51. Liu, S. & Wang, Y. Application of AFM in microbiology: a review. *Scanning* **32,** 61–73 (2010).

52. Giessibl, F. J. Forces and frequency shifts in atomic-resolution dynamic-force microscopy. *Phys. Rev. B* **56,** 16010–16015 (1997).

53. Babicz, S., Smulko, J. & Zieliński, A. Enhancing capabilities of Atomic Force Microscopy by tip motion harmonics analysis. *Bull. Polish Acad. Sci. Tech. Sci.* **61,** 535–539 (2013).

54. Tamayo, J. & García, R. Deformation, Contact Time, and Phase Contrast in Tapping Mode Scanning Force Microscopy. *Langmuir* **12,** 4430–4435 (1996).

55. ScanAsyst Exclusive, Self-Optimizing AFM Imaging Innovation with Integrity. Available at: https://www.bruker.com/fileadmin/user_upload/8-PDF-Docs/SurfaceAnalysis/AFM/Brochures/ScanAsyst-atomic-force-microscopy-imaging-mode-brochure-B071-B0.pdf. (Accessed: 17th November 2017)

56. Volkert, C. A. & Minor, A. M. Focused Ion Beam Microscopy and Micromachining. *MRS Bull.* **32,** 389–399 (2007).

57. Melngailis, J. Focused ion beam technology and applications. *J. Vac. Sci. Technol. B Microelectron. Nanom. Struct.* **5,** 469 (1987).

58. Reyntjens, S., De Bruyker, D. & Puers, R. Focused ion beam as an inspection tool for microsystem technology. in *Proc. Microsystem Symp* 125 (1998).

59. Glanville, J. Focused ion beam technology for integrated circuit modification. *Solid State Technol.* **32,** 270–272 (1989).

60. Reyntjens, S. & Puers, R. A review of focused ion beam applications in microsystem technology. *J. Micromechanics Microengineering* **11,** 287–300 (2001).

61. Stanishevsky, A., Aggarwal, S., Prakash, A. S., Melngailis, J. & Ramesh, R. Focused ion-beam patterning of nanoscale ferroelectric capacitors. *J. Vac. Sci. Technol. B* **16,** 3899–3902 (1998).

62. Liu, N. W., Datta, A., Liu, C. Y. & Wang, Y. L. High-speed focused-ion-beam patterning for guiding the growth of anodic alumina nanochannel arrays. *Appl. Phys. Lett.* **82,** 1281–1283 (2003).

63. Giérak, J. *et al.* Exploration of the ultimate patterning potential of focused ion beams. *J. Micro/Nanolithography, MEMS, MOEMS* **5,** 11011 (2006).

64. Machalett, F. *et al.* Direct patterning of gold oxide thin films by focused ion-beam irradiation. *Appl. Phys. A Mater. Sci. Process.* **71,** 331–335 (2000).

65. Hemamouche, A. *et al.* FIB patterning of dielectric, metallized and graphene membranes: A comparative study. *Microelectron. Eng.* **121,** 87–91 (2014).

66. Lugstein, A., Basnar, B., Smoliner, J. & Bertagnolli, E. FIB processing of silicon in the nanoscale regime. *Appl. Phys. A Mater. Sci. Process.* **76,** 545–548 (2003).

67. Mackenzie, R. a. D. Developments and trends in the technology of focused ion beams. *J. Vac. Sci. Technol. B Microelectron. Nanom. Struct.* **9,** 2561 (1991).

68. Yanisch-Perron, C., Vieira, J. & Messing, J. Improved M13 phage cloning vectors and host strains: nucleotide sequences of the M13mpl8 and pUC19 vectors. *Gene* **33,** 103–119 (1985).

69. Castro, C. E. *et al.* A primer to scaffolded DNA origami. *Nat. Methods* **8,** 221–9 (2011).

70. Lee, J. B. *et al.* DNA-based nanostructures for molecular sensing. *Nanoscale* **2,** 188–97 (2010).

71. Hernández-Ainsa, S. & Keyser, U. F. DNA origami nanopores: an emerging tool in biomedicine. *Nanomedicine (Lond).* **8,** 1551–4 (2013).

72. Zhu, J. *et al.* Accurate quantification of microRNA via single strand displacement reaction on DNA origami motif. *PLoS One* **8,** e69856 (2013).

73. Lund, K. *et al.* Molecular robots guided by prescriptive landscapes. *Nature* **465,** 206–10 (2010).

74. Etheridge, T. J. *et al.* Quantification of DNA-associated proteins inside eukaryotic cells using single-molecule localization microscopy. *Nucleic Acids Res.* **42,** e146–e146 (2014).

75. Mollica, M. *et al.* DNA Origami Engineered Nanostructures : A Novel Method To Study Cell Signaling. (The Ohio State University, 2014).

76. Douglas, S. M., Bachelet, I. & Church, G. M. A logic-gated nanorobot for targeted transport of molecular payloads. *Science* **335,** 831–4 (2012).

77. Yurke, B., Turberfield, A. & Mills, A. A DNA-fuelled molecular machine made of DNA. *Nature* **406,** 605–608 (2000).

78. Shen, W., Zhong, H., Neff, D. & Norton, M. L. NTA directed protein

nanopatterning on DNA Origami nanoconstructs. *J. Am. Chem. Soc.* **131,** 6660–1 (2009).

79. Voigt, N. V *et al.* Single-molecule chemical reactions on DNA origami. *Nat. Nanotechnol.* **5,** 200–3 (2010).

80. Rinker, S., Ke, Y., Liu, Y., Chhabra, R. & Yan, H. Self-assembled DNA nanostructures for distance-dependent multivalent ligand-protein binding. *Nat. Nanotechnol.* **3,** 418–22 (2008).

81. Ngo, T. A., Nakata, E., Saimura, M., Kodaki, T. & Morii, T. A protein adaptor to locate a functional protein dimer on molecular switchboard. *Methods* **67,** 142–50 (2014).

82. Castronovo, M. *et al.* Control of steric hindrance on restriction enzyme reactions with surface-bound DNA nanostructures. *Nano Lett.* **8,** 4140–5 (2008).

83. Bath, J. & Turberfield, A. J. DNA nanomachines. *Nat. Nanotechnol.* **2,** 275–284 (2007).

84. Hernández-Ainsa, S. *et al.* DNA origami nanopores for controlling DNA translocation. *ACS Nano* **7,** 6024–30 (2013).

85. Sørensen, R. S. *et al.* Enzymatic ligation of large biomolecules to DNA. *ACS Nano* **7,** 8098–104 (2013).

86. Zhao, Y.-X. *et al.* DNA origami delivery system for cancer therapy with tunable release properties. *ACS Nano* **6,** 8684–91 (2012).

87. Brus, L. E. Electron–electron and electron-hole interactions in small semiconductor crystallites: The size dependence of the lowest excited electronic state. *J. Chem. Phys.* **80,** 4403–4409 (1984).

88. Alivisatos, A. P. Semiconductor Clusters, Nanocrystals, and Quantum Dots. *Science (80-.).* **271,** 933–937 (1996).

89. Ashoori, R. C. Electrons in artificial atoms. *Nature* **379,** 413–419 (1996).

90. Murray, C. B., Kagan, C. R. & Bawendi, M. G. Synthesis and Characterization of Monodisperse Nanocrystals and Close-Packed Nanocrystal Assemblies. *Annu. Rev. Mater. Sci.* **30,** 545–610 (2000).

91. Medintz, I. L., Uyeda, H. T., Goldman, E. R. & Mattoussi, H. Quantum dot bioconjugates for imaging, labelling and sensing. *Nat. Mater.* **4,** 435–446 (2005).

92. Hermanson, G. T. *Bioconjugate Techniques*. (2013).

93. Brown, D. M. Chemical reactions of polynucleotides and nucleic acids. *Basic Princ. nucleic acid Chem.* **2,** 1–90 (1974).

94. Sánchez, A., Pedroso, E. & Grandas, A. Maleimide-dimethylfuran exo adducts: Effective maleimide protection in the synthesis of oligonucleotide conjugates.

Org. Lett. **13,** 4364–4367 (2011).

95. Chaiet, L. & Wolf, F. J. The properties of streptavidin, a biotin-binding protein produced by Streptomycetes. *Arch. Biochem. Biophys.* **106,** 1–5 (1964).

96. Chivers, C. E., Koner, A. L., Lowe, E. D. & Howarth, M. How the biotin–streptavidin interaction was made even stronger: investigation via crystallography and a chimaeric tetramer. *Biochem. J.* **435,** 55–63 (2011).

97. Holmberg, A. *et al.* The biotin-streptavidin interaction can be reversibly broken using water at elevated temperatures. *Electrophoresis* **26,** 501–510 (2005).

98. Smith, C. L., Milea, J. S. & Nguyen, G. Immobilization of Nucleic Acids Using Biotin-Strept (avidin) Systems. *Top Curr Chem* **261,** 63–90 (2006).

99. Weber, P., Ohlendorf, D., Wendoloski, J. & Salemme, F. Structural origins of high-affinity biotin binding to streptavidin. *Science (80-.).* **243,** 85–88 (1989).

100. Bäumle, M., Stamou, D., Segura, J. M., Hovius, R. & Vogel, H. Highly fluorescent streptavidin-coated CdSe nanoparticles: Preparation in water, characterization, and micropatterning. *Langmuir* **20,** 3828–3831 (2004).

101. Smyth, D. G., Blumenfeld, O. O. & Konigsberg, W. Reactions of N-ethylmaleimide with peptides and amino acids. *Biochem. J.* **91,** 589–95 (1964).

102. Feeney, R. E., Blankenhorn, G. & Dixon, H. B. F. Carbonyl-amine reactions in protein chemistry. *Adv. Protein Chem.* **29,** 135–203 (1975).

103. Hayashida, T. & Umemura, K. Atomic Force Microscopy of DNA-wrapped Single-walled Carbon Nanotubes in Aqueous Solution. *Colloids Surfaces B Biointerfaces* **143,** 526–531 (2016).

104. Hansma, H. G., Laney, D. E., Bezanilla, M., Sinsheimer, R. L. & Hansma, P. K. Applications for atomic force microscopy of DNA. *Biophys. J.* **68,** 1672–1677 (1995).

105. Huang, D., Freeley, M. & Palma, M. DNA-Mediated Patterning of Single Quantum Dot Nanoarrays: A Reusable Platform for Single-Molecule Control. *Sci. Rep.* **7,** 45591 (2017).

106. Maune, H. T. *et al.* Self-assembly of carbon nanotubes into two-dimensional geometries using DNA origami templates. *Nat. Nanotechnol.* **5,** 61–66 (2010).

107. Geng, Y. *et al.* Electrically Conductive Gold- and Copper-Metallized DNA Origami Nanostructures. *Langmuir* **29,** 3482–3490 (2013).

108. Ding, B. *et al.* Gold Nanoparticle Self-Similar Chain Structure Organized by DNA Origami. *J. Am. Chem. Soc.* **132,** 3248–3249 (2010).

109. Ko, S. H., Gallatin, G. M. & Liddle, J. A. Nanomanufacturing with DNA origami: Factors affecting the kinetics and yield of quantum dot binding. *Adv. Funct. Mater.* **22,** 1015–1023 (2012).

110. Thacker, V. V *et al.* DNA origami based assembly of gold nanoparticle dimers for surface-enhanced Raman scattering. *Nat. Commun.* **5,** 3448 (2014).

111. Pfitzner, E. *et al.* Rigid DNA beams for high-resolution single-molecule mechanics. *Angew. Chemie - Int. Ed.* **52,** 7766–7771 (2013).

112. Kershner, R. J. *et al.* Placement and orientation of individual DNA shapes on lithographically patterned surfaces. *Nat. Nanotechnol.* **4,** 557–61 (2009).

113. Scheible, M. B., Pardatscher, G., Kuzyk, A. & Simmel, F. C. Single molecule characterization of DNA binding and strand displacement reactions on lithographic DNA origami microarrays. *Nano Lett.* **14,** 1627–33 (2014).

114. Kinz-Thompson, C. D. *et al.* Robustly passivated, gold nanoaperture arrays for single-molecule fluorescence microscopy. *ACS Nano* **7,** 8158–66 (2013).

115. Chou, S. Y., Krauss, P. R. & Renstrom, P. J. Nanoimprint lithography. *J. Vac. Sci. Technol. B Microelectron. Nanom. Struct.* **14,** 4129 (1996).

116. Penzo, E., Wang, R., Palma, M. & Wind, S. J. Selective placement of DNA origami on substrates patterned by nanoimprint lithography. *J. Vac. Sci. Technol. B Microelectron. Nanom. Struct.* **29,** 06F205 (2011).

117. Gamo, K. Nanofabrication by FIB. *Microelectron. Eng.* **32,** 159–171 (1996).

118. Kubena, R. L. Resolution Limits of Focused-Ion-Beam Resist Patterning. *MRS Proc.* **279,** 567 (1992).

119. Tseng, A. A. a. Recent developments in micromilling using focused ion beam technology. *J. Micromechanics Microengineering* **14,** R15–R34 (2004).

120. Lewandowski, C. M. *Hydrophobicity, Hydrophilicity and Silane Surface Modification*. *Gelest, Inc.* **1,** (2015).

121. Waddell, T. G., Leyden, D. E. & DeBello, M. T. The nature of organosilane to silica-surface bonding. *J. Am. Chem. Soc.* **103,** 5303–5307 (1981).

122. Jenkins, M. L., Dauskardt, R. H. & Bravman, J. C. Important Factors for Silane Adhesion Promoter Efficacy: Surface Coverage , Functionality and Chain Length. *J. Adhes. Sci. Technol.* **18,** 1497–1516 (2004).

123. Mittal, K. L. *Silanes and other coupling agents*. **4,** (CRC Press, 2007).

124. Arkles, B. Tailoring surfaces with silanes. *Chemtech* **7,** 766–778 (1977).

125. Shi, H.-Q. *et al.* Synthesis of silane surface modified ZnO quantum dots with ultrastable, strong and tunable luminescence. *Chem. Commun.* **47,** 11921 (2011).

126. Sweetman, M. J., Shearer, C. J., Shapter, J. G. & Voelcker, N. H. Dual silane surface functionalization for the selective attachment of human neuronal cells to porous silicon. *Langmuir* **27,** 9497–9503 (2011).

127. Benoy, P. A. & Dellacorte, C. Au/Cr Sputter Coating for the Protection of Alumina During Sliding at High Temperatures. *Tribol. Trans.* **39,** 670–676 (1996).

128. Kubena, R. L., Stratton, F. P., Ward, J. W., Atkinson, G. M. & Joyce, R. J. Sub-20-nm-wide line fabrication in poly(methylmethacrylate) using a Ga[sup +] microprobe. *Int. Symp. electron, ion, Phot. beams* **7,** 1798–1801 (1989).

129. Kochumalayil, J. J., Meiser, A., Soldera, F. & Possart, W. Focused ion beam irradiation - morphological and chemical evolution in PMMA. *Surf. Interface Anal.* **41,** 412–420 (2009).

130. Gopinath, A. & Rothemund, P. W. K. Optimized assembly and covalent coupling of single-molecule DNA origami nanoarrays. *ACS Nano* **8,** 12030–12040 (2014).

131. Gopinath, A., Miyazono, E., Faraon, A. & Rothemund, P. W. K. Engineering and mapping nanocavity emission via precision placement of DNA origami. *Nature* **535,** 401–405 (2016).

132. Hay, E. D. *Cell biology of extracellular matrix*. (Springer Science & Business Media, 2013).

133. Gumbiner, B. M. Cell adhesion: The molecular basis of tissue architecture and morphogenesis. *Cell* **84,** 345–357 (1996).

134. Trappmann, B. *et al.* Extracellular-matrix tethering regulates stem-cell fate. *Nat. Mater.* **11,** 642–9 (2012).

135. Gray, S. D., Alipour, F., Titze, I. R. & Hammond, T. H. Biomechanical and histologic observations of vocal fold fibrous proteins. *Ann. Otol. Rhinol. Laryngol.* **109,** 77–85 (2000).

136. Zamir, E. & Geiger, B. Components of cell-matrix adhesions. *J. Cell Sci.* **114,** 3577–3579 (2001).

137. Wozniak, M. A., Modzelewska, K., Kwong, L. & Keely, P. J. Focal adhesion regulation of cell behavior. *Biochim. Biophys. Acta - Mol. Cell Res.* **1692,** 103–119 (2004).

138. Jordan, V. C. & Morrow, M. Cell adhesion molecules. **319,** 332–334 (1999).

139. Humphries, J. D., Byron, A. & Humphries, M. J. Integrin ligands at a glance. *J. Cell Sci.* **119,** 3901–3903 (2006).

140. Springer, T. A. & Wang, J.-H. in *Advances in Protein Chemistry* **68,** 29–63 (2004).

141. Danen, E. H. J. & Sonnenberg, A. Integrins in regulation of tissue development and function. *J. Pathol.* **201,** 632–41 (2003).

142. Lampugnani, M. G., Resnati, M., Dejana, E. & Marchisio, P. C. The role of integrins in the maintenance of endothelial monolayer integrity. *J. Cell Biol.* **112,** 479–490 (1991).

143. Hood, J. D. & Cheresh, D. A. Role of Integrins in Cell Invasion and Migration. *Nat. Rev. Cancer* **2,** 91–100 (2002).

144. Ni, H. & Freedman, J. Platelets in hemostasis and thrombosis: Role of integrins and their ligands. *Transfus. Apher. Sci.* **28,** 257–264 (2003).

145. Hynes, R. O. Integrins: Bidirectional, allosteric signaling machines. *Cell* **110,** 673–687 (2002).

146. Miranti, C. K. & Brugge, J. S. Sensing the environment: a historical perspective on integrin signal transduction. *Nat. Cell Biol.* **4,** E83–E90 (2002).

147. Breuss, J. M. *et al.* Expression of the β6 integrin subunit in development, neoplasia and tissue repair suggests a role in epithelial remodeling. *J. Cell Sci.* **108,** 2241–2251 (1995).

148. Lum, L. Metargidin, a Membrane-anchored Metalloprotease-Disintegrin Protein with an RGD Integrin Binding Sequence. *J. Biol. Chem.* **271,** 4593–4596 (1996).

149. Ruoslahti, E. & Pierschbacher, M. D. New perspectives in cell adhesion: RGD and integrins. *Science* **238,** 491–7 (1987).

150. Saha, A. *et al.* High-resolution in vivo imaging of breast cancer by targeting the pro-invasive integrin alphavbeta6. *J. Pathol.* **222,** 52–63 (2010).

151. DiCara, D. *et al.* Structure-function analysis of Arg-Gly-Asp helix motifs in alpha v beta 6 integrin ligands. *J. Biol. Chem.* **282,** 9657–65 (2007).

152. Thomas, G. J., Nyström, M. L. & Marshall, J. F. Avβ6 Integrin in Wound Healing and Cancer of the Oral Cavity. *J. Oral Pathol. Med.* **35,** 1–10 (2006).

153. Carpenter, G. & Cohen, S. Epidermal growth factor. *Annu. Rev. Biochem.* **48,** 193–216 (1979).

154. Schreiber, A. B., Winkler, M. E. & Derynck, R. Transforming growth factor-α: A more potent angiogenic mediator than epidermal growth factor. *Science (80-.).* **232,** 1250–1253 (1986).

155. Grotendorst, G. R., Smale, G. & Pencev, D. Production of transforming growth factor beta by human peripheral blood monocytes and neutrophils. *J. Cell. Physiol.* **140,** 396–402 (1989).

156. Woodburn, J. R. The epidermal growth factor receptor and its inhibition in cancer therapy. *Pharmacol. Ther.* **82,** 241–50 (1999).

157. Zheng, Y., Yang, W., Aldape, K., He, J. & Lu, Z. Epidermal Growth Factor (EGF)-enhanced Vascular Cell Adhesion Molecule-1 (VCAM-1) Expression Promotes Macrophage and Glioblastoma Cell Interaction and Tumor Cell Invasion *. *Publ. JBC Pap. Press* (2013). doi:10.1074/jbc.M113.499020

158. Kim, S. H., Turnbull, J. & Guimond, S. Extracellular matrix and cell signalling: The dynamic cooperation of integrin, proteoglycan and growth factor receptor.

J. Endocrinol. **209,** 139–151 (2011).

159. Bill, H. M. *et al.* Epidermal Growth Factor Receptor-Dependent Regulation of Integrin-Mediated Signaling and Cell Cycle Entry in Epithelial Cells Epidermal Growth Factor Receptor-Dependent Regulation of Integrin-Mediated Signaling and Cell Cycle Entry in Epithelial Cells. *Society* **24,** 8586–8599 (2004).

160. Cowley, G. P., Smith, J. A. & Gusterson, B. A. Increased EGF receptors on human squamous carcinoma cell lines. *Br. J. Cancer* **53,** 223–229 (1986).

161. Masui, H. *et al.* Growth inhibition of human tumor cells in athymic mice by anti-epidermal growth factor receptor monoclonal antibodies. *Cancer Res* **44,** 1002–1007 (1984).

162. Gill, G. N., Bertics, P. J. & Santon, J. B. Epidermal growth factor and its receptor. *Mol. Cell. Endocrinol.* **51,** 169–86 (1987).